Universität Rostock

Traditio et Innovatio

The network of signaling pathways

Analysis of the Notch and Wnt signaling pathway in the differentiation of human neural progenitor cells

Dissertation

zur

Erlangung des akademischen Grades

doctor rerum naturalium (Dr. rer. nat.)

der Mathematischen-Naturwissenschaftlichen Fakultät

der Universität Rostock

vorgelegt von

Carolin Mußmann geb. Mahler

geb. am 14.04.1986 in Neustadt am Rübenberge

Rostock, 14.01.2014

urn:nbn:de:gbv:28-diss2015-0044-6

Gutachter:

1. Gutachter:
   Prof. Dr. Reinhard Schröder,
   Institut für Biowissenschaften Abt. Genetik, Universität Rostock

2. Gutachter:
   Prof. Dr. Arndt Rolfs,
   Albrecht-Kossel-Institute for Neuroregeneration, Universität Rostock

Datum der Einreichung: 14. Januar 2014
Datum der Verteidigung: 05. Dezember 2014

Erklärung

Ich versichere hiermit an Eides statt, dass ich die vorliegende Arbeit selbstständig angefertigt und ohne fremde Hilfe verfasst habe, keine außer den von mir angegebenen Hilfsmitteln und Quellen dazu verwendet habe und die den benutzten Werken inhaltlich und wörtlich entnommenen Stellen als solche kenntlich gemacht habe.

Rostock, 14.01.2014_____

(Carolin Mußmann)

Content

1 Introduction 1
1.1 Stem cells 1
1.1.1 Neural Progenitor Cells 2
1.2 Regulation of the neuronal differentiation 3
1.2.1 The Wnt pathways 4
1.2.2 The Notch pathway 11
1.2.3 The BMP pathway 14
1.2.4 The JAK/STAT3 pathway 16
1.3 Aim of the study 17
2 Materials and Methods 20
2.1 Materials 20
2.1.1 Technical equipment 20
2.1.2 Software 21
2.1.3 Consumables 21
2.1.4 Chemicals 22
2.1.5 Antibodies 23
2.1.6 Oligonucleotides 25
2.1.7 Vectors 27
2.1.8 Enzymes 28
2.1.9 Bacterial strains and media 28
2.1.10 Cell lines and media 29
2.1.11 Cell culture media, buffers and supplements 29
2.2 Methods 32
2.2.1 Cell culture 32
2.2.2 Protein analysis 35
2.2.3 Molecular biological methods 38
3 Results 42
3.1 Generation of expression vectors 42
3.1.1 Generation of pCAGGS-h*HES1* 42
3.1.2 Generation of pCAGGS-h*HES5* 43
3.2 The Notch pathway in ReNcell VM cells 44
3.2.1 Inhibition of the Notch pathway 45
3.2.2 Activation of the Notch pathway 46

3.3 The effect of Wnt-3a in the differentiation of ReNcell VM cells 48
3.3.1 Modulation of the Notch target genes by Wnt-3a 49
3.3.2 The additive effect of Wnt-3a treatment and Notch inhibition 50
3.3.3 Time dependency of Wnt-3a/DAPT effects on neurogenesis 54
3.4 The mechanism behind the Wnt-3a effect 57
3.4.1 Analysis of the Wnt pathway dependency 58
3.4.2 Analysis of the Notch pathway dependency 63
3.4.3 Analysis of the BMP pathway dependency 69
3.4.4 Analysis of the JAK/STAT3 pathway dependency 73
3.5 Induced pluripotent stem cell derived neural progenitor cells (iPS-NPCs) 77
3.5.1 The Notch pathway in iPS-NPCs 78
3.5.2 The effect of Wnt-3a in differentiating iPS-NPCs 78
3.5.3 The Wnt-3a and DAPT effect in the differentiation of iPS-NPCs 80
4 Discussion 82
4.1 Generation of pCAGGS-hHES vectors 82
4.2 The Notch pathway in ReNcell VM cells 83
4.3 The effect of Wnt-3a treatment and Notch inhibition in the differentiation of ReNcell VM cells 85
4.4 Time dependency in the differentiation of ReNcell VM cells 89
4.5 The mechanism behind the Wnt-3a effect 90
4.5.1 Wnt pathway dependency 91
4.5.2 Notch pathway dependency 93
4.5.3 BMP pathway dependency 95
4.5.4 JAK/STAT3 pathway dependency 96
4.6 Induced pluripotent stem cell derived neural progenitor cells (iPS-NPCs) 98
4.7 ReNcell VM cells 99
4.8 Outlook 100
5 Summary 102
6 Literature I
7 Appendix I
7.1 ReNcell VM cells I
7.2 iPS-NPCs I
7.3 Efficiency of transfection and lipofection of ReNcell VM cells II
7.4 Generation of pCAGGS-HA-HES vectors II

7.4.1 Generation of pCAGGS-HA-hHES1 II
7.4.2 Generation of pCAGGS-HA-hHES5 III
7.5 Treatment of ReNcell VM cells with Dkk-1 IV

Abbreviations:

%	percent
(R)-SMADs	receptor regulated SMADs
°C	degree Celsius
AD	Alzheimer disease
ADAM	A disintegrin and metalloproteinase
AICAR	5-aminoimidazole-4-carboxamide-1-D-ri-bofuranoside
AKos	Albrecht-Kossel-Institute
AP2	adaptor protein 2
APC	adenomatous-polyposis-coli
ASCL1	Mash1
AXIN2	axin inhibition protein 2
bFGF	basic fibroblast growth factors
bHLH	basic helix-loop-helix
BMP	Bone morphogenetic proteins
bp	base pair(s)
BSA	bovine serum albumin
CADASIL	cerebral autosomal dominant arteriopathy with subcortical infarcts and leukoencephalopathy
CAG	chicken β-actin promoter
CAMKII	calmodulin-dependent kinase II
CBP	CREB binding protein
cDNA	copy DNA
CIAP	calf intestine alkaline phosphatase
CK1α	casein kinase 1α
cLSM	confocal laser scanning microscope
CNS	central nervous system
Co-A	coactivators
Co-R	corepressor
CSL	CBF-1, Suppressor of Hairless, Lag-2
C_t	cycle threshold
d	day(s)
DAAM	Dishevelled-associated activator of morphogenesis 1
DAG	1,2 diacylglycerol
DAPI	4′,6-Diamidin-2-phenylindol
DAPT	N-[N-(3,5-difluorophenacetyl)-L-alanyl]-S-phenylglycine-t-butyl ester

DCC	deleted in colorectal cancer
Dkk1	Dickkopf1
Dll	Delta-like
DMEM	Dulbecco's modified eagle medium
DMSO	dimethylsulfoxide
DNA	desoxyribonucleic acid
dNTP	deoxyribonucleotide
Dvl	Dishevelled
E	embryonic stage
E. coli	*Escherichia coli*
EDTA	ethylendiamin-tetraacetat
EGF	epidermal growth factor
EGFR	epidermal growth factor receptor
EGTA	ethylene glycol tetraacetic acid
ER	endoplasmatic reticulum
ERBB4	v-erb-a erythroblastic leukemia viral oncogene homolog 4
ESC	embryonic stem cells
et al.	et alii
FACS	fluorescence activated cell sorting
FCS	fetal calf serum
Fz	Frizzled
G6PD	Glucose-6-phosphate dehydrogenase deficiency
GAPDH	Glyceraldehyde 3-phosphate dehydrogenase
GFAP	glial fibrillary acidic protein
GFP	green fluorescent protein
GRPs	glial restricted precursors
GSK3	glycogen synthase kinase 3
h	hour(s)
h	human
HA	hemagglutinin-tag
HAT	acetyltransferases
HBSS	Hank`s balanced salt solution
HDAC	histone deacetylase
HEK293H	human embryonic kidney 293H
HES	hairy and enhancer of split
HLH	helix-loop-helix

HSA	human serum albumin
IC	immunochemistry
ICD	intracellular domain
ID	inhibitor of differentiation
IgG	immunoglobulin G
int-1	integration 1
IP3	inositol 1,4,5-triphosphate
iPSCs	induced pluripotent stem cells
IPTG	Isopropyl-β-D-thiogalactopyranosid
JAG	Jagged
JAK	Janus family kinases
JAK-I-1	JAK-Inhibitor 1
JNK	JUN-N-terminal kinase
kDa	kilo Dalton
LB-medium	Luria-Bertani broth medium
LEF	lymphoid enhancing factor
LIF	leukemia inhibitory factor
LRP5/6	LDL receptor-related proteins 5 and 6
m	mouse
MAM	Mastermind
MAPK p38	mitogen-activated protein kinase pathway p38
MASH1	ASCL1
min	minute(s)
Mio	Million
ml	milliliter
mRNA	messenger RNA
MS	Multiple Sclerosis
MSCs	Mesenchymal Stem Cells
MVBs	multivesicular bodies
N-cadherin	neural cadherin
NECD	notch extracellular domain
NFAT	nuclear factor associated with T cells
ng	nanogramm
NICD	Notch intracellular domain
nm	nanometer
NP-40	detergent

NPCs	Neural Progenitor Cells
NSCs	Neural Stem Cells
N^{TM}	Notch transmembrane fragment
PBS	phosphate buffered saline
PCR	polymerase chain reaction
PFA	paraformaldehyde
PIP2	phosphatidylinositol (4,5)-bispho-sphate
PKC	protein kinase C
PLC	phospholipase C
PPIP	phospholipid phosphatidyl inositol 4,5-bisphosphate
PSM	presomitic mesoderm
pSTAT3	phospho-STAT3
PTK7	Tyrosine-protein kinase-like 7
qRT-PCR	quantitative real-time PCR
RAC1	Ras-related C3 botulinum toxin substrate 1
Rap7	receptor-associated protein 7
RHOA	Ras homologous A
RIPA buffer	radioimmunoprecipitation buffer
RNA	ribonucleic acid
ROCK	RHO kinase
ROR	receptor orphan
RYK	transmembrane receptor tyrosine kinase
S1/2/3	cleavage sites1/2/3
S100β	“soluble in 100 % saturated ammonium sulfate solution”
S33Y	stabilized β-catenin
SB21	SB216763
SDS	sodium dodecyl sulfate
sec	second(s)
sFRPs	secreted Fz-related proteins
Shh	sonic hedgehog
siRNA	small interfering RNA
SOX2	RY-related HMG-box gene 2
SRC	non-receptor tyrosine kinase
STAT3	Signal transducer and activator of transcription 3
T705	tyrosine 705 phosphorylation
TAS	Trichostatin A

TCF	T cell factor
TGF-β	transforming growth factor β
TLE	transducin-like enhancer of split
Tuj1	class III β-tubulin
V	Voltage
WB	western blot
wg	wingless
WHO	World Health Organization
Wnt	**w**ingless/i**nt**egration 1
WST	Cell Proliferation Reagent
ZFP423	zinc-finger protein 423
µ	micro

1 Introduction

The neurodegenerative diseases are defined by the European Commission as hereditary and sporadic conditions which are characterized by progressive nervous system dysfunction. They include diseases such as Alzheimer Disease (AD), Degenerative Nerve Diseases, Epilepsy, Stroke, Parkinson Disease, Multiple Sclerosis (MS), Huntington Disease and others. Alzheimer disease is here chosen to illustrate the impact of neurodegenerative diseases on the human society. The World Health Organization (WHO) revealed AD as the fourth highest source of overall disease burden in the high-income countries (WHO statistics, table 13). All these diseases have the degeneration of neuronal cells in common. In addition, injuries can also lead to neuronal deletions. The fact that the capacity for neural regeneration is limited in evolutionarily higher organisms including humans, leads to the requirement of replacement of nerve cells in humans. The replacement of neural cells by stem cells or induced pluripotent stem cells is highly discussed to be an emerging approach to treat neurodegenerative diseases (Steward et al., 2013).

1.1 Stem cells

Stem cells are defined by their ability to self-renew as well as their ability to differentiate into multiple cell types (Zhu et al., 2013), and therefore can serve as a source for cell replacement of damaged neurons. Stem cells are able to self-renew by symmetric division and differentiate by asymmetric cell divisions (Martin-Rendon and Watt, 2003). Stem cells are classified by their potency to develop into other cell types, as totipotent, pluripotent, and multipotent. Totipotent stem cells have the ability to differentiate into every cell type of an organism and are resulting out of a fertilized ovum (zygote) and their daughter cells up to the fourth cell division. Pluripotent cells, for example embryonic stem cells (ESC), have the ability to give rise to all three germ layers: mesoderm, ectoderm and endoderm (Loebel et al., 2003). Multipotent stem cells are cells which are restricted to differentiate into cell types depending on their cell source (Korbing and Estrov 2003).

Traditionally, as a source of neural stem cells for replacement purposes, have served adult stem cells isolated from the hippocampus and subventricular zone (Steward et al., 2013). But due to the low amount of adult stem cells it was needed to establish other stem cell sources, including human embryonic stem cells (hESCs) and human induced pluripotent stem cells (hiPSCs). Especially the method of hiPSC generation is a great breakthrough to improve the

production of mature neuronal cell types from a patient-specific somatic cell source and, therefore, negate the ethical and immune-rejection concerns.

1.1.1 Neural Progenitor Cells

Neural stem cells can divide into neural progenitor cells (NPCs) which are more restricted in their differentiation potential and can be found in the hypothalamus, the dentate gyrus of the hippocampus, the forebrain, the subventricular zone, and the subgranular zone of the dentate gyrus (Temple and Alvarez-Byulla, 1999). They derive out of the neural tube which forms the central nervous system and differentiate due to mesodermal initiated signaling (Kandel et al., 2000). NPCs have the ability to differentiate into neurons which are classified by the expression of the neuronal specific β-tubulin Tuj1 (also known as class III β-tubulin) which is able to heterodimerize with α-tubulins to form microtubules, which are essential components of the cytoskeleton. In addition, differentiating NPCs express HuC/D. Hu proteins are RNA-binding proteins who stabilize specific target mRNAs (Perrone-Bizzozero and Bird 2013). Furthermore, they can differentiate into glial cells, like the myelinating oligodendrocytes which express the surface antigene O4 and into astrocytes, which are positive for the calcium binding protein S100β (Perrone-Bizzozero and Bird 2013).
Differentiation of NPCs is controlled by a multitude of different pathways, which regulate the neurogenesis as well as gliogenesis. Understanding these mechanisms will definitely provide the basis for directing differentiation of human NPCs for clinical applications.

1.1.1.1 ReNcell VM cells

Most of the knowledge how NPCs differentiate is based on murine models. Therefore, the cells of choice for identifying the pathways underlying neuronal differentiation are human neuronal progenitor cells, like the ReNcell VM cells, which have defining properties: self-renewal, human origin, multipotency, fast growth, virtually unlimited availability, and they are suitable for molecular manipulation. These cells have the ability to differentiate into multiple neuronal cell types and make them attractive as powerful tools in research. ReNcell VM cells are a v-myc retrovirally immortalized human cell line and were derived from the ventral midbrain of a 10-week old male fetus (Donato et al., 2007). Recent studies have shown that v-myc induction can enhance the self-renewal of neural progenitors derived from

fetal human brain with no tumorigenic potential either *in vitro* or *in vivo* and creates karyotypically stable cell lines (Kim et al., 2012). This cell line is able to differentiate after 3 days into HuC/D and Tuj1 positive neurons (Morgan et al., 2009; Hübner et al., 2010; Schmöle et al., 2010). Furthermore, proliferating cells express the neuronal marker Nestin (Donato et al., 2007) - an intermediate filament expressed in many neural precursor cells (Lendahl et al., 1990) - and SOX2 (SRY-related HMG-box gene 2; Donato et al., 2007) which is a known transcription factor expressed in neural precursor/stem cells (Episkopou 2005; Jiang et al., 2008). For phase contrast pictures see appendix 7.1.

1.1.1.2 Induced pluripotent stem cell derived neural precursor cells (iPS-NPCs)

By reprogramming somatic cells into pluripotent state using defined transcription factors, Yamanaka´s group provided a new basis for cell replacement therapy using stem cells (Takahashi and Yamanaka, 2006). This method enabled the generation of induced pluripotent stem cells with abilities comparable to that of embryonic stem cells, but without the ethical and immune-rejection concerns. Therefore, the iPSCs are widely used for patient-specific analyzes of different diseases (Ito et al., 2012). Moreover, recently a substantial function of them in pre-clinical models of ischemic brain injury has been revealed (Zhu et al., 2013).
The here used iPS-NPCs were derived via dual SMAD inhibition by using the human iPS cell line hFib2-iPS5 (Park et al., 2008; Trilck et al., 2013). Cells are positive for the stem cell markers Nestin and SOX2, like ReNcell VM cells. In addition, they are able to differentiate into HuC/D positive cells after 18 days of growth factor removal. For phase contrast pictures see appendix 7.2.

1.2 Regulation of the neuronal differentiation

The neural induction starts with the development of the neural plate out of the ectoderm of the blastocyst, which afterwards forms the neural tube. Out of the front part of the neural tube the forebrain and midbrain arise while the hindbrain and the spinal cord resulting out of the back part of the neural tube. Differentiation is initiated by defined temporal sequences from the mesoderm (Kandel et al., 2000). These temporal sequences are widely conserved in vertebrate species (Bayer and Altmann, 1991). Diverse studies have revealed numerous signaling pathways that control the temporal sequences and discovered that the effects on neuronal

progenitor cells are highly dynamic, depending on the stage of development and the local niche (Denham et al., 2009). The main pathways which are regulating the differentiation and analyzed in this work are the Wnt signaling pathway, the Notch pathway, the BMP pathway and the JAK/STAT3 pathway. All of these pathways regulate target genes, representing different basic helix-loop-helix (bHLH) transcription factors. These factors form hetero dimers with ubiquitously expressed bHLH E proteins, such as E12 and E47, through their HLH domain. Hetero dimers bind to DNA through their basic domain and activate the transcription of genes that have E boxes in their promoter region (Hsieh, 2012).

1.2.1 The Wnt pathways

The Wnt signaling pathway plays an important role in the development of the central nervous system. Wnts are required for early patterning by acting as posteriorising signal, for the development of neural progenitor cells, cell proliferation, for cell fate determination, and stem cell renewal (Ciani and Salinas, 2005). Furthermore, the Wnt signaling pathway is substantially involved in neuronal polarization (Habib et al., 2013), neuronal migration, axon guidance, dendrite development, and synapse formation (Inestrosa and Arenas, 2010). Strikingly, the effect of Wnt is strongly depended on time and vicinity, for example it can either induce or repress the growth of human breast cancers depending on molecular pathways which are expressed in the affected cells (Green et al., 2013).

The Wnt pathway is named for its ligands and was discovered more than 30 years ago. Sharma and Chopra described in 1976 *Drosophila melanogaster* mutants that exposed reduced or absent wings and named this gene wingless (wg) (Sharma and Chopra 1976). Later, in 1984 Nusse and Varmus identified the gene int-1, short for integration 1, which induced mouse mammary tumors, which revealed to be a homolog of wg (Nusse et al., 1984). The names were merged into the today well known Wnt. The Wnt ligands are secreted glycoproteins with 19 known family members which are highly conserved among animal species (van Amerongen and Nusse, 2009). Many Wnt proteins are posttranslational modified by glycosylation and palmitoylation as shown for Wnt-3a (Willert et al., 2003, Takada et al., 2006).

A variety of different Wnt signaling pathways is known and on the basis of early studies, they have been classified as either canonical (β-catenin dependent) or non-canonical

(β-catenin independent). However, this classification is not appropriate, due to the fact that various cross talks are known in different cellular contexts (Niehrs, 2012).

The best described pathway is the β-catenin dependent pathway afterwards follows the β-catenin independent pathways; the PCP (planar cell polarity) pathway and the Ca^{2+} pathway. But there are more than 15 different Wnt-receptors and co-receptors, and the specific combination of these together with 19 different Wnt ligands determines the downstream pathway and the effect on the cell, whereas the main part seems to depend on the co-receptor (Figure 1; Niehrs, 2012).

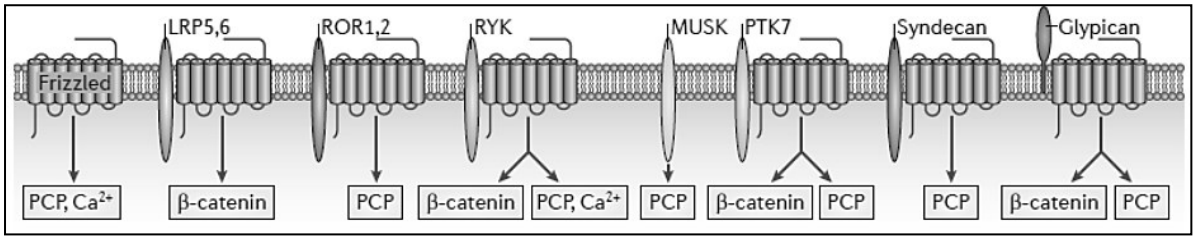

Figure 1: Overview of major Wnt pathways, receptors and co-receptors. PCP= planar cell polarity, LRP= LDL receptor-related proteins, ROR= receptor orphan, RYK= transmembrane receptor tyrosine kinase, MUSK= muscle-specific receptor kinase, PRK7= Tyrosine-protein kinase-like 7 .Diagram from Niehrs, 2012.

Wnt ligands can activate more than one pathway at the same time. For example, Wnt-3a can activate both, the β-catenin dependent pathway and the Ca^{2+} pathway in human articular chondrocytes, with distinct transcriptional targets (Nalesso et al., 2011).

In addition, the Wnt pathways are known to interact with a variety of different other pathways. The glycogen synthase kinase 3 (GSK3) for example has potentially 20 % of all proteins in a cell as substrates and can therefore likely affect plenty of other signaling pathways (Taelmann et al., 2010).

1.2.1.1 The β-catenin dependent pathway

When the β-catenin dependent pathway is not activated, β-catenin is targeted for ubiquitin-mediated proteasome degradation of the E3 ubiquitin ligase complex (Figure 2, A). This targeting is performed by the β-catenin destruction complex, consisting of the scaffold proteins axin inhibition protein (AXIN), adenomatous-polyposis-coli (APC), GSK3, and casein kinase 1α (CK1α). In the active state, this destruction complex is inhibited (Figure 2, B). This leads to an increase of active β-catenin in the cytosol and its translocation into the

nucleus, where it triggers the transcription of Wnt target genes by association with the transcription factor T cell factor/lymphoid enhancing factor (TCF/LEF; Gordon and Nusse, 2006).

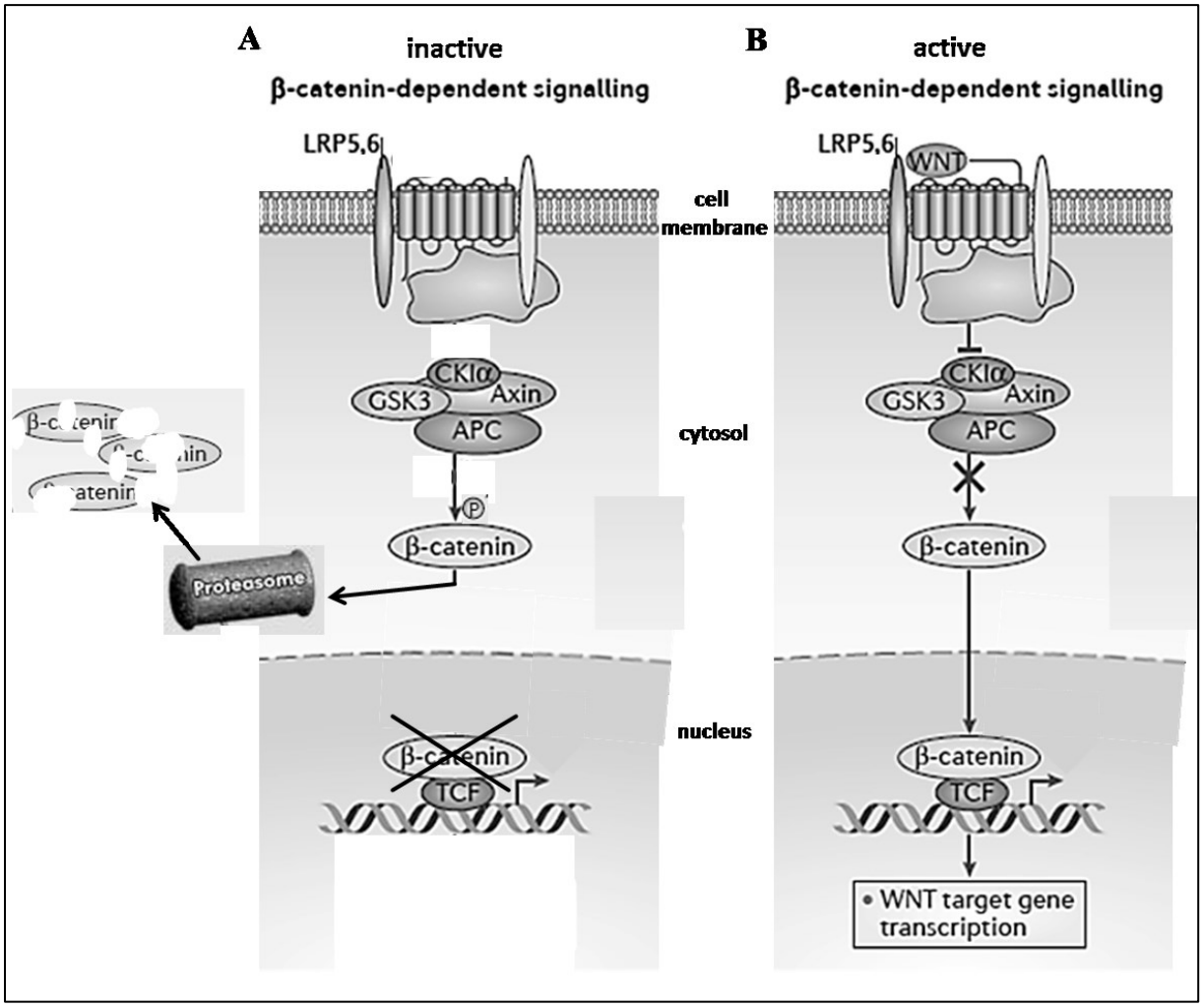

Figure 2: Simplified scheme of the β-catenin dependent Wnt pathway. A: Glycogen synthase kinase 3 (GSK3) phosphorylates β‑catenin, which triggers its degradation. **B**: In the presence of Wnt ligand, the destruction complex (comprising GSK3, CK1α, AXIN and APC) is recruited to the Wnt–receptor complex and inactivated. This allows β‑catenin to accumulate and translocate to the nucleus, where it activates the transcription of target genes under the control of T cell factor (TCF), among others. Modified diagram from Niehrs, 2012.

In detail, Wnt ligands bind to members of the Frizzled (Fz) family of seven transmembrane domain receptors, which are G-protein-coupled receptors (Koval et al., 2011). In addition, Wnts bind to the single-pass transmembrane co-receptors LDL receptor-related proteins 5 and 6 (LRP5/6; He et al., 2004), which results in the phosphorylation of LRP5/6, the activation of cytoplasmatic protein Dishevelled (Dvl) and the production of phosphatidylinositol (4,5)-bisphosphate (PIP2; Pan et al., 2008). Increased PIP2 induces oligomerization and clustering

of LRP5/6, furthermore, it forms a signalosome which recruits AXIN and Axin-bound GSK3 complexes to the cell surface (Zeng et al., 2008 and Tanneberger et al., 2011). This, and the fact that AXIN is the scaffold protein that directly binds to many of the involved components and brings them within close proximity to each other, makes it to the limiting component of the β-catenin destruction complex (Lee et al., 2003). Furthermore, clathrin and adaptor protein 2 (AP2) are required for the formation of LRP6 signalosomes (Kim et al., 2013). Taelman et al., 2010 clearly showed a sequestration of the Wnt induced receptor signaling complex, the signalosom, into multivesicular bodies (MVBs) which are positive for the lysosomal marker Rap7. In addition, they found that GSK3 is sequestered into the lumen of these MVBs, thus blocking its ability to affect its target substrates in the cytoplasm such as β-catenin (Figure 3).

The phosphorylated cytoplasmic domain of LRP6 is able to bind and therefore inhibit the GSK3. This inhibition of the GSK3 activity leads to blocking of the β-catenin phosphorylation which is now able to translocate into the nucleus and bind to the TCF/LEF. TCF binds to the Wnt-responsive element [CCTTTGWW (W can be either T or A)] and starts the expression of the Wnt target genes like AXIN2 (Wu et al., 2009, Hatzis et al., 2008). In addition, there is a verity of studies showing that diverse DNA-binding transcription factors (e.g. SMAD3) bind to β-catenin to activate or repress β-catenin dependent Wnt target genes. Due to the large number of TCF binding sites and numerous transcriptional co-regulators, it is clear that the gene expression may induce dramatic changes in the cell (Cadigan, 2012). In ReNcell VM cells, for example, the treatment of Wnt-3a leads to an induction of AXIN2 (Hübner et al., 2010).

In addition, β-catenin is a constitutively expressed protein connecting cadherin cell adhesion molecules to the cytoskeleton (Aberle et al., 1996). Furthermore, there are evidences which support potential influence of cadherins on Wnt signaling. Some studies demonstrating that proteolytic cleavage of cadherins by proteases such as ADAM10 and presenilin-1 (γ-secretase) is able to release β-catenin and therefore activates transcription of β-catenin dependent Wnt target genes (Reiss et al., 2005, Uemura et al., 2006).

There are plenty of substances which are able to inhibit the β-catenin dependent Wnt pathway. One of the best described is Dickkopf-1 (Dkk-1) which binds the co-receptor LRP5/6 and blocks its interaction with Wnt ligands (Semenov et al. 2001; Mao et al. 2002). Recently, X-ray crystal structure analysis revealed that the extracellular region of LRP6 binds to the C-terminal domain of Dkk1 (Ahn et al. 2011; Cheng et al. 2011). In addition, secreted

Fz-related proteins (sFRPs) are able to bind and sequester Wnt ligands to block their association with Wnt-receptors (Bovolenta et al., 2008). Another way to modulate the β-catenin dependent Wnt pathway is to inhibit GSK3 with a small molecule named SB216763 which was extensively analyzed in our work group (Schmöle et al., 2010).

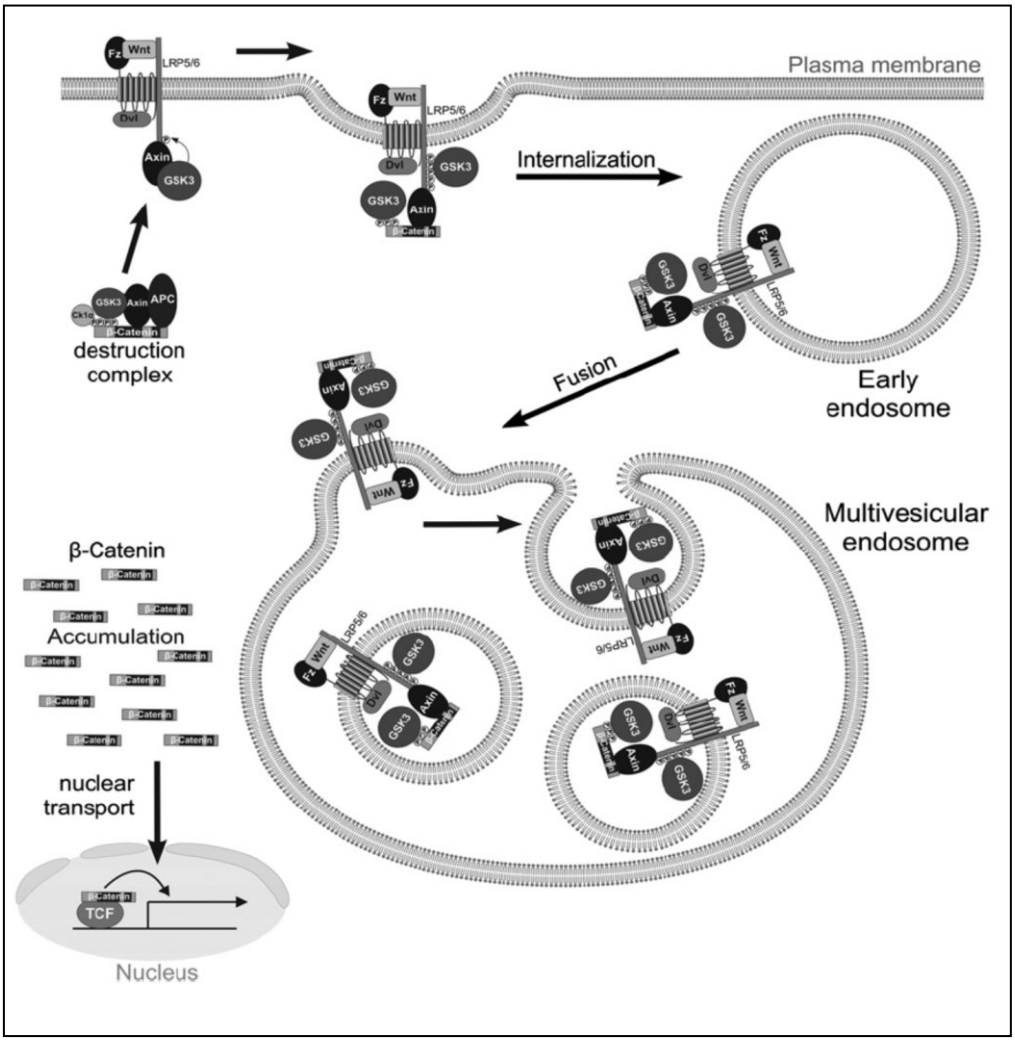

Figure 3: Scheme of the β-catenin dependent Wnt signaling through the sequestration of GSK3 inside MVBs. Binding of GSK3 to the Wnt-receptor complex sequestrates GSK3 inside small intraluminal MVB vesicles, causing its cytosolic substrates such as β-catenin and many other proteins to become stabilized. The initial GSK3 molecules are recruited to the receptor complex bound to Axin, ensuring that the GSK3 fraction bound to the destruction complex is depleted first. Diagram from Taelman et al., 2010.

1.2.1.2 The β-catenin independent pathways

The β-catenin independent pathways are named due to their independency of β-catenin. The best described pathways are the PCP pathway and the Ca^{2+} pathway. In addition, an

increasing number of other pathways are starting to emerge which are named after the specific combination of essential receptor and ligand (e.g. Wnt-5a-ROR-, RYK-Wnt-, PTK7-Wnt-pathways etc.). Increasing evidences suggesting that in vertebrates the PCP and Wnt-5a–ROR signaling pathways substantially overlap (Ho et al., 2012).

The PCP pathway

The PCP pathway is essential for the organization of multicellular structures and tissue remodeling as well as the control of polarized cell migration and coordinated cell movements. The Wnt ligand binds to a combination of Frizzeld and a co-receptor (e.g. ROR or RYK) which leads to an activation of Ras-related C3 botulinum toxin substrate 1 (RAC1) and subsequently of JUN-N-terminal kinase (JNK) which starts the transcription of the PCP target genes (Figure 4). Furthermore, the small GTPase Ras homologous A (RHOA) is activated through activated Dishevelled associated activator of morphogenesis (DAAM), which in turn activate RHO kinase (ROCK) and therefore modulates actin polymerization (Nomachi et al., 2008, Schlessinger et al., 2009). While the RYK dependent PCP signaling can activate the β-catenin dependent signaling (Berndt et al., 2011), the ROR2 dependent signaling inhibits the β-catenin dependent pathway (Winkel et al., 2008). The list of additionally factors which cooperate with the core PCP genes is continually expanding (Dworkin et al., 2011). Furthermore, the γ-secretase can cleave the RYK receptor and induce the target genes of the RYK-Wnt pathway (Lyu et al., 2008).

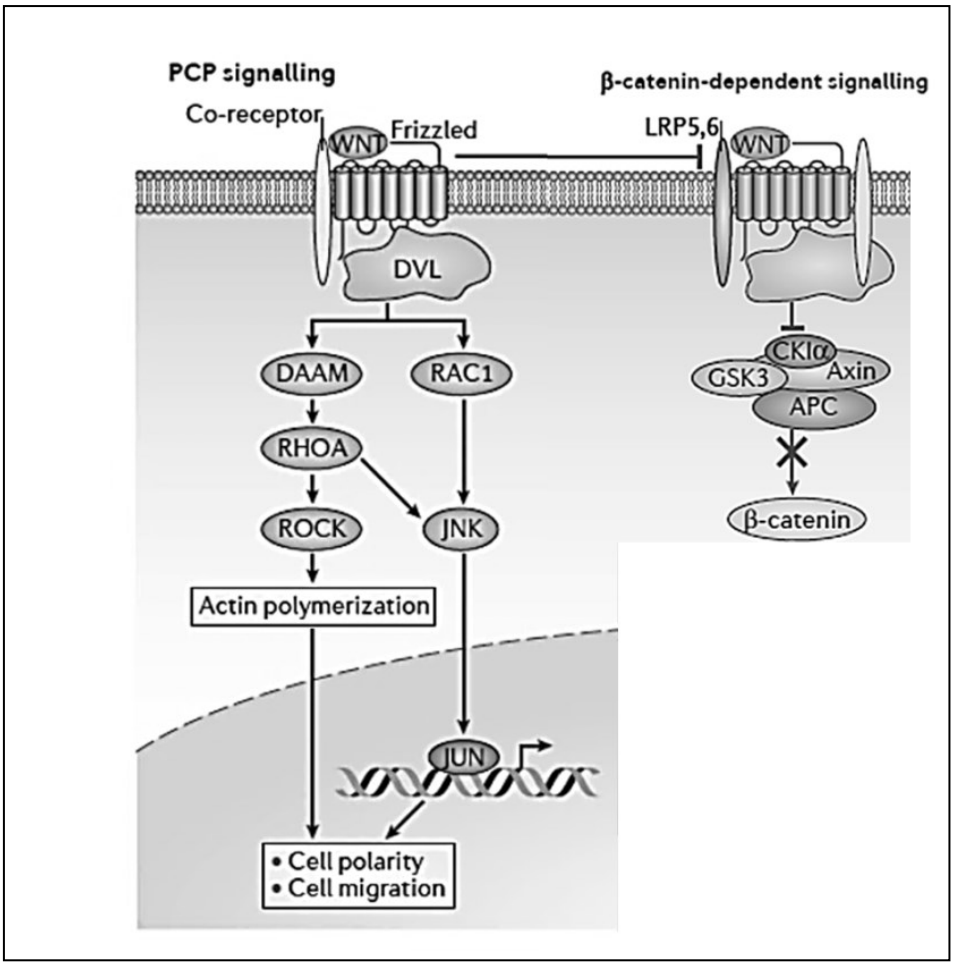

Figure 4: Scheme of the planar cell polarity (PCP) pathway. PCP signaling triggers activation of the small GTPases RHOA and RAC1, which in turn activate RHO kinase (ROCK) and JUN-N-terminal kinase (JNK), respectively, leading to actin polymerization and microtubule stabilization. Diagram from Niehrs, 2012.

The Ca^{2+} dependent pathway

The second β-catenin independent pathway that has been described is the Wnt-Ca^{2+} pathway. Here, the Wnt ligands bind to Frizzled and defined co-receptors (Figure 1) which activate phospholipase C (PLC). Subsequently, this activation leads to a short-lived increase of the intracellular signaling molecules inositol 1,4,5-triphosphate (IP3), 1,2 diacylglycerol (DAG), and Ca^{2+} (Figure 5). This elevation of secondary messengers - which are derived from membrane-bound phospholipid phosphatidyl inositol 4,5-bisphosphate (PPIP) - promotes the release of calcium ions from the endoplasmatic reticulum (ER). The Ca^{2+} release activates calmodulin-dependent kinase II (CAMKII), Calcineurin and protein kinase C (PKC; Kühl et al., 2000). CAMKII and PKC are able to inhibit the β-catenin dependent pathway (De et al., 2011). PKC activates CDC42 subsequently induce actin polymerization. In contrast the

activation of Calcineurin by Ca^{2+} induced the transcriptional regulator nuclear factor associated with T cells (NFAT) and its target genes (Saneyoshi et al., 2002).

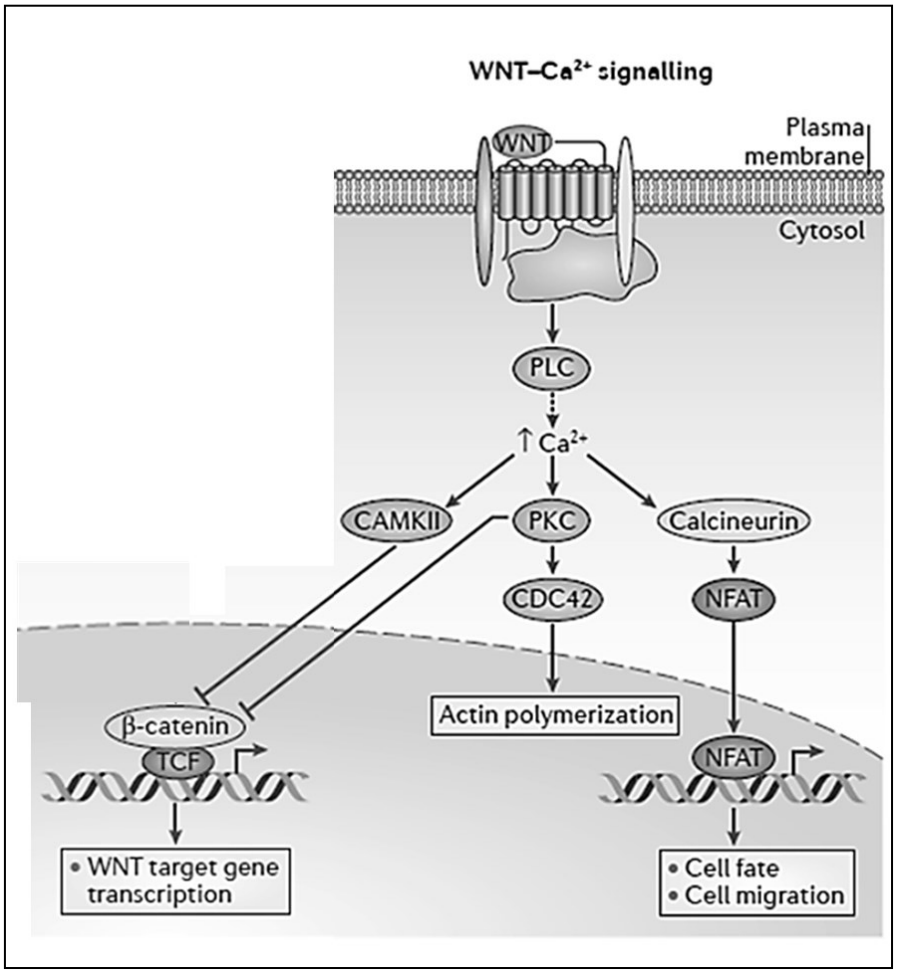

Figure 5: The Wnt- Ca^{2+} pathway. Wnt binding to Frizzeld and co-receptors activates Ca^{2+}- and Calmodulin-dependent kinase II (CAMKII), protein kinase C (PKC) and Calcineurin. Calcineurin activates nuclear factor of activated T cells (NFAT), which regulates the transcription of genes controlling cell fate and cell migration. The Ca^{2+} pathway inhibits β-catenin signaling. Diagram from Niehrs, 2012.

1.2.2 The Notch pathway

The Notch signaling pathway is well known as an important signaling mechanism for communication between neighboring cells which is essential for specification of neuronal identity, division, survival and migration. This pathway plays a major role in the process of the lateral inhibition which regulates the differentiation of an initially homogenous cell population into distinct cell types (Kopan et al., 2009, Kageyama et al., 2009). Furthermore, the Notch pathway is associated with human diseases such as cerebral autosomal dominant

arteriopathy, subcortical infarcts and leukoencephalopathy (CADASIL) and certain cancers (Louvi et al., 2012).

In the Notch signaling pathway are usually two cells involved. One cell expresses the Notch ligands Delta-like (Dll1, 3, and 4) and/or Jagged (JAG1 and JAG2) while the second cell expresses at least one of the four receptors (Notch1–4). The Notch receptor has three cleavage sites (S1, S2, S3). The first cleavage (S1) occurs during maturation and trafficking to the cell surface membrane which converts the notch polypeptide into a heterodimer, composed of the notch extracellular domain (NECD), the transmembrane fragment (N^{TM}) and the intracellular domain (NICD). This Notch receptor is now, upon Dll1 activation, cleaved by ADAM-family metalloproteases at site 2 (S2) which releases NECD. Finally, Notch is cleaved by presenilin proteases of the γ-secretase complex progressively from site 3 (S3) to site 4 (S4; Fortini et al., 2009). The cleaved intracellular domain of the notch receptor (NICD) is released from the cell membrane and translocates to the nucleus, where it associates with the DNA binding protein RBP-Jκ (Figure 6). The transcriptional coactivator Mastermind (MAM) then recognizes the NICD/RBPjκ interface, and this triprotein complex recruits additional coactivators (Co-A) to activate the transcription of Notch target genes. In the absence of NICD, RBP-J may associate with ubiquitous corepressor (Co-R) proteins and histone deacetylases (HDACs) to repress transcription of some target genes (Kopan et al., 2009, Imayoshi et al., 2013).

The best described target genes of the Notch pathway are the HES and related HEY genes which encode a family of basic helix–loop–helix (bHLH) transcriptional repressors. They inhibit the transcription of their target genes, such as MASH1 (ASCL1) and Neurogenins by directly binding to the specific promotor or by dominant negative function on E protein availability, thereby preventing undifferentiated precursor cells from achieving differentiated phenotypes (Kageyama et al., 1997). Among the target genes, HES5 expression has been shown to be mostly dependent on notch signaling. Other notch target genes, including HES1, HES3, and HES7, are also regulated by signaling pathways other than notch signaling (Androutsellis-Theotokis et al., 200; Wall et al., 2009; Niwa et al., 2007). Moreover, the target genes expression oscillates in various cell types, such as fibroblasts, NSCs, and embryonic stem cells (Kageyama et al., 2009). In somitogenesis, they are periodically expressed in a wave-like fashion initiating at the posterior end and moving towards the anterior region of the presomitic mesoderm (PSM), where every wave leads to the generation of a pair of somites (Kageyama et al., 2012).

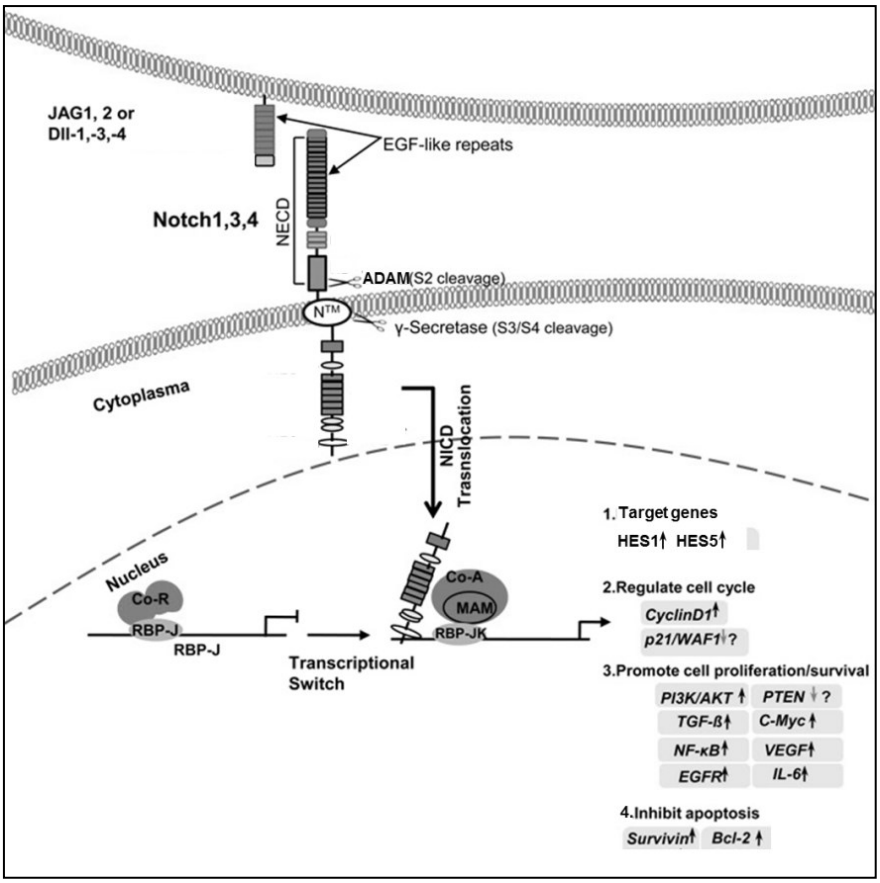

Figure 6: Scheme of the Notch signaling pathway. The Notch receptor is activated by binding to a ligand presented by a neighboring cell. A conformational change, then, exposes site 2 (S2) in Notch for cleavage by ADAM metalloproteases. γ-secretase then cleaves the Notch transmembrane domain progressively from site 3 (S3) to site 4 (S4) to release the Notch intracellular domain (NICD). Subsequently, NICD enters the nucleus where it associates with the DNA-binding protein RBP-Jκ and starts the transcription of the target genes. Diagram from Guo et al., 2011.

The main point in Notch activation is the release of the Notch intracellular domain by cutting the Notch receptor with a γ-secretase. To inhibit γ-secretase activity the small molecule DAPT (N-[N-(3,5-difluorophenacetyl)-L-alanyl]-S-phenylglycine-t-butyl ester) is widely used (Ong et al., 2006, Nelson et al., 2006). But it inhibits not only the release of the Notch intracellular domain but also affects other γ-secretases, which can lead to multifarious ramifications (Bay and Pfaff, 2011). Another approach to inhibit the Notch signaling pathway is the downregulation of the co-transcription factor MAM. In contrast, the transcription factor RBP-J is difficult to efficiently downregulate due to its long protein half-life (Kopan et al., 2009).

1.2.3 The BMP pathway

Bone morphogenetic proteins (BMPs) are members of the transforming growth factor β (TGF-β) superfamily (Miyazono et al., 2010). BMPs were originally described as factors that induce bone formation (Urist, 1965). Meanwhile, they were described to play a role in various cell types and tissues and controlling embryogenesis and the formation and maintenance of the nervous system including dendritic and axonal growth, synapse formation and stabilization etc. (Mehler et al., 1997, Chen et al., 2004).

The BMPs are with 33 members the largest subfamily of the TGF-β superfamily. They are able to signal through a canonical SMAD dependent pathway (TGF-β/BMP ligands, receptors and SMADs) and a non-canonical SMAD independent pathway (e.g. mitogen-activated protein kinase pathway p38, MAPK p38). The specific ligand-receptor combinations to activate these non-canonical pathways and specific signaling outcomes are still in discussion and need to be studied.

In the canonical pathway, the BMPs bind to a heterotetrameric complex of transmembrane receptors known as type I and II serine/threonine kinase receptors (Mueller et al., 2012). A ligand-receptor specific combination of interaction is still in discussion and seems to be cell type dependent (Hinck, 2012). The activation of type I receptors leads to a phosphorylation of receptor regulated (R)-SMADs (SMAD1, 2, 3, 5, and 8) which induce the formation of a multimeric complex composed out of R-SMADs and SMAD4 that translocate into the nucleus where it starts the transcription of BMP target genes (Figure 7; Feng et al., 2005, Hill, 2009). The main target genes of the BMP pathway are the inhibitor of differentiation 1 and 3 (ID1 and ID3) which are HLH transcription factors. They lack the basic region which makes them unable to bind to DNA but dimerization of IDs with other bHLH leads to an inhibition of the DNA binding ability of the bHLH transcription factors (Norton, 2000). Moreover, IDs not only inhibit transcriptional function but also promote the degradation of neurogenic bHLH by sequestering ubiquitous E proteins (Vinals et al., 2004). Takizawa et al. (2003) described that ID and HES play a major role in the negative effects of BMPs on differentiation of neuronal precursors.

There are several known molecules which are able to inhibit the BMP pathway. The most frequent used is Noggin which binds to the BMP ligand and therefore impairs the binding to the receptor and inhibits the SMAD1, 5, 8, and MAPK p38 (Yu et al., 2008). The compound C (Dorsomorphin) is a potent inhibitor of AMP-activated protein kinase (AMPK) and inhibits BMP4 induced signaling and does not affect MAPK p38 (Yu et al., 2008). The small

molecule SB431542 inhibits ALK1 as well as ALK7 and therefore SMAD2 and 3 (Inman and Hill, 2002). In addition, the inhibitory SMADs, SMAD6 and SMAD7, block BMP signaling by preventing phosphorylation of R-SMADs by binding to active receptor complexes (Derynck and Zhang, 2003). Another known mechanism is the degradation of SMADs through the ubiquitin proteasome pathway or by mitogen-activated protein (MAP) kinase and GSK3 phosphorylation (Wicks et al., 2006, Fuentealba et al., 2007).

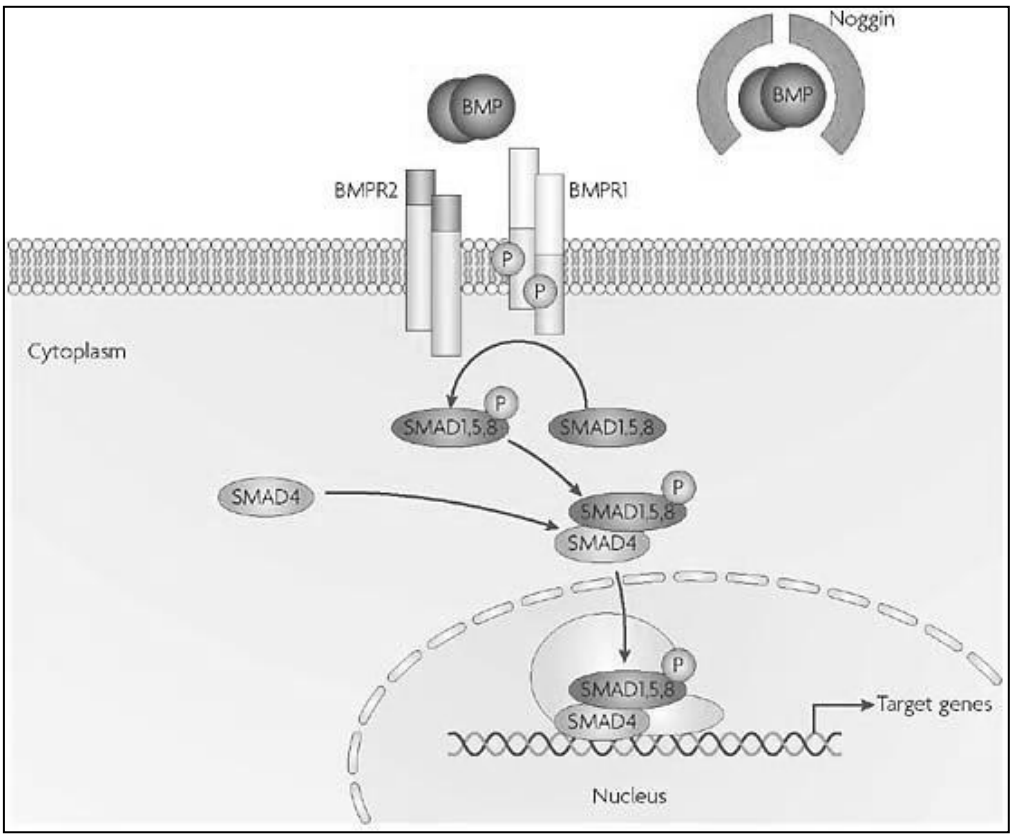

Figure 7: Simplified scheme of the BMP pathway. BMP ligands bind to the BMP receptors BMPR1 and BMPR2. Phosphorylated BMPR1 subsequently phosphorylates SMAD1, SMAD5 and SMAD8, which associate with SMAD4 and enter the nucleus, where they regulate gene expression. The BMP signal can be blocked by extracellular antagonists, such as Noggin, which bind BMP ligands and prevent their association with the BMP receptors. Diagram from Hardwick et al., 2008.

Moreover, BMPs were described to promote astrocytic differentiation together with leukemia inhibitory factor (LIF) by activating astrocyte specific promotors through a STAT3-p300/CBP-SMAD1 complex (Nakashima et al., 1999). Scholl et al. (2012) revealed that the ability of BMPs and STAT3 to promote astrogliogenesis dependends on the histone acetylation/deacetylation machinery. This machinery regulates the chromatin structure and therefore is essential for the regulation of gene transcription. Chromatin is dynamically

regulated through a variety of mechanisms and enzymes including the histone acetyltransferases (HAT) and deacetylases (HADAC). This will finally lead to an open or closed nucleosomal DNA structure and therefore enables transcription factors to bind to promotors and regulate transcription. The inhibiton of HDAC by TSA (Trichostatin A) leads to an increase of STAT3 levels (Scholl et al., 2012), which in turn regulates together with BMP the astrogliogenesis (Nakashima et al., 1999).

In addition, the BMP pathwaywas described to affect plenty of different other pathways and proteins, for example HES5 (Nakashima et al., 2001) and SMAD was discovered to interact with Dvl-1 in mouse MSCs (Liu et al., 2006). Moreover, Masserdotti et al. (2010) revealed that the zinc-finger protein ZFP423 triggers a cooperative interaction between NICD and the SMAD complex, which leads to a strong activation of HES5. Finally, AXIN can facilitate TGF-β signaling by presenting SMAD3 to the type I TGF-β receptor (Furuhashi et al., 2001).

1.2.4 The JAK/STAT3 pathway

Signal transducer and activator of transcription 3 (STAT3) belongs to a family of seven transcription factors which are able to modulate a variety of biological processes like cell growth, inflammation, embryological development, and axonal regeneration in the spinal cord (Qiu et al., 2005).

STAT3 is activated in response to growth factors, cytokines, and hormones. Binding of these ligands to the epidermal growth factor receptor (EGFR) activates Janus kinase (JAK), which phosphorylates STAT3 at tyrosine 705 (Figure 8). This phosphorylation leads to a dimerization and translocation of STAT3 into the nucleus where the dimer is able to trigger STAT3 target genes Bcl-xL, cyclin D1, c-myc, Twist and Survivin (Dziennis and Alkayed, 2008). Another mechanism of STAT3 activation is the phosphorylation by non-receptor tyrosine kinases such as SRC and activation by G-protein coupled receptors (Ram and Iyengar, 2001). The STAT3 signaling can be inhibited through an inhibition of JAK e.g. the substance JAK-Inhibitor 1 which inhibits the phosphorylation of STAT3 by JAK (Pedranzini et al., 2006). In contrast, the activation and translocation of STAT3 can be activated with the small molecule 5-aminoimidazole-4-carboxamide-1-D-ri-bofuranoside (AICAR; Zang et al., 2008).

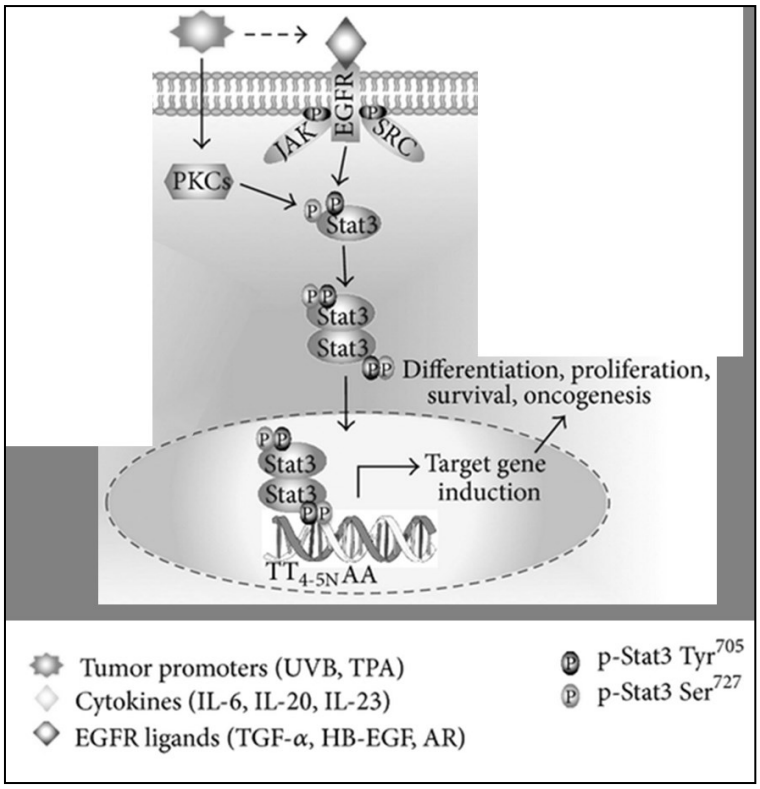

Figure 8: Scheme of the JAK/STAT3 pathway. STAT3 is activated downstream of receptor tyrosine kinases (e.g., EGFR), cytokine receptors via associated Janus family kinases (JAKs). Transcriptional induction of cytokines and EGF ligands can lead to autocrine stimulation and sustained STAT3 phosphorylation. After phosphorylation, STAT3 dimerizes and translocates to the nucleus, where STAT3 dimers directly regulate gene expression of transcriptional targets including Bcl-xL, cyclin D1, c-myc, Twist and Survivin. Diagram from Macias et al., 2013

1.3 Aim of the study

Hübner et al. (2010) demonstrated the induction of the β-catenin dependent Wnt pathway by treatment of Wnt-3a and transfection with Wnt-3a as well as stabilized β-catenin overexpression plasmid in the human neural progenitor cell line (ReNcell VM). However, only Wnt-3a but not overexpression of stabilized β-catenin led to an increase of neuronal differentiation as judged by HuC/D and Tuj1 positive cells. In addition, pharmacological inhibition of Notch signaling in these cells resulted in increased neuronal differentiation suggesting an important role for the Notch pathway in controlling neuronal differentiation. Moreover, further studies revealed that Wnt-3a, in contrast to stabilized β-catenin, was able to modulate Notch target genes HES1/HES5 and GFAP in ReNcell VM cells (Rayk Hübner, personal communication). These data pointed out a mechanism by which Wnt-3a independently of β-catenin increases neuronal differentiation, which may be based on Notch target gene modulation.

Therefore the aim of this study was at first to verify the active Notch pathway in differentiating ReNcell VM cells by pharmacological inhibition with DAPT. The differentiating cells should be treated with DAPT and analyzed via FACS to detect the amount of cells positive for the glial marker GFAP, S100β and neuronal marker Tuj1 and HuC/D, and by qRT-PCR to analyze the mRNA levels of the Notch target genes HES1 and HES5 as well as the neurogenic MASH1 and the glial marker GFAP. This will, in addition, reveal the importance of the Notch pathway in the differentiation of ReNcell VM cells. The detection of the mRNA levels will be useful due to the fact that there are no post-translational modifications known which would regulate these genes independent of their mRNA levels. In contrast, the activation of the Notch pathway by overexpression of the Notch intracellular domain 1 (NICD1) should prove through a rescue experiment the Notch dependency of DAPT and simultaneously emphasize the importance of Notch in the differentiation of human neural progenitor cells.

The second step is to verify the effect of Wnt-3a on Notch target genes HES1 and HES5 by treatment of ReNcell VM cells with recombinant Wnt-3a and to extend the analysis by detecting the mRNA levels of MASH1 and GFAP. Furthermore, the effect of Wnt-3a on the amount of the cells for the marker Tuj1, HuC/D, S100β and GFAP should be measured via FACS. Due to the fact that Wnt-3a as well as DAPT are able to reduce HES5 and affect the differentiation of neural progenitor cells, it will be analyzed if this effect is additive. In addition, the time dependency of this effect should be further evaluated by analyzing time points between 1 and 72 hours of differentiation and by determining the time frame where progenitor cell differentiation can be modulated by Wnt-3a and other substances.

Because we found Wnt-3a to regulate HES genes independent of β-catenin it was the aim of this study to reveal the underlying mechanism. Therefore, it should be investigated if upstream proteins of the β-catenin dependent pathway are involved in the Wnt-3a effect. Single components of the Wnt pathway should be inhibited through specific inhibitors to analyze their impact in the differentiation. SB216763 should be used to inhibit GSK3, Dkk-1 to inhibit Wnt-3a - LRP5/6 interactions and sFRP1 to impair the connection between Frizzled and Wnt. The inhibition of these interactions will reveal if they are essential for the effect of Wnt-3a. In addition, the dependency of the Wnt-3a effect on single Notch pathway components should be determined by overexpression of NICD1, HES1 and HES5 in order to reveal their importance for the Wnt-3a effect and for the differentiation of ReNcell VM cells.

Moreover, other pathways should be analyzed which potentially might link Wnt-3a and the modulation of Notch target genes. It was, for example, hypothesized that Wnt-3a may act via inhibition of BMP. To assess that possibility, it should be analyzed whether inhibition of this pathway using Noggin, Dorsomorphin and SB431542 is able to mimic the Wnt-3a effect. Since SMAD1 is known to modulate together with STAT3 the level of GFAP (Nakashima et al., 1999), on this account, a potential modulation of the STAT3 activity should be assessed via western blot analysis. For analysis of the JAK/STAT3 pathway in ReNcell VM cells the pSTAT3 activator AICAR and inhibitor Jak-Inhibitor-1 should be investigated. If an active JAK/STAT3 pathway is detectable, nuclear pSTAT3 in Wnt-3a and DAPT treated cells should be quantified.

Moreover, to rule out the possibility that the observed Notch modulations and the effect on neuronal differentiation are not strictly a cell-type specific phenomenon a second, neural cell system based on iPS cells should be utilized.

2 Materials and Methods

2.1 Materials

2.1.1 Technical equipment

Table 1: Technical equipment

Type	Name	Supplier
agarose gel chamber	Mini-SubII	Bio-Rad
balance	MCBA 100	Sartorius
cell counter	CASY	Innovatis
cell culture microscope	Eclipse TS100	Nikon
centrifuge	Z383K	Hermle
centrifuge	Z233MK-2	Hermle
centrifuge	Universal 30 RF	Hettich
centrifuge	Microfuge 16	Beckman Coulter
centrifuge	Avanti J-25	Beckman Coulter
FACS	FACSCalibur	Becton Dickenson
fluorescence microscope	Biozero	Keyence
fluorescence microscope	Eclipse TS200	Nikon
gel documentation camera	C-5050	Olympus
gel documentation system	TransilluminatorBioview	biostep
heating block	Thermomixer	eppendorf
incubator	WTC	Binder
incubator	T6	Heraeus
nucleofector	NucleofectorII	Amaxa
PCR-Cycler	GeneAmp9700	ABI
PCR-Cycler	Mastercycler	eppendorf
pH-meter		Mettler Toledo
pipets	Reference	eppendorf
plate reader	Magellan	Tecan
power supplies	PowerPacHC	Bio-Rad
real-time PCR Cycler	LightCyclernano 1.0	Roche

SDS-PAGE chamber	Criterion	Bio-Rad
semi-dry transfer chamber	Trans-Blot SD	Bio-Rad
shaker	KM-2Akku	Edmund Bühler
shaker	K2-50	Noctua
shaker	Titramax 100	Heidolph
spectrophotomteter	Ultrospec3100pro	Amersham
sterile working bench	Antares 48	Sterile
vortexer	MS1	IKA
water bath	AL12	Lauda

2.1.2 Software

ArgusX1

BioEdit (http://www.mbio.ncsu.edu/BioEdit/bioedit.html)

BLAST (http://www.ncbi.nlm.nih.gov/BLAST/)

CellQuest Pro (BD Biosciences)

GIMP 2 (www.gimp.org)

Microsoft Office 2010

Vector NTI Advance 11

NCBI database (http://www.ncbi.nlm.nih.gov/)

MultAlin (http://multalin.toulouse.inra.fr/multalin/)

Reverse Complement tool (http://www.bioinformatics.org/sms/rev_comp.html)

2.1.3 Consumables

Table 2: Consumables

Type	Size/Specification	Supplier
bacteria culture tubes	15 ml	Falcon
bacteria culture plates	9 cm	Greiner
cell culture pipets	5,10, 25 ml	Greiner
cell culture plasticware	96-,48-,24-,6-well,T-75	Greiner
cell culture plasticware	48-,24-,6-well	Sarstedt
cell culture plasticware	4-well	Nunc

FACS tubes	5 ml	Falcon
gloves	nitrile	Kimberly-Clark
LightCycler strips		Roche
nitrocellulose membrane	Hybond-ECL	Amersham
PCR reaction tubes	0.2 ml	Biozym
pipet tips	10, 100, 1000 µl	Eppendorf, Biozym, Sarstedt
reaction tubes	1.5, 2 ml	Eppendorf, Sarstedt
reaction tubes	15, 50 ml	Falcon, Sarstedt
sterile filter units	0.22 µM	Millipore
Whatmanpaper	58x58 cm	Schleicher und Schüll

2.1.4 Chemicals

Often used chemicals were purchased with „pro analysis“ grade and were supplied if not otherwise stated by Calbiochem, Fluka, Merck, Sigma and Roth.

Table 3: Buffers and solutions

Type	Compostion / Supplier
Buffers for agarose gel electrophoresis	
6x DNA loading dye	fermentas
50x TAE	2 M Tris-HCl, pH 8.0, 1 M acetic acid, 50 mM EDTA
Lysis buffers for cell extracts	
RIPA buffer (radioimmunoprecipitation buffer)	20 mMTris pH 7.4, 137 mMNaCl, 0.1% SDS, 0.1 % sodiumdesoxycholate, 1 % Triton X-100, 10 % glycerol, 2 mM EDTA, 1 mM EGTA, 1 mMNaF, 20 mM sodiumpyrophosphate plus protease and phosphatase inhibitor cocktail (Roche)
Solutions for western blot	
5x Sample buffer	50 mMTris, 2 % SDS, 5 % glycerol, 5 % β-mercaptoethanol, 0.2 mg/ml bromphenol

	blue
10x SDS electrophoresis buffer	250 mM Tris, 188 mM glycine, 3.5 mM SDS
SDS Transfer buffer	48 mM Tris, 39 mM glycine, 3.5 mM SDS, 20 % methanol
Blocking solution	TBST with 2 % or 5 % BSA (Roth)
Blocking solution	TBST with 5 % skim milk powder (Sigma)
TBS	20 mM Tris-HCl, 150 mM NaCl, pH 7.6
TBST	TBS with 0.1 % Tween 20
Solutions for FACS analysis and immunocytochemistry	
PBS (w/o Mg, Ca)	Biochrom
FACS fixing solution	1 % PFA in PBS
FACS saponin buffer	0.5 % BSA, 0.5 % saponin, 0.02 % NaN_3 in PBS
FACS wash buffer	0.5 % BSA, 0.02 % NaN_3 in PBS
IC blocking buffer	5 % normal goat serum, 0.3 % Triton-X100 in PBS
IC antibodyincubationbuffer	1 % normal goat serum in PBS
Mounting medium with DAPI	VectaShield

Table 4: Kits

Type	Supplier
BCA Protein Assay Kit	Pierce
Endo-Free Plasmid Maxi Kit	Qiagen
FastLane cDNA Kit	Qiagen
GFX purification Kit	GE healthcare
Nucleofection Kit V	Lonza
T4 DNA Ligase Kit	Promega
ZYPPY Plasmid Mini Kit	Zymo Research

2.1.5 Antibodies

Antibodies for FACS analysis, immunocytochemistry or western blot.

Table 5: Primary antibodies

Target	Type	Company	Application	Dilution
β-actin	mouse monoclonal IgG_1	Sigma (AC-15)	WB	1:10.000
Tuj1	mouse monoclonal IgG_1	Santa Cruz (sc-51670)	FACS, IC	1:100 1:500
Flag-tag	mouse monoclonal IgG_1	Sigma (F1804)	WB	1:10.000
GAPDH	mouse monoclonal IgG_1	Abcam (ab8245)	WB	1:10.000
GAPDH	rabbit polyclonal IgG	Santa Cruz (FL-335)	WB	1:1000
GFAP	rabbit polyclonal IgG	Dako (Z0334)	FACS, IC, WB	1:500
HuC/D	mouse monoclonal IgG_1	Invitrogen (A-21271)	FACS	1:100
HES5	rabbit polyclonal IgG	Lifespan Biosciences (LS-C136917)	WB	1:1000
HES1	rabbit polyclonal IgG	abcam (ab71559)	WB	1:1000
Lamin A/C	mouse monoclonal IgG_1	BD (612162)	WB	1:1000
pGSK3β (Ser9)	rabbit polyclonal IgG	Cell Signaling (9336)	WB	1:1000
pSTAT3 (Tyr705)	rabbit monoclonal IgG	Cell Signaling (9139)	WB	1:2000
S100β	rabbit polyclonal IgG	Dako (Z0311)	FACS, IC	1:500
STAT3	mouse monoclonal IgG_{2a}	Cell Signaling (9145)	WB	1:2000
HA-tag	mouse monoclonal IgG_1	Cell Signaling (6E2)	WB	1:10.000
negative control	normal mouse IgG	Santa Cruz (sc-2025)	FACS, IC	1:100
negative control	normal rabbit IgG	Santa Cruz (sc-2027)	FACS, IC	1:100
NICD1 (Val1744)	rabbit monoclonal IgG	Cell Signaling (4147)	WB	1:1000

non-phospho-β-catenin (Ser33/37/Thr41)	rabbit polyclonal IgG	Cell Signaling (4270)	WB	1:1000

Table 6: Secondary antibodies

Target	Host	Conjugate	Company	Application	Dilution
rabbit IgG	goat	Alexa Fluor 680	Invitrogen (A-21076)	WB	1:10.000
mouse IgG	goat	Alexa Fluor 680	Invitrogen (A-21057)	WB	1:10.000
rabbit IgG	goat	IRDye 800	Rockland (611-131-122)	WB	1:10.000
mouse IgG	goat	IRDye 800	Rockland (610-131-003)	WB	1:10.000
mouse IgG	goat	Alexa Fluor 488	Invitrogen (A11029)	FACS, IC	1:1000
rabbit IgG	goat	Alexa Fluor 647	Invitrogen (A21245)	FACS, IC	1:1000

2.1.6 Oligonucleotides

Oligonucleotide sequences were from references if indicated and were obtained from MWG Biotech AG or from Qiagen. Stock solutions (100 µM) of primers in water were stored at -20 °C.

Table 7: Oligonucleotides for sequencing

Name	Purpose	Sequence 5'-3'
T7_fw	Sequencing of pcDNA3.1/HisA / pGEM-T easy	TAATACGACTCACTATAGGG
SP6_rc	Sequencing of pcDNA3.1/HisA / pGEM-T easy	ATTTAGGTGACACTATAG
pCAGGS-fw	Sequencing of pCAGGS	TTCCTACAGCTCCTGGGCAACG
pCAGGS-rc	Sequencing of pCAGGS	TCAGATGCTCAAGGGGCTTC

Table 8: Oligonucleotides for cloning

Target name	Purpose	Forward primer sequence 5'-3' *Reverse primer sequence 5`-3`*	Annealing temperature
hHES1	pCAGGS-hHES1	tctcgagttgaccaccATGCCAGCTGATATAATGGAGAAAAAT *AGCCAGGGCATTGGTTATCAGTTCCGCCACGG*	64,2 °C
hHES1	pCAGGS-HA-hHES1	tctcgagttgaccaccATGggctacccatatgatgttccagattacgctCCAGCTGATATAATGGAGAAAAAT *AGCCAGGGCATTGGTTATCAGTTCCGCCACGG*	51,6 °C
hHES5	pCAGGS-hHES5	tctcgagttgaccaccATGGCCCCCAGCACTGTG *AGCCAGGGCATTGGTTATCACCAGGGCCGCC*	64,2 °C
hHES5	pCAGGS-HA-hHES5	TctcgagTTGACCACCATGGGCTACCCATATGATGTTCCAGATTACGCTGCCCCCAGCACTGTG *AGCCAGGGCATTGGTTATCACCAGGGCCGCC*	64,2 °C

ctcgag = *Xho*I restriction site
ccannnnnntgg = *Bst*XI restriction site

Table 9: Oligonuclrotides for quantitative real-time PCR

Gene name	Annealing temp.	Ampliconlenght [bp]/melting temp. [°C]	Forward primer sequence 5'-3' *Reverse primer sequence 5'-3'*	Reference
hAXIN2	55 °C	202/86	AGTCAGCAGAGGGACAGGAA *AGCTCTGAGCCTTCAGCATC*	Hübner 2010
hG6PD	55 °C	191/88	ATCGACCACTACCTGGGCAA *TTCTGCATCACGTCCCGGA*	http://medgen.ugent.be/rtprimerdb/ ID: 1031
hGFAP	55 °C	158/84	CGATCAACTCACCGCCAACA *GTGGCTTCATCTGCTTCCTGTC*	Böhm et al., 2003
hHES1	60 °C	100/88	proprietary	Qiagen, Cat. No. QT00039648
hHES5	55 °C	232/90	TCAGCCCCAAAGAGAAAAAC *TAGTCCTGGTGCAGGCTCTT*	Chen et al., 2006

hID1	55 °C	127/86	proprietary	Qiagen, Cat. No. QT00230650
hID3	55 °C	101/86	proprietary	Qiagen, Cat. No. QT01673336
hMASH1	55 °C	66/55	proprietary	Qiagen, Cat. No. QT00237755

2.1.7 Vectors

Table 10: Cloning-, reporter and -expression vectors

Name	Insert / total size [bp]	Properties	Reference
pCAGGS	4790	P_{CAG}	J. Luo, AKos
pCAGGS-HES1	984/4790	hHES1	this work
pCAGGS-HES5	525/4790	hHES5	this work
pCAGGS-HA-HES1	1011/4790	hHES1 tagged N-terminally with HA-Tag	this work
pCAGGS-HA-HES5	552/4790	hHES5 tagged N-terminally with HA-Tag	this work
pCAGGS-GFP	723/5534	mutGFP, P_{CAG}	J. Luo, AKos
pCAGGS-NICD1	2500/4790	mouse notch intracellular domain 1	Addgene 26891
pCAGGS-mS33Y β-catenin-HA	2387/7178	mS33Y β-catenin tagged C-terminally with HA-Tag	Hübner et al., 2010
pCAGGS-mWnt3a-HA	1116/5842	mWnt-3a tagged C-terminally with HA-Tag	Hübner et al., 2010
pGEM-T easy	3015	cloning vector, blue/white screening	Promega

pCMV6-XL4-HES1	4700	hHES1	Origene SC301536
pCMV6-XL4-HES5	4700	hHES5	Origene SC116707
pmaxGFP	3486	P_{CMV}, maxGFP	Amaxa

2.1.8 Enzymes

Enzymes (polymerases, restriction enzymes, ligases, phosphatases) were purchased from Promega, New England Bioloabs, Fermentas, Stratagene and Qiagen.

2.1.9 Bacterial strains and media

As host bacterium the *E. coli* K12 derived strain JM109 with genotype e14–(mcrA–) *recA1 endA1 gyrA96 thi-1 hsdR17* ($r_K^- m_K^+$) *supE44 relA1* Δ(*lac-proAB*) [F′ *traD36 proABlacI*^{q}*ZΔM15*] (Promega) was used.

Table 11: Bacterial media

Type	Supplier	Composition
LB-medium	Roth	15 g/l H_2O, autoclave
LB-agar	Roth	25 g/l H_2O, autoclave

If needed for selection, 100 µg/ml ampicillin (Roth) or 25 µg/ml kanamycin (Roth) were added after autoclaving. For blue/white screening, 1 mM IPTG (Roth) and X-Gal (Invitrogen) were added after autoclaving.

2.1.10 Cell lines and media

Table 12: Eukaryotic cell lines and media

Line	Type	Proliferation medium	Reference
HEK293H	human embryonic kidney	DMEM 4.5 g/l glucose 10 % FCS 1x Pen/Strep	Invitrogen
ReNcell VM	human ventral-midbrain derived neural precursor cells, v-myc immortalized	DMEM/F12 10 ng/ml bFGF 20 ng/ml EGF 2 mMGlutaMax, 1xB27, 10 U/ml heparin sodium salt, 50 µg/ml gentamycin	ReNeuron/Millipore
iPS-NPC	iPS-derived Neural progenitor cells (Human iPS cell line hFib2-iPS5; Park et al., 2008)	DMEM/F12; Neurobasal Medium 1:1 1x N2 supplement 1x B27 2 mMGlutaMax, 0,25x Pen/Strep 10 ng/ml bFGF/EGF	Derived from hFib2-iPS5; (Park et al., 2008) NPCs derived by: Dr. R. Hübner as described (Trilck et al., 2013)

2.1.11 Cell culture media, buffers and supplements

Table 13: Culture media and buffers

Type	Supplier
B27	Invitrogen
Benzonase	Merck
bFGF	Roche/ GlobalStem
DMEM (Dulbecco`s Modified Eagle Medium) 4.5 g/l glucose	Invitrogen
DMEM/F12	Invitrogen
EGF	Roche

FCS (fetal calf serum)	Invitrogen
Gentamycin	Invitrogen
HBSS (Hank`s balanced salt solution)	Invitrogen
heparin sodium salt	Invitrogen
HSA (human serum albumin)	OctaPharma
mouse laminin	Trevigen
N2	Invitrogen
Neurobasal medium	Invitrogen
noggin Fc- chimera	R&D
normal goat serum	Invitrogen
Pen/Strep 100x	PAA
Poly-D-ornithine	Sigma
Poly-L-ornithine	Sigma
Trypsin/Benzonase solution	25 U/ml Benzonase in Trypsin-EDTA
Trypsin/EDTA	Invitrogen
Trypsin-Inhibitor	Sigma
Trypsin-inhibitor/Benzonase	1 % HSA , 25 U/ml Benzonase, 0,55 mg/ml trypsin-inhibitor in DMEM/F12

If not dissenting indicated supplements were used with following concentrations.

Table 14: Supplements

Substance	Solvent	Stock Solution	End Solution	Supplier
AB199 (IM12)	DMSO	10 mM	3 µM	M. Beller, LIKAT
AICAR	H_2O	250 mM	1 mM	Santa Cruz
DAPT	DMSO	10 mM	5 µM	Sigma
DMSO		100 %	depending on compared substance (0,2 % -4 %)	Sigma
Dorsomorphin	DMSO	10 mM	1 µM	Sigma
HSA	PBS	0,1 %	0,001 %	OctaPharma
Jak-Inhibitor-1	DMSO	1 mM	1 µM	Santa Cruz
recombinant	HSA	100 µg/ml	400 ng/ml	R&D

human Dkk1				
recombinant human Noggin	PBS	250 µg/ml	500 ng/ml	R&D
recombinant human sFRP1	HSA	100 µg/ml	500 ng/ml	R&D
recombinant mouse Wnt-3a	HSA	100 µg/ml	100 ng/ml	R&D
SB216763	DMSO	10 mM	3 µM	Sigma
SB431542	DMSO	10 mM	20 µM	Sigma

2.2 Methods

2.2.1 Cell culture

2.2.1.1 Cultivation of ReNcell VM cells

ReNcell VM cells were initially provided by ReNeuron (Guildford, UK) and are distributed now from Millipore (Billerica, USA). It is a v-myc retrovirally immortalized human cell line and was derived from the ventral midbrain of a 10-week old male fetus. The cells were cultivated in cell culture flasks at 37 °C with 5 % CO_2 and 20 % O_2. For growing as adherent monolayers cell culture flasks needed to be coated with Laminin (10 µg/ml). For coating it was diluted 1:100 in ice-cold DMEM:F12 and incubated with culture plastic ware for at least one hour at 37 °C. Laminin was removed by washing with pre-warmed DMEM:F12. Cells were cultivated in proliferation medium and passaged when reaching around 70 % confluence. Therefore, cells were washed with pre-warmed HBSS and incubated with Trypsin/Benzonase until detaching. Reaction was stopped by adding Trypsin inhibitor/Benzonase. The suspension was centrifuged for 5 min at 100 x g at room temperature. The supernatant was discharged and the cell pellet was resuspended in pre-warmed proliferation medium. A defined number (Table 15) of cells were seeded in Laminin coated culture vessels.
Differentiation was induced by withdrawal of growth factors. Therefore, cells were washed with pre-warmed HBSS and incubated with differentiation medium at 37 °C for up to 3 days. ReNcell VM cells are able to differentiate into neurons, astrocytes and oligodendrocytes (Donato et al., 2007, Hübner et al., 2010 and Morgan et al., 2010).

2.2.1.2 Cultivation of HEK293H

HEK293H cells were grown as adherent monolayers at 5 % CO_2, 20 % O_2 at 37 °C and were passaged when reaching around 80 % confluence. Cells were washed with pre-warmed PBS (Biochrom) and incubated with Trypsin/EDTA (Invitrogen) until detaching. Reaction was stopped by adding medium. The suspension was centrifuged for 5 min at 100 x g at room temperature. The supernatant was discharged and the cell pellet was resuspended in pre-warmed medium. A defined number (Table 15) of cells were seeded in culture vessels.

2.2.1.3 Cultivation of iPS cell derived neuronal progenitor cells (iPS-NPCs)

Human iPS cell line hFib2-iPS5 (Park et al., 2008), was maintained on a layer of mitotically inactivated murine embryonic fibroblasts (GlobalStem) and cultured as described (Trilck et al., 2013) and manually passaged every 5-7 days. iPS routine cell culture was carried out by Michaela Trilck and Rayk Hübner (AKos).

iPS-NPCs were derived via dual SMAD inhibition. Cells were obtained after 10 days of differentiation in N2B27 medium containing Neurobasal, DMEM/F12, 1xN2 supplement, 1xB27 supplement and GlutaMax (all from Invitrogen) complemented with human recombinant noggin Fc- chimera (500 ng/ml; R&D) and SB431542 (20 µM; Sigma). After 10 days, Noggin and SB431542 were omitted from the medium and 10 ng/ml hEGF (Roche) and hFGF-2 (GlobalStem) were included. After 14 days appearing rosette clusters were manually isolated using a hooked glass needle. Clusters were gently triturated using Tryp/Benz and reaction was stopped with Trit/Benz. iPS-NPCs were cultured on Poly-L-ornithin (15 µg/ml) /Laminin (10 µg/ml) coated dishes for 3–5 days (medium was changed every day) until 70 % confluence and passaged as described (2.2.1.1). Differentiation was induced by washing the cells with HBSS followed by withdrawal of growth factors FGF2 and EGF from the medium at a confluence of 70 %.

2.2.1.4 Cultivation of *E. coli*

E. coli was cultivated at 37 °C and 200-250 rpm on a rotatory shaker in LB-medium with appropriate antibiotics in Erlenmeyer vials or polystyrene tubes. For storage of bacterial clones 0.8 ml of culture was mixed with 0.2 ml glycerol and stored at -80 °C. For seeding, a small amount of the glycerol stock was added into 5 ml of fresh LB medium with appropriate antibiotics.

2.2.1.5 Measuring and seeding of cell numbers

For cell number measurement 50 µl of cell suspension was added to 10 ml CASYton and analyzed by CASY cell counter (Innovatis, Reutlingen, Germany) with the appropriate program. The seeded cell numbers are shown in Table 15.

Table 15: Seeding cell numbers

Cell line	Vessel size	Cell number/ Experiment	Proliferation time
ReNcell VM	6-well (greiner)	250.000/treatment 350.000/transfection	48 h
ReNcell VM	4-well (Nunc) 24-well (greiner)	100.000/treatment 150.000/transfection	24 h
ReNcell VM	96-well (greiner)	5.000/treatment	48 h
HEK293H	4-well (Nunc) 24-well (greiner)	200.000/transfection	24 h
iPS-NPCs	4-well (Nunc) 24-well (greiner)		24 h
iPS-NPCs	6-well (greiner)		48 h

2.2.1.6 Transfection of ReNcell VM cells

ReNcell VM cells were transfected by Nucleofaction (Lonza, Cologne, Germany). Briefly, cells were resuspended in 100 µl of Nucleofection solution (Kit V) mixed with 2-4 µg plasmid/1 Mio cells and transfected with program X-001 according to the manufacturer´s instructions. Cells were plated on Laminin coated vessels up to 70 % confluence and were differentiated upon withdrawal of growth factors. The transfection efficiency was about 90 % using positive control pmaxGFP (Lonza) as judged by microscopy (see appendix 7.1).

2.2.1.7 Transfection of HEK293H cells

For Transfection of HEK293H cells, 24 h cultivated cells were washed with pre-warmed PBS and incubated with medium without antibiotics (Table 15). 2 h later cells were transfected with 1 to 2 µg of plasmid with Lipofectamine 2000 according to the manufacturer´s instructions. After 6 h of incubation at 37 °C, medium was changed to medium containing antibiotics. The transfection efficiency was about 95 %, using positive control pCAGGS-GFP as judged by microscopy (see appendix 7.1).

2.2.1.8 Transformation and selection of *E. coli*

50 µl of competent cells were thawed on ice and 1 to 5 µl of DNA was added, incubated on ice for 5 min, plated onto LB-agar plates (37 °C) with appropriate antibiotics and incubated overnight at 37 °C in an incubator (Heraeus, Hanau, Germany). For blue/white screening, 1 mM IPTG and X-Gal were added to agar medium. For selection of transformed cells, single white colonies were picked, grown overnight in 6 ml LB-medium with appropriate antibiotics and were further analyzed.

2.2.1.9 Treatment of cells

For treatment of ReNcell VM cells and NPCs, cells were washed with pre-warmed HBSS. Differentiation was induced by withdrawal of growth factors and simultaneously cells were treated - if not otherwise indicated - once with substances (Table 14). In experiments using iPS-NPCs, medium was changed every 2 days, without additional treatment.

2.2.1.10 WST-1 assay

For cell viability measurement the colorimetric assay WST-1 (Roche, Penzberg, Germany) was used that determines the enzyme activity of mitochondrial dehydrogenases, which cleave a tetrazolium substrate resulting in colored formazan. The enzyme activity correlates with the metabolic activity of viable cells (Hipper and Isenberg, 2000). 5.000 ReNcell VM cells were plated on Laminin coated 96-well plates in proliferation media and treated after 4 hours of incubation at 37 °C with substances. Cell viability was analyzed after 48 h by adding 10 µl WST-1 reagent per well and 2 h incubation at 37 °C. The optical density at 450 nm wavelength was determined using genios microplate reader (Tecan, Crailsheim, Germany). 650 nm was used as reference wavelength. Six wells per condition were measured.

2.2.2 Protein analysis

2.2.2.1 Preparation of total cell lysates and protein measurement

Cells were harvested as described and lysed in ice cold RIPA buffer containing protease and phosphatase inhibitor cocktails (Roche) for 15 min on ice, slightly shaking. Suspension was

centrifuged at 15.000 g for 15 min at 4 °C and the supernatant was stored at -80 °C. Protein concentrations were measured using the bicinchoninic acid assay (BCA, Pierce, Rockford, IL, USA) according to manufacturer`s instructions using a plate reader (Tecan).

2.2.2.2 Preparation of nuclear cell lysates

Cells were washed twice with ice-cold PBS and then harvested with 1 ml ice-cold PBS, scraped with a cell scraper and centrifuged for 10 sec. The pellet was triturated 5 times with 1 ml ice-cold 0.1 % NP40-PBS, the remainder was pop-spun for 10 sec and the supernatant was transferred in a new tube, this was the cytoplasmic fraction. Next, the pellet was resuspended with 1 ml ice-cold 0.1 % NP40-PBS, afterwards, the remainder was centrifuged for 10 sec and the supernatant was discarded. For SDS-PAGE sample preparation, remaining pellets were mixed with 200 µl 1x sample buffer, sonificated twice for 5 sec, placed on ice and were subsequently boiled for 5 min.

2.2.2.3 Western blot

For protein analysis via western blot a defined amount of protein was mixed with 5x sample buffer and incubated for 5 min at 95 °C. Samples were loaded on a vertical Tris-HCl gel with 4-15 % acrylamide concentration gradient (Criterion Precast, Bio-Rad) and were run in a Criterion Cell (Bio-Rad) at 100-120 V until the running front of the gels reached the bottom. The prestained peqGOLD marker IV (PEQLAB, Erlangen, Germany) was used as molecular weight marker. Proteins were transferred via a Semi-dry blotting system (Trans-BlotSD, Bio-Rad) onto nitrocellulose membranes (Hybond-ECL, Amersham) at 200 mA for 1,5 h. Membranes were blocked with blocking solution (2 % BSA or 5 % milk) in TBST for 1 h followed by incubation with primary antibodies overnight at 4 °C on a shaker. Blots were washed 3 times for 5 min with TBST and incubated in darkness with appropriate fluorescent secondary antibodies for 1 h. Afterwards membranes were washed 3 times for 5 min with TBS, air-dried and stored in the dark. To visualize and quantify proteins the Odyssey infrared imaging system (LI-COR Biosciences GmbH, Bad Homburg, Germany) was used. The membranes were scanned at a wavelength of 700 nm for Alexa Fluor 680-labeled antibodies and at a wavelength of 800 nm for IRDye 800CW-labeled antibodies, respectively using

Odyssee software version 1.2. Values from total cell lysates were normalized to GAPDH which was used as a loading control. Nuclear cell lysates were normalized to Lamin A/C.

2.2.2.4 FACS analysis

To analyze proteins in different cell populations FACS analysis was used. Therefore cells were differentiated in 6-well plates, harvested and fixed with 1 % PFA in PBS for 15 min at room temperature. After centrifugation at 100 x g at 4 °C, the pellet was resuspended in 500 µl FACS-Wash buffer and stored at 4 °C.

For staining, cells were centrifuged at 100 x g at 4 °C and the pellet was resuspended in 25 µl saponin buffer containing diluted primary antibodies and incubated for two hours at room temperature on a shaker. As negative control, cells were incubated with normal mouse and normal rabbit IgG. Cells were washed with 300 µl saponin buffer and resuspended in 25 µl saponin buffer containing appropriate secondary antibodies. The samples were incubated for one hour in darkness at room temperature with gentle shaking. Cells were washed with 300 µl saponin buffer, resuspended in 500 µl FACS wash buffer and stored in the dark at 4 °C until analysis.

50.000 cells per sample were counted and analyzed using FACSCalibur (BectonDickinson, San Jose, USA) in combination with CellQuest Pro software. Cell debris was filtered out of the data set prior to analysis. Gates were set referred to cells stained with negative control antibodies.

2.2.2.5 Immunocytochemistry

For immunocytochemistry cells were cultured on coverslips and fixed on them with 4 % PFA in PBS for 15 min at room temperature. Afterwards, cells were washed with PBS and conserved with 0.02 % NaN_3 in PBS at 4 °C. Following blocking and permeabilization with IC blocking buffer for 30 min, cells were incubated for 30 min with primary antibodies diluted in IC antibody incubation buffer. Cells were washed 3 times with PBS and incubated for 30 min at room temperature in darkness with secondary antibodies diluted in IC antibody incubation buffer. Afterwards, cells were washed with PBS and covered with mounting medium containing DAPI (VectaShield). Slips were plated on object plates, sealed using nail polish and stored at 4 °C in the dark until analysis. Staining without primary antibodies served

as a control for background staining. Fluorescent images were generated by using a Biozero microscope (Keyence).

2.2.3 Molecular biological methods

2.2.3.1 Polymerase chain reaction (PCR)

For primer testing colony PCR and optimizing PCR conditions HotStartTaq (Qiagen) was used in combination with the gradient cycler (Eppendorf). For cloning purposes the proofreading blend Herculase II (Stratagene, La Jolla USA) was used in combination with the ABI cycler. Colony PCR was run with HotStartTaq on the ABI cycler in combination with the sequencing primers for pCAGGS (Table 7).

Table 16: PCR Mixes

Compound	HotStartTaq	Herculase II
buffer	-	5 µl (5 x)
enzyme	10 µl (MasterMix)	0,25 µl (5 U/µl)
dNTPs (10 mM)	-	0,5 µl
primer (10 pmol/µl)	0,8 µl	1 µl
template (ca. 10 ng/µl)	1 µl	2 µl
H_2O	7,2 µl	15 µl
DMSO	1 µl	1,25 µl

Table 17: Cycling conditions

Cycler	Eppendorf (HotStartTaq)		ABI (Herculase II)	
Step	**Temperature**	**Time**	**Temperature**	**Time**
denaturation	95 °C	15 min	98 °C	4 min
denaturation	94 °C	30 sec	98 °C	20 sec
annealing	60±10 °C	30 sec	see Table 8	20 sec
extension	72 °C	60 sec	72 °C	23 sec

2.2.3.2 Agarose gel electrophoresis

To generate gels, 1-2 % agarose (Biozym) was dissolved in 1xTAE buffer and heated in a microwave. Ethidium bromide (1 µg/ml working concentration) was added and gels were poured into prepared gel chambers. DNA samples were mixed with appropriate volume of 6x loading dye (Fermentas, St.-Leon-Roth, Germany). Gels were run at 100 V and photographed using UV gel documentation system (Herolab/biostep) in combination with a digital camera sytem (C-5050; Olympus, Japan). Size estimation of DNA fragments was done by using the GeneRuler DNA Ladder Mix (Fermentas).

2.2.3.3 Isolation and purification of DNA

To isolate vectors from *E. coli* cultures, the ZYPPY Plasmid Mini Kit (Zymo Research) was used. 6 ml of culture were centrifuged for 5 min at 14.000 g at room temperature and processed according to manufacturer's instructions. For large-scale purification of DNA, the Endo-Free Plasmid Maxi Kit (Qiagen, Hilden, Germany) was used according to manufacturer`s instructions. DNA was resuspended in endotoxin-free TE-buffer to yield a concentration of ~1 µg/µl. Vectors were sterile filtered (0.22 µM) and stored at -20 °C.
For purification of DNA fragments from solutions or gels, the GFX purification Kit (GE healthcare, Munich, Germany) was used according to manufacturer's instructions. DNA was eluted in 30 µl H_2O.

2.2.3.4 Photometric DNA concentration measurement

DNA concentration and purity was estimated by measuring absorption at 260 and 280 nm using a spectrophotometer (Ultrospec 3100pro, Amersham, Munich, Germany).

2.2.3.5 Digestion, dephosphorylation and ligation of DNA

For digestion the FastDigest enzymes (Fermentas) were used. Therefore 500 ng of DNA was incubated with 0,5 µl of each enzyme together with appropriate amount of buffer and water for 20 min at 37 °C.

To avoided re-ligation, vectors were dephosphorylated by adding 1 µl of calf intestine alkaline phosphatase (CIAP, Promega, USA) and appropriate amount of reaction buffer and were incubated for 30 min at 37 °C.
For ligation, 50 ng of linearized and dephosphorylated vector together with a 3-fold molar amount of fragment were incubated overnight at 4 °C or for 4 h at room temperature with T4 DNA ligase (T4 DNA Ligase Kit, Promega)

2.2.3.6 Sequencing of DNA

To check the identity of DNA, the purified DNA samples were sequenced at Qiagen Sequencing Service (Qiagen, Hilden) or MWG (eurofinsmwg|operon, Ebersberg). Sequences were aligned and analyzed using MultAlin software.

2.2.3.7 cDNA synthesis

To generate cDNA the FastLane cDNA Kit (Qiagen) was used according to manufacturer's instructions. Briefly, cells were grown in a 24 or 96-well plate and were washed with 200 µl or 100 µl FCW buffer, respectively. After 10 min incubation with 80 µl or 16 µl FCP buffer, lysates were stored at -80 °C. The lysates were used to synthesize cDNA according to manufacturer's instructions with the exception, that only half amount of the buffers was used per sample due to cost-effective reasons.

2.2.3.8 Quantitative real-time PCR (qRT-PCR)

For quantitative real-time PCR a LightCycler Nano 1.0 (Roche) was used in combination with FastStart Essential DNA Green Master Mix (Roche) according to manufacturer's instructions. For primer information see Table 9. The primer efficiency was calculated by plotting the C_q-values against the cDNA amounts of a serial diluted positive control (human total brain cDNA, Clontech). As a template, 1 µl cDNA generated with FastLane Cell cDNA Kit (Qiagen) was used. All samples were run in duplicates and as a negative control template was omitted from the reaction. For cycling parameters see Table 18. PCR products were verified by melting point analysis and by size in agarose gel electrophoresis. Relative changes of mRNA amount were calculated using the delta-delta C_t method (Pfaffl et al., 2000). Amount

of mRNA of interest was normalized to the housekeeping gene Glucose-6-phosphate-dehydrogenase (G6PD) and was calculated as relative changes compared to control.

Table 18: Cycling parameters

Step	Temperature	Time
denaturation	95°C	10 min
denaturation	95 °C	20 sec
annealing	See Table 9	20 sec
extension	72 °C	23 sec
melting curve	60-95 °C	

2.2.3.9 Statistical analysis

Statistical evaluation was carried out using the two-tailed Student's t-test with Excel software (Microsoft, USA). Difference was considered to be statistically significant $p \leq 0.05$.

3 Results

3.1 Generation of expression vectors

For overexpression in ReNcell VM cells the backbone plasmid pCAGGS was used. pCAGGS contains a CAG promoter (Niwa et al., 1991) which has been shown to drive efficient expression in ReNcell VM cells compared to other promoters like CMV (Hübner et al., 2010 and data not shown). In addition, HA-HES plasmids were generated (see appendix 7.1).

3.1.1 Generation of pCAGGS-h*HES1*

To amplify h*HES1* the plasmid pCMV6-XL4-*HES1* (Origene) was used as a template, together with the forward primer which includes the *Xho*I restriction site and the reverse primer which includes the *Bst*XI restriction site. After amplification of h*HES1* (Figure 9, A) the insert was purified and ligated into pGEM-T easy (Promega) for subsequent blue/white screening and selection. Positive clones were analyzed by digestion with *Eco*RI, expected fragments were ca. 3000 bp and 981 bp (Figure 9, B). All positive clones were sequenced and used for insert production. The purified insert was ligated into pCAGGS and resulting clones were analyzed by colony PCR. Consequential positive clones were sequenced and transfected in ReNcell VM cells. The expression of HES1 was tested via western blot analysis. Therefore, transfected ReNcell VM cells were proliferated for 24 h after transfection and then differentiated for 24 h. Western blot analysis revealed a specific band at ca. 25 kDa (Figure 9, D). The predicted size of hHES1 is 30 kDa, the variance may be due to alternative splicing of HES (Hirata et al., 2000).

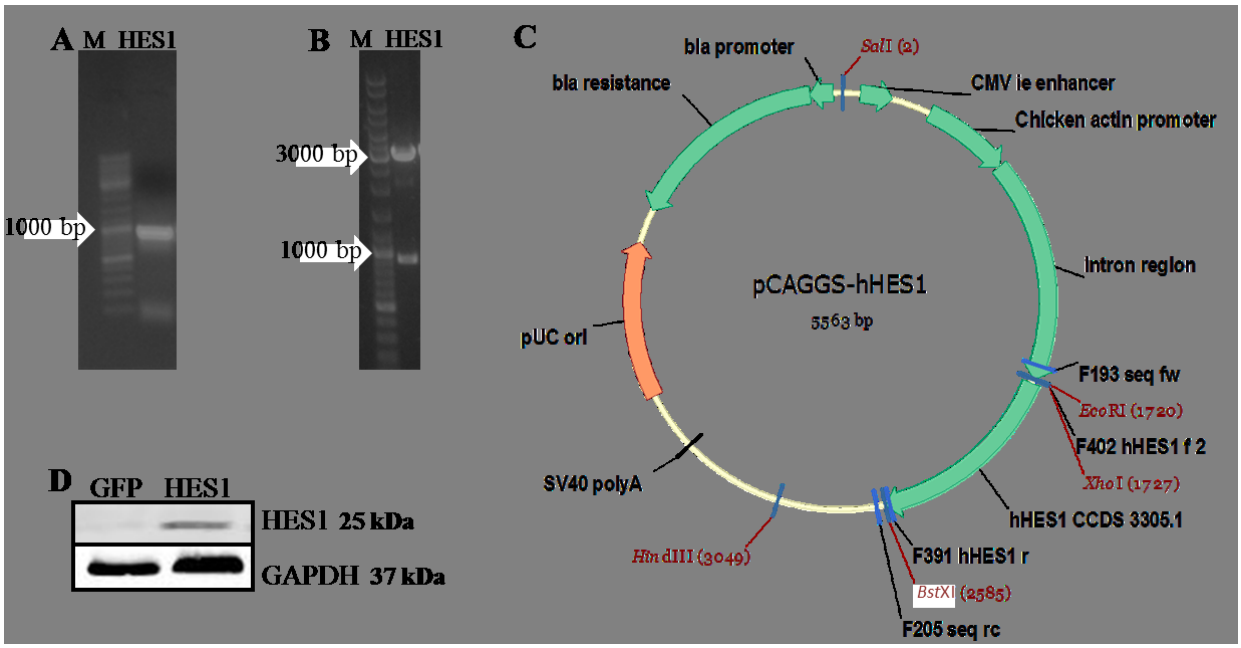

Figure 9: Generation ofpCAGGS-h*HES1*. A: Product of h*HES1* amplification (M=DNA ladder). **B**: Digestion of pGEM-T easy-h*HES1* by *Eco*RI; expected fragments were 3000 bp and 981 bp. **C**: Plasmid map of pCAGGS-h*HES1*. **D**: Western blot of pCAGGS-h*HES1* transfected ReNcell VM cells after 24 h of differentiation, pCAGGS-GFP transfected cells were used as control and GAPDH as loading control.

3.1.2 Generation of pCAGGS-h*HES5*

To amplify h*HES5* the plasmid pCMV6-XL4-HES5 (Origene) was used as a template, together with the forward primer which includes *Xho*I restriction site and the reverse primer which includes a *Bst*XI restriction site. After amplification of h*HES5* (Figure 10, A) the insert was purified and ligated into pGEM-T easy (Promega) for subsequent blue/white screening and selection. Positive clones were analyzed by digestion with *Eco*RI, expected fragments were ca. 3000 bp and 550 bp (Figure 10, B). All positive clones were sequenced and used for insert production. The purified insert was ligated into pCAGGS and resulting clones were analyzed by colony PCR. Consequential, positive clones were sequenced and transfected in ReNcell VM cells. The expression of Hes5 was tested via western blot analysis. Therefore, transfected ReNcell VM cells were proliferated for 24 h after transfection and then differentiated for 24 h. Western blot analysis revealed a specific band at ca. 20 kDa (Figure 10, D). This fits to the predicted size of 19 kDa of hHES5.

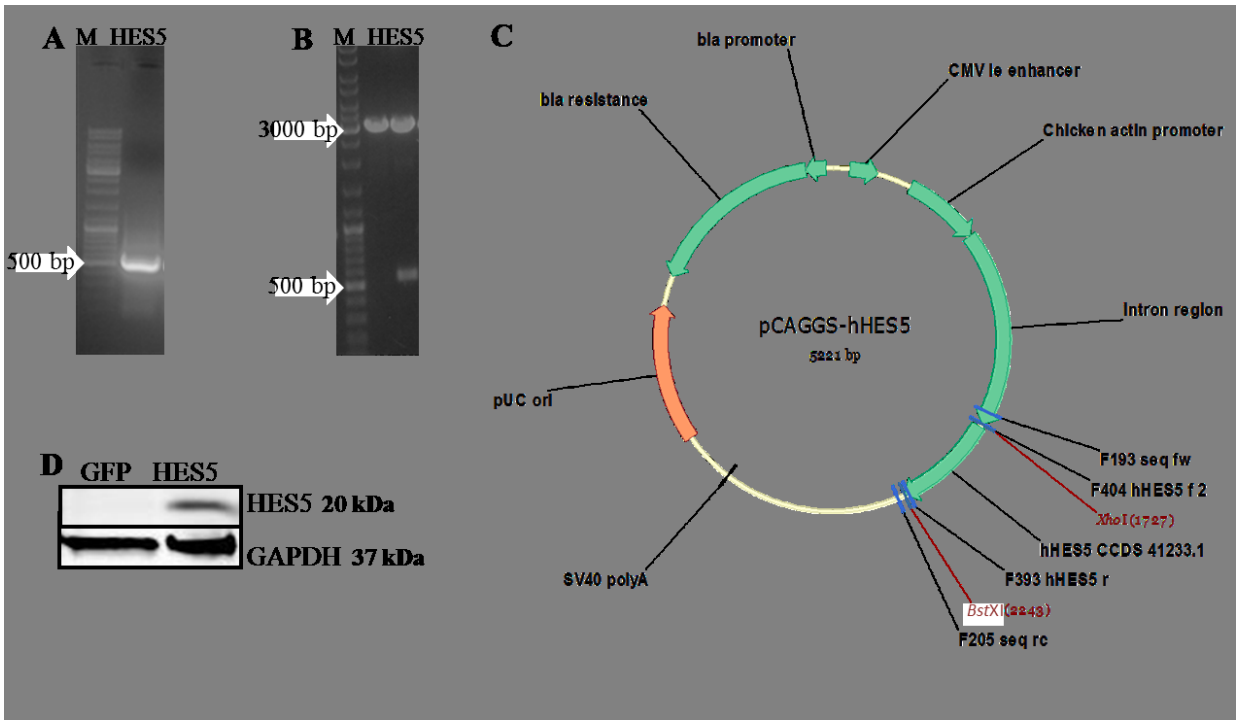

Figure 10: Generation of pCAGGS-h*HES5*. **A**: Product of h*HES5* amplification (M=DNA ladder). **B**: Digestion of pGEM-T easy-h*HES5* with *Eco*RI; expected fragments were 3000 bp and 550 bp. **C**: Plasmid map of pCAGGS-h*HES5*. **D**: Western blot of pCAGGS-h*HES5* transfected ReNcell VM cells after 24 h of differentiation, pCAGGS-GFP transfected cells were used as control and GAPDH as loading control.

3.2 The Notch pathway in ReNcell VM cells

It was shown before in several different organisms and cell lines, that the Notch pathway is decidedly important in the neuronal differentiation (Ables et al., 2011). The main point in Notch activation is the release of the Notch intracellular domain by cutting the Notch receptor with a γ-secretase. To demonstrate an active Notch pathway in differentiating ReNcell VM cells, the γ-secretase activity was inhibited by the widely used small molecule DAPT (N-[N-(3,5-difluorophenacetyl)-L-alanyl]-S-phenylglycine-t-butyl ester) as shown before in other systems (Ong et al., 2006, Nelson et al., 2006). It inhibits not only the release of the Notch intracellular domain but also affects other γ-secretases, which can lead to multifarious ramifications (Bay and Pfaff 2011). Therefore, cells were differentiated and simultaneously treated with 5 µM DAPT (Hübner, 2010) at 0 h. In addition, in other experiments, the Notch pathway was activated by overexpression of Notch intracellular domain 1 (NICD1). NICD1 was described as the most prominent Notch intracellular domain in mice neuronal cells (Ables et al., 2010). The following experiments were performed to elucidate the impact of Notch signaling on the cell fate of differentiating ReNcell VM cells.

3.2.1 Inhibition of the Notch pathway

Treatment of ReNcell VM cells with DAPT for 3 days of differentiation led to an increased net like growth pattern (Figure 11, A), which was not observable in control treated cells (solvent DMSO). Western blot analysis showed a decrease of endogenous NICD1 level after 3 h of DAPT treatment, while the control protein level GAPDH (Glyceraldehyde 3-phosphate dehydrogenase) was not affected (Figure 11, B).

The main target genes of the Notch pathway are the basic helix-loop-helix (bHLH) transcription factors hairy and enhancer of split 1 and 5 (HES1 and HES5; Bailey et al., 1995). Both are expressed in ReNcell VM cells and were able to be down regulated by DAPT treatment (Figure 11, C and D). Strikingly the HES1 mRNA level was less affected than the HES5 level. NICD seemed to have a stronger effect on HES5 than on HES1 regulation. Furthermore, both target genes responded fast (already after 2 h of treatment) and continuing (up to 72 h of treatment), which suspects a direct and permanent regulation. A detection of the endogenous HES1 and HES5 protein level reduction via western blot was, due to the low protein level, not possible.

HES1 and HES5 are described to induce the glial fibrillary acidic protein (GFAP) (Kabos et al., 2004, Kamakura et al., 2004) and reduce expression of proneural genes like MASH1 (ASCL1), Neurogenin 1, and Neurogenin 2 (Castella et al., 1999, Kageyama 2009). DAPT was able to decrease the GFAP mRNA level after 12 h up to 72 h of treatment (Figure 11, E). This indicated a indirect regulation of GFAP by DAPT over the Notch target genes HES1 and/or HES5 in ReNcell VM cells. Upregulation of MASH1 mRNA by DAPT after 6 h up to 24 h of treatment also indicated a indirect regulation of MASH1 by HES1 and/or HES5. The detection of Neurogenin 1 and 2 mRNA levels in ReNcell VM cells via qRT-PCR was not possible due to very low mRNA level (data not shown).

Thus, DAPT was able to inhibit the endogenous Notch pathway in ReNcell VM cells apparently by reduction of NICD1, which leads to a reduction of the Notch target genes HES1 and HES5. Moreover, DAPT was able to reduce GFAP and induce MASH1 mRNA levels.

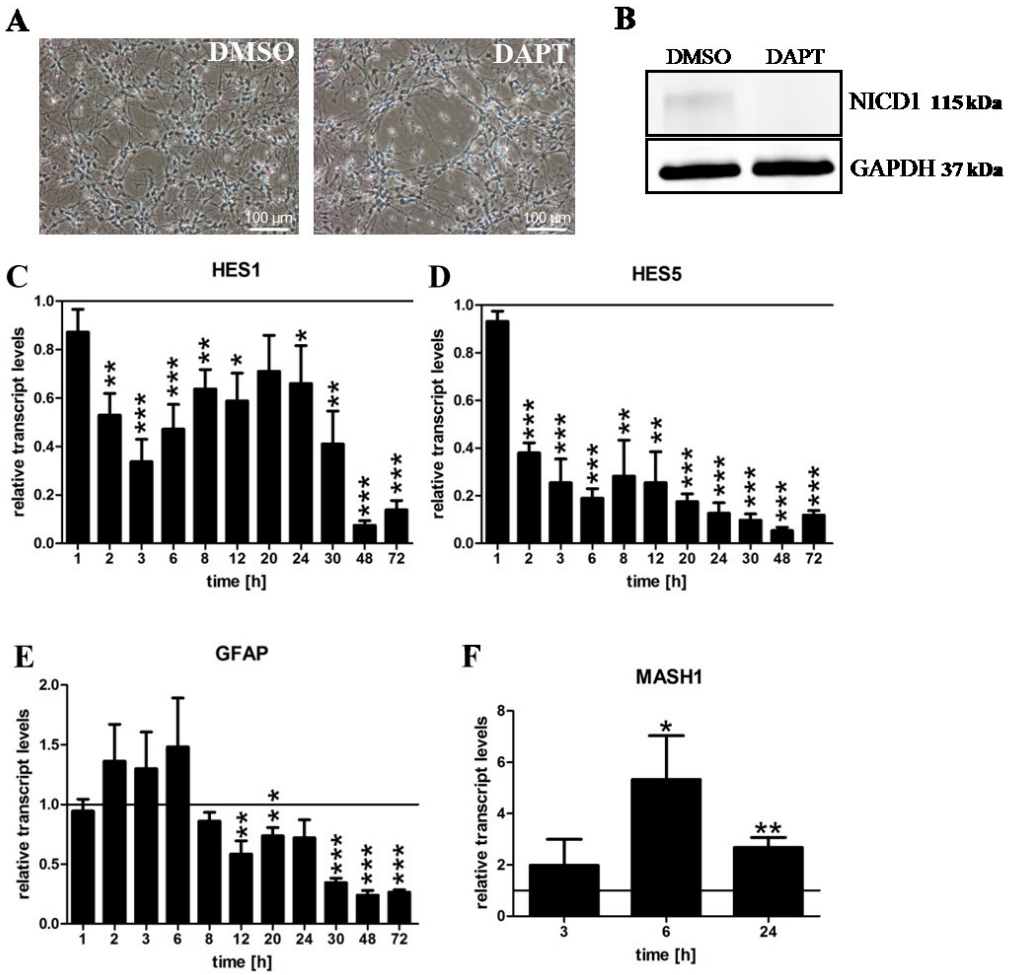

Figure 11: Inhibition of the Notch pathway by DAPT. Analysis of ReNcell VM cells in differentiation **A**: Phase contrast of 3 days differentiated cells treated with DMSO or DAPT, respectively. Scale bar 100 µm. **B**: Western blot analysis of Notch intracellular domain 1 (NICD1) under 3 h DAPT treatment. **C-F:** qRT-PCR of HES1 (**C**), HES5 (**D**), GFAP (**E**) and MASH1 (**F**) in cells treated with DAPT. Data are normalized to DMSO treated cells (time point control, indicated as black line). Data are presented as means ± SEM from at least three independent experiments. *p<0.05, **p<0.01, *** p<0.001 compared to time point control.

3.2.2 Activation of the Notch pathway

The plasmid pCAGGS-NICD1 encoded for the cleaved Notch intracellular domain 1 (110 kDa) and therefore was used to activate the Notch pathway. It was transfected in ReNcell VM cells and the overexpression of NICD1 was validated by western blot using a specific antibody against NICD1 after 24 h of transfection (Figure 12, A). The NICD1 antibody detects endogenous levels of the Notch intracellular domain 1 only when released by cleavage between Gly1753 and Val1754. qRT-PCR analysis revealed at the same time point an 2-fold induction of HES5 and a slightly reduction of HES1 mRNA levels (Figure 12, B). Therefore, HES5 seems to be the main target of the Notch intracellular domain 1.

To demonstrate the Notch specificity of the DAPT effect, a rescue experiment was performed. Therefore, NICD1 and GFP as control were overexpressed in ReNcell VM cells for 3 days of differentiation. Simultaneously, the cells were treated with DAPT or DMSO as control. The percentage of cells positive for the neuronal marker HuC/D and Tuj1 or the stem cell/ glial marker GFAP were measured by flow cytometry. DAPT treatment of GFP transfected control cells showed a clear increase in the percentage of cells positive for the neuronal marker HuC/D and Tuj1 (Figure 12, C and D). The amount of cells positive for HuC/D increases from 8 % up to 23 % and cells positive for Tuj1 from 3 % up to 15 %. Under DAPT treatment the percentage of GFP transfected control cells positive for GFAP was not significantly affected, but clearly decreased by tendency (Figure 12, E). Conversely, activation of Notch signaling via overexpression of NICD1 in ReNcell VM cells resulted in a reduction of cells positive for the neuronal marker HuC/D and Tuj1 (Figure 12, C and D). The amount of DMSO treated cells positive for HuC/D decreased from 8 % (GFP transfected control cells) to 4 % (NICD1 transfected cells), cells positive for Tuj1 decreased from 3 % (GFP transfected control cells) to 1 % (NICD1 transfected cells). In contrast, an induction of GFAP positive cells by NICD1 overexpression was not observable (Figure 12, E). The increase of cells positive for neuronal marker by DAPT treatment could be prevented by NICD1 overexpression (Figure 12, C and D). In this case, the induction was reduced to nearly control levels of positive cells. Furthermore, the percentage of DAPT treated cells positive for GFAP was induced by NICD1 transfected cells compared to GFP transfected cells. A regulation of the glial marker S100β was not observable (data not shown).

In summary, the NICD1 overexpression was able to activate the Notch pathway by increasing HES5 mRNA level. In addition, DAPT was able to induce cells positive for neuronal markers like HuC/D and Tuj1 and reduced cells positive for GFAP by tendency. NICD1 overexpression largely abolished the DAPT effect on differentiating ReNcell VM cells and therefore underscores the specificity of DAPT as an inhibitor of the Notch pathway.

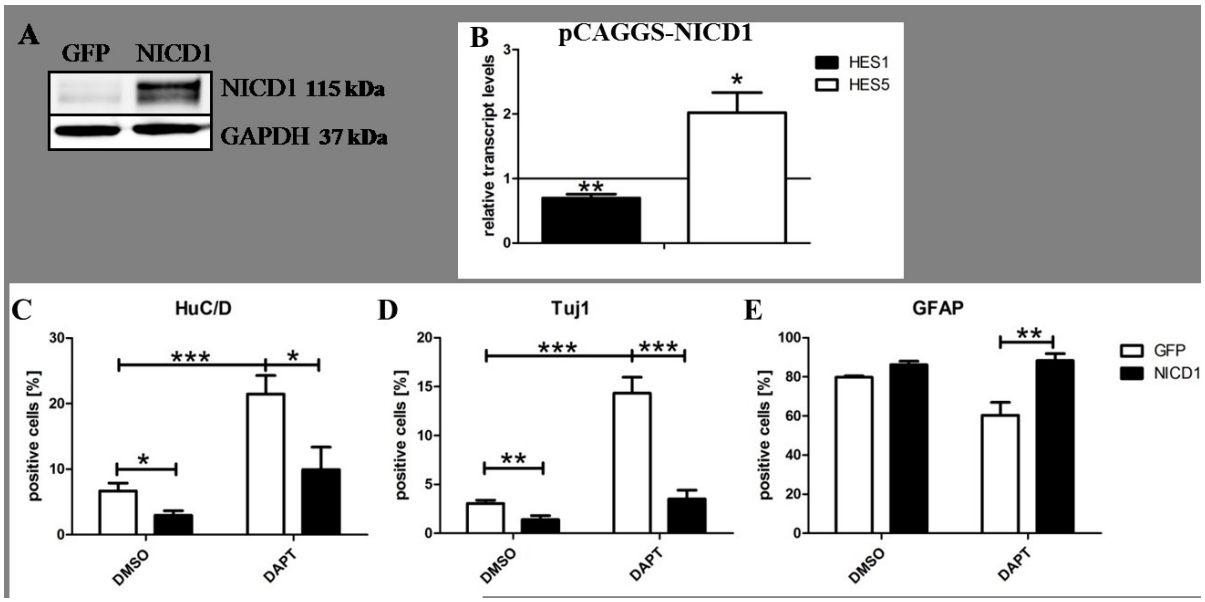

Figure 12: Activation of the Notch pathway in ReNcell VM cells rescued neuronal differentiation. A: Western blot analysis of Notch intracellular domain 1 (NICD1) of cells transfected with pCAGGS-NICD1 or control vector pCAGGS-GFP, harvested after 24 h of differentiation. **B**: qRT-PCR of HES1 and HES5 in NICD1 transfected cells, harvested after 24 h of differentiation. Data are normalized to GFP transfected cells (indicated as black line). **C-E:** Flow cytometric data showing percentages of NICD1 or GFP transfected cells positive for HuC/D (**C**), Tuj1 (**D**) and GFAP (**E**) differentiated for 3 days in the presence of DAPT or DMSO as control. Data are presented as means ± SEM from at least three independent experiments. *p<0.05, **p<0.01, *** p<0.001 compared to time point control.

3.3 The effect of Wnt-3a in the differentiation of ReNcell VM cells

As previously shown, Wnt-3a overexpression was able to increase the neuronal differentiation in ReNcell VM cells (Hübner et al., 2010). To verify this result, ReNcell VM cells were treated with 100 ng/ml of recombinant Wnt-3a and the expression of the neuronal markers HuC/D and Tuj1, the mature glial marker S100β and the stem/glial marker GFAP were analyzed after 3 days of differentiation via flow cytometry.

Wnt-3a treatment resulted in an increase in neuronal marker HuC/D (Figure 13, A) from 8 % up to 13 % and in an increase of Tuj1 positive cells (Figure 13, B) from 5 % up to 8 %. The glial marker S100β was not significantly affected by Wnt-3a treatment (Figure 13, C). Simultaneously, the percentage of cells positive for GFAP decreased under Wnt-3a treatment (Figure 13, D) from 74 % to 60 %.

In summary, Wnt-3a treatment was able to induce neurogenesis in ReNcell VM cells and coincidentally reduced the stem/glial marker GFAP, while S100β was not significantly affected.

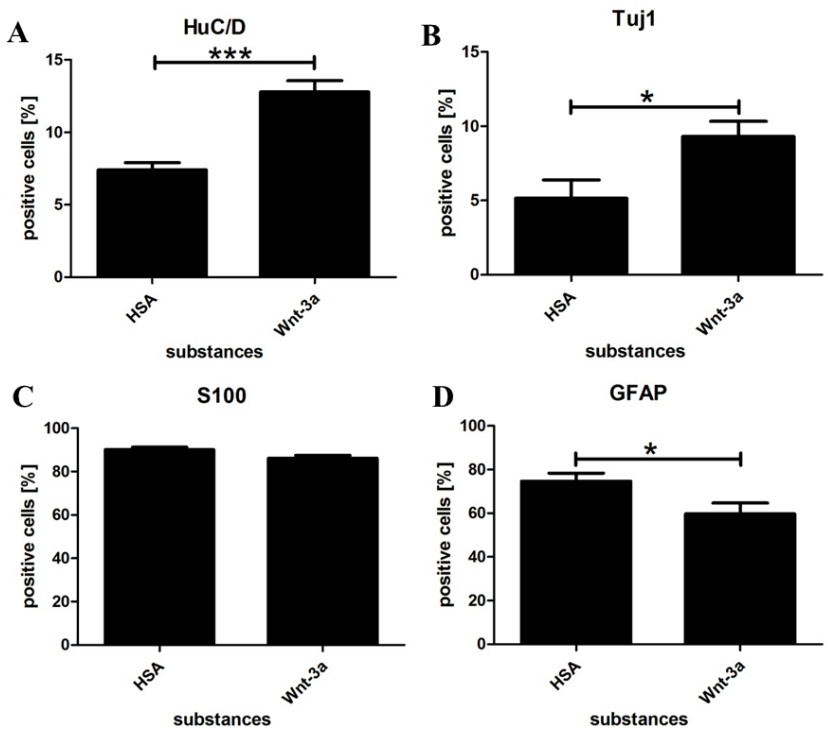

Figure 13: Induction of neurogenesis in ReNcell VM cells by Wnt-3a treatment. Flow cytometric data showing percentages of Wnt-3a treated cells positive for HuC/D (**A**), Tuj1 (**B**), S100β (**C**) and GFAP (**D**) differentiated for 3 days in the presence of Wnt-3a or HSA as control. Data are presented as means ± SEM from at least three independent experiments. *p<0.05, **p<0.01, *** p<0.001 compared to time point control.

3.3.1 Modulation of the Notch target genes by Wnt-3a

To get a deeper insight into the regulation of the Notch target genes by Wnt-3a, a time series analysis was performed in which differentiating ReNcell VM cells were treated for 1 h up to 72 h with 100 ng/ml of Wnt-3a. Afterwards, an analysis of the mRNA levels of HES1, HES5, GFAP and MASH1 was performed by qRT-PCR (Figure 14).

Wnt-3a treatment resulted in an increase of HES1 at 2 h, 6 h and 8 h but this effect was lost in later time points where no regulation was detected (Figure 14, A). In contrast, HES5 was rapidly downregulated by Wnt-3a after 2 h up to 24 h except of 8 h and 12 h of treatment (Figure 14, B) with a surprisingly strong regulation after 24 h. Interestingly, HES5 mRNA levels seemed to oscillate under Wnt-3a treatment, in combination with a time frame without significantly regulation between 8 h and 12 h. After 30 h up to 72 h a regulation was no longer observable. Strikingly, GFAP mRNA levels were significantly downregulated not until 6 h but constantly up to 72 h of treatment with exception of 20 h and 30 h. The proneural gene MASH1, in contrast, was upregulated after 24 h of Wnt-3a treatment, interestingly at the same time point when the strongest HES5 mRNA downregulation was observed.

In summary, Wnt-3a was able to induce HES1 mRNA level only in early time points while HES5 mRNA level was downregulated. Both Notch target genes seemed to be directly affected by Wnt-3a but were differentially regulated in time span and direction. The later regulation of GFAP led to the suggestion, that GFAP is an indirect target of Wnt-3a. The potentially mediator of this effect is HES5, because of its fast and continuous downregulation compared to HES1. Simultaneously, MASH1 was upregulated after 24 h of Wnt-3a treatment, which was the same time point when Wnt-3a had a strong effect on HES5 mRNA level.

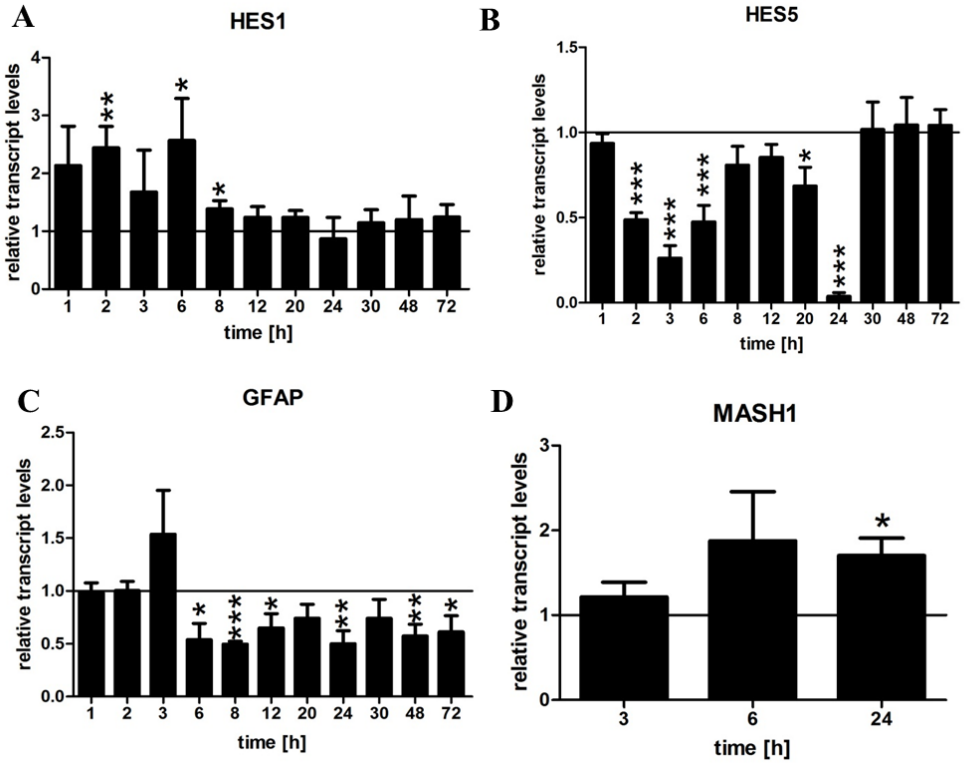

Figure 14: Modulation of Notch target genes in ReNcell VM cells by Wnt-3a. qRT-PCR of HES1 (**A**), HES5 (**B**), GFAP (**C**) and MASH1 (**D**) in cells treated with Wnt-3a. Data are normalized to HSA treated cells (time point control, indicated as black line). Data are presented as means ± SEM from at least three independent experiments. *p<0.05, **p<0.01, *** p<0.001 compared to time point control.

3.3.2 The additive effect of Wnt-3a treatment and Notch inhibition

Due to the fact that DAPT treatment as well as Wnt-3a treatment resulted in a downregulation of HES5 and GFAP mRNA levels, it arose the question, whether combined treatment is able to intensify the single effects. Therefore ReNcell VM cells were differentiated for up to 72 h under 5 µM DAPT and 100 ng/ml Wnt-3a treatment. mRNA levels of HES1, HES5, GFAP,

and MASH1 were compared to 5 µM DAPT treatment to illustrate the additive effect of Wnt-3a.

Addition of Wnt-3a was able to induce the HES1 mRNA level after 2 h of treatment compared to DAPT alone. But after 6 h and 48 h, Wnt-3a addition led to a decrease of HES1 mRNA while in other time points no significant regulation was detectable (Figure 15, A). Simultaneously, HES5 mRNA level was stronger downregulated by Wnt-3a in addition to its downregulation by DAPT alone (Figure 15, B). This regulation appeared already after 2 h up to 48 h of treatment except of 20 h and 30 h. Interestingly, double treatment with DAPT and Wnt-3a acted in the same time frame like Wnt-3a alone. Similar to HES5, GFAP mRNA level were decreased under double treatment and showed already after 3 h a significant and strong downregulation up to 72 h except of 12 h to 24 h (Figure 15, C). In contrast, double treatment resulted in no significant additive effect on MASH1 mRNA level. At 24 h time point however, Wnt-3a addition led to MASH1 upregulation by tendency.

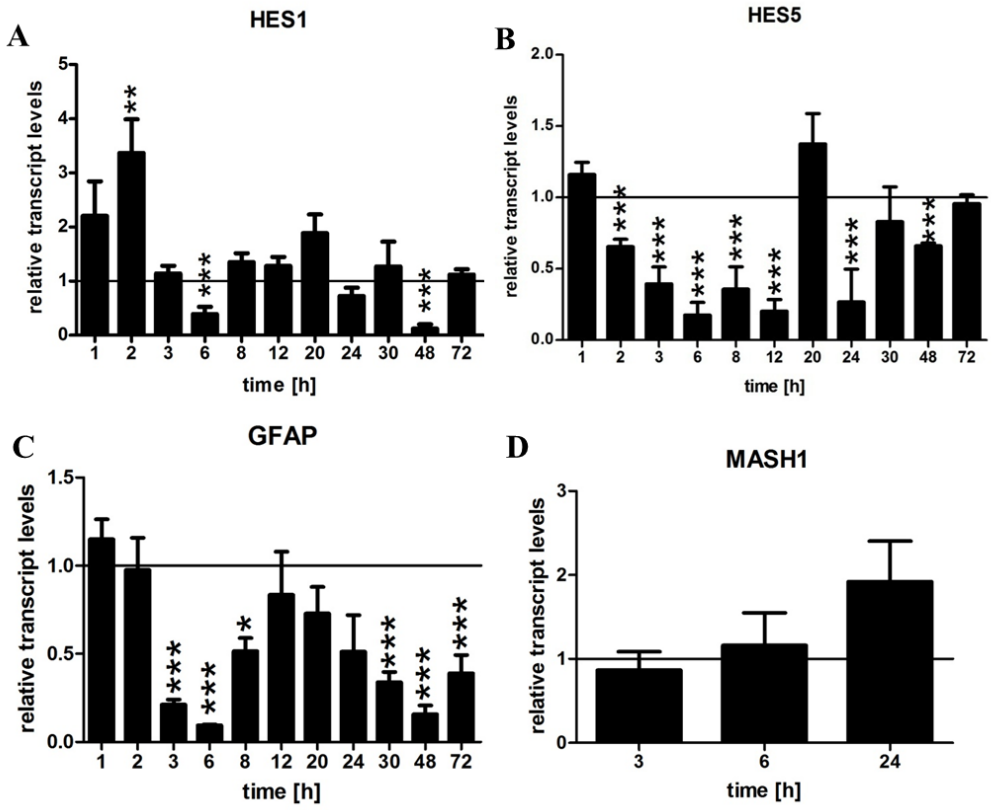

Figure 15: Modulation of Notch target genes in ReNcell VM cells by DAPT+Wnt-3a qRT-PCR of HES1 (**A**), HES5 (**B**), GFAP (**C**) and MASH1 (**D**) in cells treated with DAPT+Wnt-3a. Data are normalized to DAPT treated cells (time point control, indicated as black line). Data are presented as means ± SEM from at least three independent experiments. *p<0.05, **p<0.01, *** p<0.001 compared to time point control.

Thus, Wnt-3a was clearly able to affect the HES5 and GFAP mRNA levels in addition to DAPT alone. Precisely, Wnt-3a was able to downregulate GFAP as well as HES5 in addition to DAPT, but did have no significant additional effect on HES1 and MASH1 mRNA levels. But it was a slight upregulation of MASH1 mRNA by tendency supposable.

FACS analysis of 3 days differentiated cells positive for the neural marker HuC/D and Tuj1 revealed no significant induction of positive cells under DAPT+Wnt-3a treatment compared to only DAPT treated cells (Figure 16, A and B), which fits well with the MASH1 mRNA analysis. Simultaneously, the inductive effect of DAPT treatment on ReNcell VM cells positive for neural markers HuC/D and Tuj1 (Figure 12, C and D) was verified for treated (but not transfected, like Figure 12) cells compared to DMSO treated control cells. S100β was not affected by DAPT or DAPT+Wnt-3a treatment (Figure 16, C). In contrast, GFAP was clearly decreased by DAPT compared to DMSO from 74 % to 58 % and especially by DAPT+ Wnt-3a (down to 40 %) compared to DMSO as well as DAPT treatment alone (Figure 16, D).

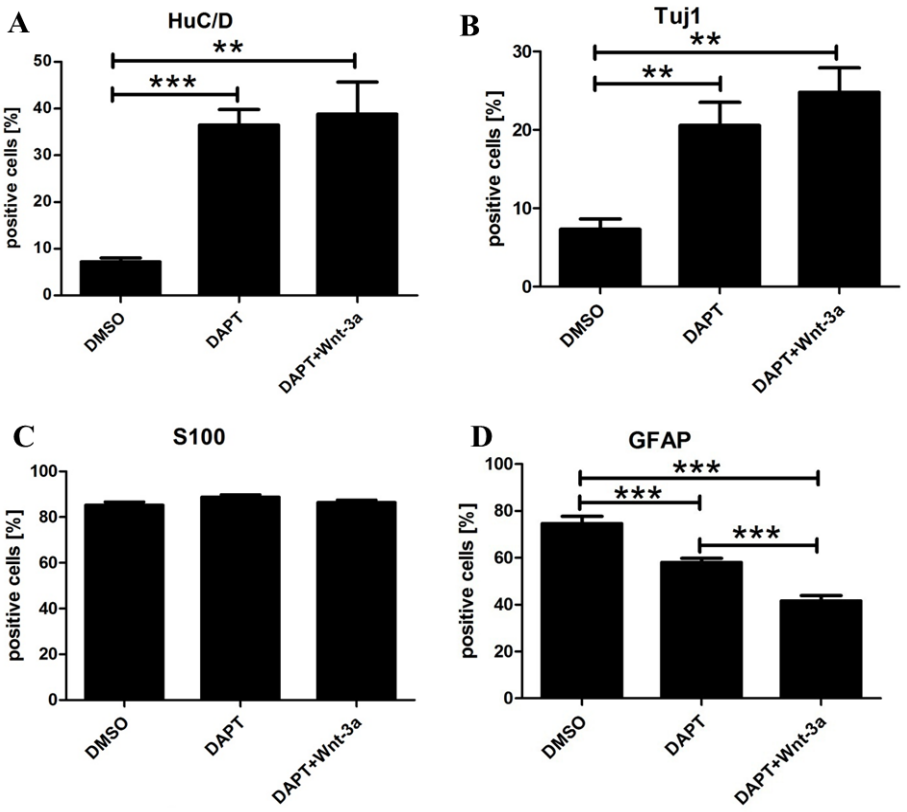

Figure 16: Induction of Neurogenesis in ReNcell VM cells by DAPT+Wnt-3a treatment. Flow cytometric data showing percentages of DAPT and DAPT+Wnt-3atreated cells positive for HuC/D (**A**), Tuj1 (**B**), S100β (**C**) and GFAP (**D**) differentiated for 3 days in the presence of DAPT and DAPT+Wnt-3a or DMSO as control. Data are presented as means ± SEM from at least three independent experiments. *p<0.05, **p<0.01, *** p<0.001 compared to time point control.

In summary, only DAPT was able to increase cells positive for HuC/D and Tuj1 compared to DMSO. But only GFAP was significantly downregulated by DAPT compared to DMSO and by DAPT+Wnt-3a compared to DMSO as well as DAPT.

Similar to the FACS data, immunocytochemistry cLSM-pictures (confocal laser scanning microscope) showed an increase in cells positive for Tuj1 when treated with Wnt-3a compared to HSA (Figure 17, A and B) and DAPT compared to DMSO (Figure 17, C and D). In addition, the amount of cells positive for GFAP decreased under DAPT and DAPT+Wnt-3a treatment compared to DMSO treated cells (Figure 17, C, D and E). Moreover, under DAPT treatment a net like growth pattern was observable (Figure 17, D) which got more distinct by treatment with DAPT+Wnt-3a (Figure 17, E). This net like structure of these cells led to a thicker cell layer where more cells were grown over each other and did not build a monolayer anymore. Therefore it was not possibly to count the cells or nuclei. Interestingly, GFAP positive cells were only encountered in the inner part of the net like structure while Tuj1 positive cell branches were visibly across the whole surface.

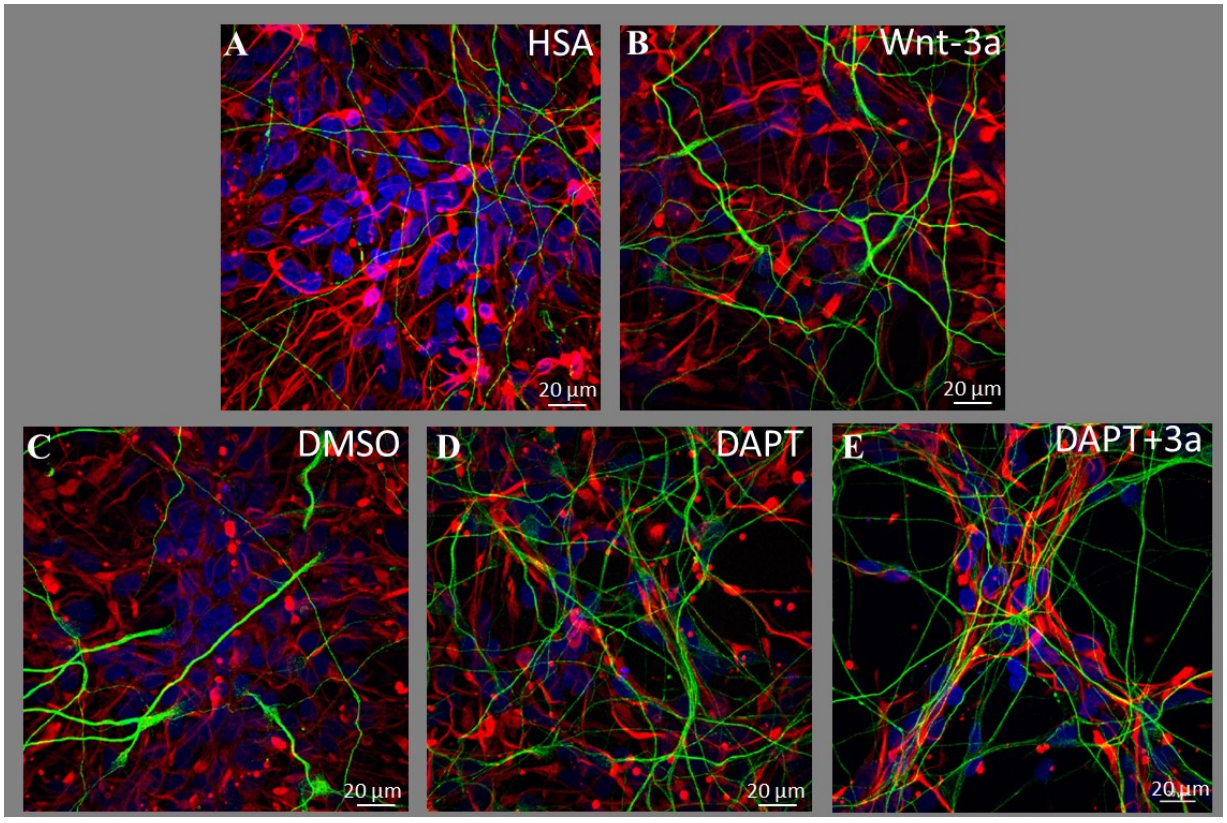

Figure 17: Induction of neurogenesis in ReNcell VM cells. Immunocytochemistry of cells positive for DAPI (**blue**), Tuj1 (**green**) and GFAP (**red**) differentiated for 3 days in the presence of Wnt-3a (**B**), DAPT (**D**) and DAPT+Wnt-3a (**E**) or HSA (**A**) and DMSO (**C**) as control. Representative pictures were acquired by cLSM in the center of Microscopy of the University of Rostock with help of Heiko Lemcke.

3.3.3 Time dependency of Wnt-3a/DAPT effects on neurogenesis

As shown before, Wnt-3a, DAPT as well as DAPT+Wnt-3a were able to induce neurogenesis and to reduce GFAP, mRNA levels as well as amount of positive cells, compared to their controls. All substances were acting very fast but only Wnt-3a seemed to lose its effect after 24 h of treatment but nevertheless it was able to upregulate neuronal markers after 3 days of differentiation. These data led to the question whether Wnt-3a and DAPT are able to induce neurogenesis even if they are not present during the whole differentiation period. Therefore, ReNcell VM cells were differentiated for 3 days and were treated only for 3 h, 6 h, 24 h, 48 h and 72 h. After treatment cells were washed and differentiated for up to 3 days without substances.

After 24 h treatment with DAPT and DAPT+Wnt-3a treatment, Tuj1 showed the first induction of positive cells (Figure 18, A). Since the standard deviation was untypically high in some time points a clear distinction was difficult. But an increase in cells positive for Tuj1 in long compared to short substance-exposure was supposable. Interestingly, HuC/D was the only marker which was affected when treated for short time frames. It showed already after 3 h of treatment an increase in positive cells when treated with Wnt-3a, DAPT or DAPT+Wnt-3a compared to HSA or DMSO (Figure 18, B). The amount of positive cells was only increasing if cells were treated longer with substances. Strikingly, no difference in HuC/D positive cells was detectable between 48 h of treatment compared to 72 h. Similar to Tuj1, GFAP was initially regulated after at least 24 h of treatment with DAPT+Wnt-3a compared to DMSO. Between 48 h and 72 h there were no clear differences visible under DAPT or DAPT+Wnt-3a treatment, only Wnt-3a compared to HSA treatment showed after 72 h the first significant downregulation of GFAP positive cells (Figure 18, C). Surprisingly, S100β showed after 48 h a downregulation of positive cells by DAPT+Wnt-3a treatment compared to DMSO as well as DAPT. This is the only time that a significant regulation of S100β was detectable (Figure 18, D).

In summary, HuC/D is a very early neuronal marker which is modifiable by treatments with short time frames. In contrast, Tuj1 and GFAP needed at least 24 h to be regulated by DAPT and DAPT+Wnt-3a, while Wnt-3a alone needed 72 h to modulate GFAP. The downregulation of S100β by DAPT+Wnt-3a was visible in all time points beginning from 24 h by tendency but it was only significant at 48 h.

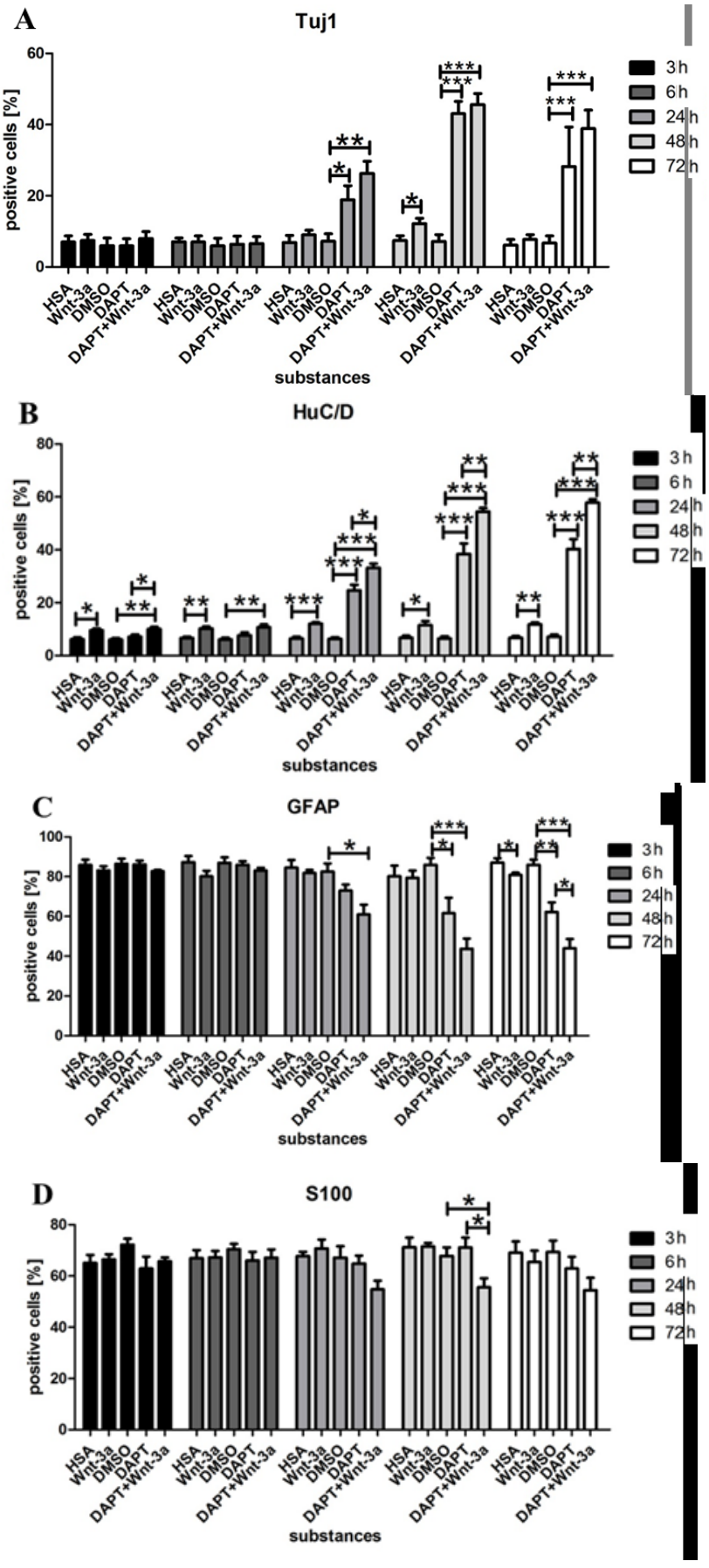
A
Tuj1
positive cells [%]
substances
3h
6h
24h
48h
72h
HSA
Wnt-3a
DMSO
DAPT
DAPT+Wnt-3a
B
HuC/D
C
GFAP
D
S100

Figure 18: Time dependency of ReNcell VM cell treatment. Flow cytometric data showing percentages of cells positive for Tuj1 (**A**), HuC/D (**B**), GFAP (**C**) and S100β (**D**) differentiated for 3 days in the presence of HSA, Wnt-3a, DMSO, DAPT and DAPT+Wnt-3a. Cells were treated at time point 0 h and were washed after 3 h, 6 h, 24 h, 48 h or 72 h, respectively. Data are presented as means ± SEM from at least three independent experiments. *p<0.05, **p<0.01, *** p<0.001 compared to time point control.

To further analyze the fast increase of HuC/D positive cells under DAPT and DAPT+Wnt-3a treatment, ReNcell VM cells were differentiated and treated for 1 day instead of 3 days. After just 1 day of differentiation a significant increase of HuC/D positive cells was visible when treated with DAPT compared to DMSO or treated with DAPT+Wnt-3a compared to DMSO as well as DAPT (Figure 19). In contrast, 1 day of differentiation was not sufficient to give rise to Tuj1 positive cells and no differences were observable for the marker GFAP and S100β (data not shown).

This underlines that HuC/D is a very early marker of neurogenesis in ReNcell VM cells and is useful to predict early progenitor cell fate.

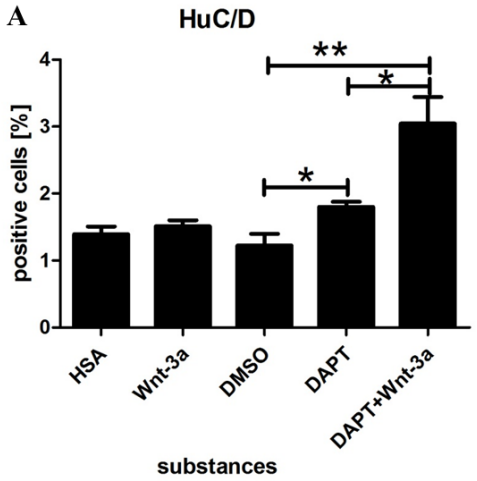

Figure 19: HuC/D positive ReNcell VM cells after 24 h of differentiation under treatment. Flow cytometric data showing percentages of cells positive for HuC/D (**A**) differentiated for 1 day in the presence of HSA, Wnt-3a, DMSO, DAPT and DAPT+Wnt-3a. Data are presented as means ± SEM from at least three independent experiments. *p<0.05, **p<0.01, *** p<0.001 compared to time point control.

Not only is the duration of treatment is important for the differentiation but also the point when the treatment starts. Taking this into account, ReNcell VM cells were treated after 18 h, 24 h and 66 h of differentiation with HSA, Wnt-3a, DMSO, DAPT and DAPT+Wnt-3a until a total length of 72 h of differentiation.

Interestingly, only DAPT+Wnt-3a were able to induce Tuj1 positive cells when treated after 18 h of differentiation (Figure 20, A). Later in differentiation no regulation is detectable. HuC/D positive cells were able to be induced after 18 h and even after 24 h of differentiation

(Figure 20, B). In this case, the percentage of positive cells under Wnt-3a treatment was after 18 h of differentiation as high as after treatment for full 72 h (Figure 18, B). In contrast, DAPT and DAPT+Wnt-3a treated cells were induced only up to 15 % instead of 40 % and 28 % instead of 58 %. Thus, DAPT compared to Wnt-3a needed to act at the beginning of the differentiation to develop its whole potential. In contrast, no regulation of GFAP or S100β was observable in all time points (Figure 20, C and D).

In summary, Wnt-3a as well as DAPT displayed a time frame where they were able to influence the differentiation of ReNcell VM cells. This time frame starts at the differentiation induction and seemed to end at 48 h after differentiation.

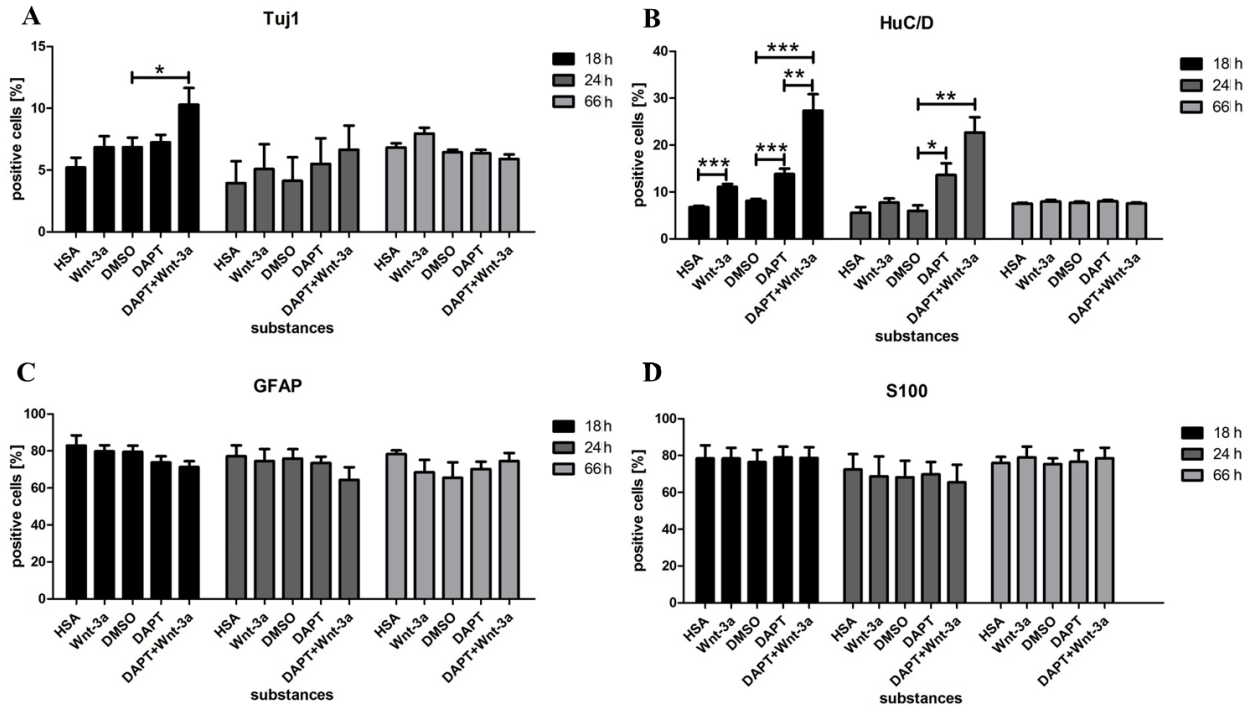

Figure 20: Time dependency of ReNcell VM cell treatment. Flow cytometric data showing percentages of cells positive for Tuj1 (**A**) HuC/D (**B**), GFAP (**C**) and S100β (**D**) differentiated for 3 days in the presence of HSA, Wnt-3a, DMSO, DAPT and DAPT+Wnt-3a. Cells were treated at time point 18 h, 24 h, or 66 h after start of differentiation, respectively. Data are presented as means ± SEM from at least three independent experiments. *p<0.05, **p<0.01, *** p<0.001 compared to time point control.

3.4 The mechanism behind the Wnt-3a effect

Wnt-3a was shown before to modulate different pathways, e.g.Notch and BMP, depended on cell type and vicinity (Peignon et al., 2011). In addition, Hübner et al. (2010) showed that the activation of the Wnt pathway in ReNcell VM cells by Wnt-3a but also that overexpression of stabilized β-catenin could activate Wnt signaling as assessed by target gene analysis.

However, β-catenin overexpression was not sufficient to increase neuronal differentiation in ReNcell VM cells (Hübner et al., 2010). Moreover, it was not able to modulate Notch target genes HES1/HES5 or GFAP (Rayk Hübner, personal communication). These results suggested a mechanism resulting in increased neuronal differentiation which is independent of β-catenin and lead to the question: which other pathway(s) is/are involved in the Wnt-3a mediated modulation of HES1 and HES5, as well as downregulation of GFAP, which are accompanied by an increase in neuronal differentiation of ReNcell VM cells?
To analyze the mechanism behind the Wnt-3a effect and the involved pathways, at first the Wnt pathway and its main proteins were tried to be excluded to be essential for the signalling. Afterwards the relevance of the Notch, BMP (Bone Morphogenetic Protein) and the JAK/STAT3 pathway was analyzed. Wnt ligands were already described to affect the Notch and BMP pathway, but STAT3 was only known to be modulated by HES1 and/or HES5 (Kamakura et al., 2004).

3.4.1 Analysis of the Wnt pathway dependency

As described before, the effect of Wnt-3a on the Notch target genes and the differentiation of the ReNcell VM cells are independent of β-catenin (see 1.3). This leads to the question if the effect is only independent of β-catenin or independent of the whole β-catenin dependent Wnt pathway. In addition, a crosstalk between Wnt and Notch pathway was already described in 1999 by Cooper and colleagues. They postulated that Fz/Dvl promotes activity of the Notch ligand Delta and inhibits Notch receptor activity in R3 *Drosophila melanogaster* eyes. In 2009 Ribeiro et al. described that GSK3β phosphorylation of Notch2 inhibits transcription of the Notch target gene HES1. Furthermore, while Wnt signaling inhibits GSK3β, and since overexpression of Wnt-1 upregulates HES1, Espinosa et al. (2003) suggested that Notch phosphorylation by GSK3β regulates cross-talk between the Notch and Wnt pathways. This leads to the suggestion that Wnt-3a may modulate the Notch pathway in ReNcell VM cells via Wnt-pathway-proteins upstream of β-catenin. To answer these questions, the impact of upstream proteins like GSK3β, LRP6 and Frizzeld were analyzed.

3.4.1.1 GSK3 dependency

One of the main points of the Wnt pathway activation is the inhibition of GSK3 by Wnt-3a, where the exact mechanism is still under discussion (Metcalfe and Bienz, 2011). There are also small molecules available like SB216763 and IM12 which are able to specifically inhibit

GSK3 and therefore activating the β-catenin dependend Wnt pathway (Schmöle et al., 2010). IM12 was described before by Schmöle et al., 2010. If the Wnt-3a effect depends solely on GSK3 these small molecules would be able to mimic the effect.

Treatment of cells with SB216763 significantly induced the mRNA level of Wnt target gene AXIN2 after 3 h and 6 h and after 12 h and 24 h by tendency (Figure 21, A) thus demonstrating GSK3 inhibition .While Wnt-3a was able to induce HES1 mRNA level (Figure 14, A) SB216763 reduced it after 3 h, 8 h and 24 h (Figure 21, B). Interestingly, HES5 was induced after 6 h of treatment but reduced after 8 h and 24 h (Figure 21, C). However, GFAP was slightly reduced only after 24 h compared to control treated cells (Figure 21, D).

In summary, SB216763 was able to induce the Wnt pathway as judged by increasing AXIN2 mRNA level. HES1 was reduced and HES5 was slightly induced at an early time point but reduced in later time points, while GFAP was not affected until 24 h after treatment and was subsequently marginally reduced.

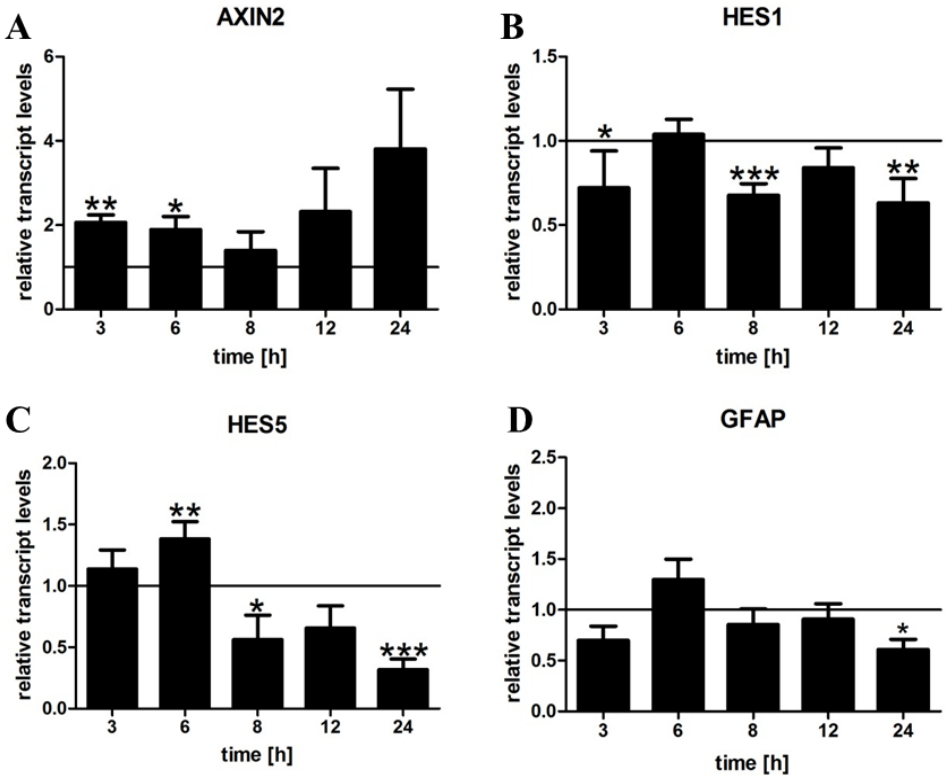

Figure 21: Modulation of genes in ReNcell VM cells by GSK3 inhibition via SB216763. qRT-PCR of AXIN2 (**A**), HES1 (**B**),HES5 (**C**) and GFAP (**D**) in cells treated with SB216763. Data are normalized to DMSO treated cells (time point control, indicated as black line). Data are presented as means ± SEM from at least three independent experiments. *p<0.05, **p<0.01, *** p<0.001 compared to time point control.

As shown before, Wnt-3a was able to induce the neural marker HuC/D and Tuj1 and reduced the stem/glial marker GFAP but did not affect the glial marker S100β. To further analyze the impact of GSK3, 3 days differentiated ReNcell VM cells were stained for the mentioned markers.

The amount of cells positive for the neural marker HuC/D and Tuj1 of IM12 or SB216763 treated ReNcell VM cells was not significantly induced but slightly by tendency (Figure 22, A and B). Furthermore, there was no difference between the amount of cells positive for GFAP treated cells and control cells (Figure 22, D). Strikingly, SB216763 as well as IM12 were able to significantly reduce S100β positive cells (Figure 22, C).

In conclusion, inhibition of GSK3 was not able to mimic the effect of Wnt-3a on differentiating ReNcell VM cells.

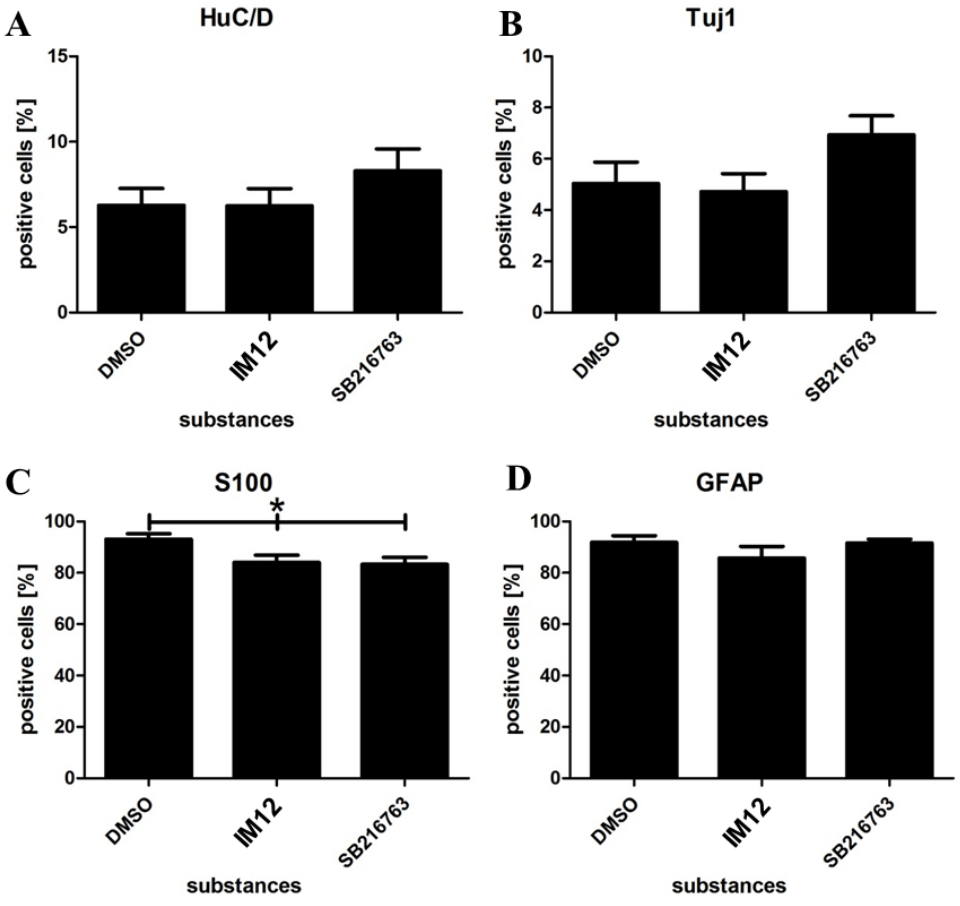

Figure 22: Modulation of ReNcell VM cells by GSK3β inhibitors. Flow cytometric data showing percentages of IM12 and SB216763 treated cells positive for HuC/D (**A**), Tuj1 (**B**), S100β (**C**) and GFAP (**D**) differentiated for 3 days in the presence of IM12, SB216763 or DMSO as control. Data are presented as means ± SEM from at least three independent experiments. *p<0.05, **p<0.01, *** p<0.001 compared to time point control.

3.4.1.2 LRP5/6 dependency

Low-density lipoprotein receptor-related proteins 5/6 are the best described co-receptors of the β-catenin dependent Wnt signaling pathway. They form receptor complexes with Frizzled and the ligand Wnt-3a. This interaction is able to be blocked by Dickkopf-related protein 1 as shown by Munji et al. (2011) in cortical intermediate progenitors. Therefore, Dkk-1 was used to analyze whether Wnt-LRP5/6 interaction would be required to influence HES gene regulation. If this effect is independent of LRP5/6, an inhibition by Dkk-1 would not inhibit Wnt-3a effects on HES gene expression and vice versa. The Wnt target gene AXIN2 was maximally increased in ReNcell VM cells upon 3 h of Wnt-3a treatment (Hübner et al., 2010). A concentration of 400 ng/ml of Dkk-1 was chosen, since this concentration appeared to efficiently inhibit the Wnt-3a induced AXIN2 upregulation and the increase of cytosolic β-catenin compared to other concentrations (Kathleen Müller, 2012). Higher concentration failed to maximize the effect. Therefore, the cells were differentiated and, after pretreatment for 1 h with Dkk-1, treated with Wnt-3a (100 ng/ml) for additional 3 h.

Wnt-3a treatment induced to a 20-fold increase of AXIN2 transcript levels while Dkk-1 was significantly able to inhibit this induction down to 7-fold (Figure 23). In addition, Wnt-3a decreased GFAP levels down to 0.7-fold as well as HES5 down to 0.8-fold, while HES1 was not significantly affected, but increased by tendency. Strikingly, Dkk-1 mediated inhibition of signaling did not affect the downregulating effect of Wnt-3a on HES5 and GFAP. In contrast, Wnt-3a +Dkk-1 treatment was able to significantly further downregulate HES5 compared to Wnt-3a treatment.

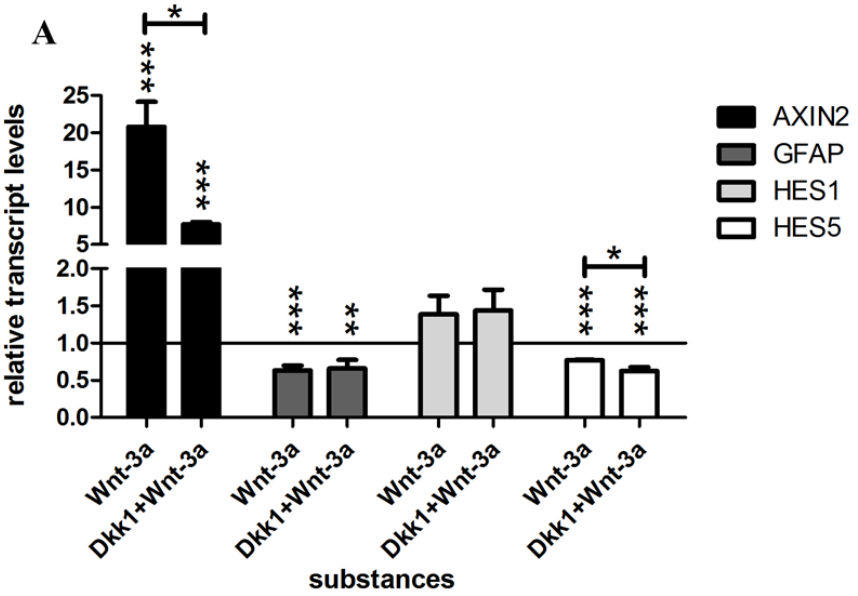

Figure 23: Modulation of genes in ReNcell VM cells by Dkk-1 (400 ng/ml). qRT-PCR of AXIN2, GFAP, HES1 and HES5 in cells treated for 3 h with 100 ng/ml Wnt-3a or Dkk-1+Wnt-3a. Data are normalized to HSA treated cells (time point control, indicated as black line). Data are presented as means ± SEM from at least three independent experiments. *p<0.05, **p<0.01, *** p<0.001 compared to time point control.

3.4.1.3 Frizzled dependency

The Frizzled receptors are one part of the receptor complex which is required for the activation of the β-catenin dependent Wnt pathway, but also are involved in β-catenin independent Wnt pathways (Kikuchi et al., 2009). The secreted Frizzled related protein 1 (sFRP1) is able to inhibit the interaction of Wnt-3a to its receptor Frizzled (Wawrzak et al., 2007). 500 ng/ml was used to inhibit the Wnt-3a derived AXIN2 induction, where higher concentrations were not able to maximize the effect, 6 h of treatment was chosen due to the fact, that there was the best AXIN2 reduction detectable by sFRP1 (data not shown). Cells were differentiated and treated with sFRP1+Wnt-3a (100 ng/ml) for 6 h.

Wnt-3a induced AXIN2 expression after 6 h of treatment up to 10-fold and this was significantly reduced by sFRP1 down to 5-fold (Figure 24). In addition, neither Wnt-3a nor sFRP1+Wnt-3a were able to significantly affect the mRNA level of GFAP and HES1 after 6 h of treatment, but both decreased GFAP and increased HES1 by tendency. Interestingly, the Wnt-3a evoked reduction of HES5 was not significantly affected by sFRP1 but was increased by tendency from 0.3-fold to 0.5-fold.

In summary, sFRP1 was able to reduce the Wnt-3a induced upregulation of AXIN2 but did not significantly influence the modulation of GFAP, HES1 or HES5 mRNA levels.

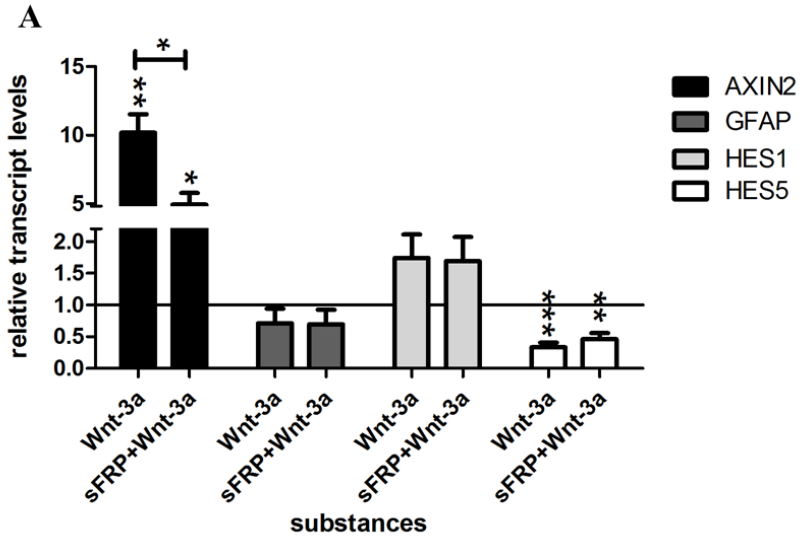

Figure 24: Modulation of genes in ReNcell VM cells by sFRP1 (500 ng/ml). qRT-PCR of AXIN2, GFAP, HES1 and HES5 in cells treated for 6 h with Wnt-3a or sFRP1+Wnt-3a. Data are normalized to HSA treated cells (time point control, indicated as black line). Data are presented as means ± SEM from at least three independent experiments. *p<0.05, **p<0.01, *** p<0.001 compared to time point control.

3.4.2 Analysis of the Notch pathway dependency

As described before, the effect of DAPT on ReNcell VM cells depends on the Notch intracellular domain 1 (NICD1). It was further analyzed whether Wnt-3a also depends on NICD1. Furthermore, HES1 as well as HES5 were overexpressed to show their relevance in the Wnt-3a effect on neuronal differentiation.

3.4.2.1 Notch1 dependency

To further analyze the impact of the Notch pathway, NICD1 overexpressing cells were treated with Wnt-3a.

NICD1 overexpression reduced the amount of positive cells for the neural marker HuC/D and Tuj1 in control as well as in Wnt-3a treated cells (Figure 25, A and B). Interestingly, in control treated cells NICD1 overexpression lead to a slightly increase in GFAP positive cells compared to control transfected cells. As described above, DAPT was not able to increase NICD1 transfected cells positive for neural markers compared to DMSO treated cells. The increase of HuC/D positive cells treated with DAPT compared to control might be explained

by the fact that not all cells were transfected and the non-transfected-cells were still able to respond to DAPT.

As long as NICD1 was overexpressed, neither DAPT nor Wnt-3a was able to increase neurogenesis as judged by Tuj1 positive cells. This led to the suggestion that the DAPT as well as Wnt-3a effect on neuronal differentiation depended on the NICD1.

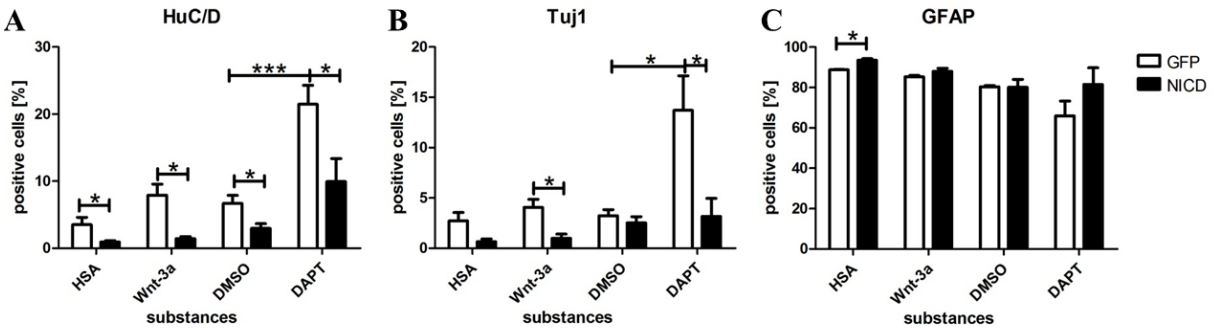

Figure 25: NICD1 overexpression in ReNcell VM cells. Flow cytometric data showing percentages of pCAGGS-NICD1 transfected cells positive for HuC/D (**A**), Tuj1 (**B**), and GFAP (**C**) differentiated for 3 days in the presence of Wnt-3a (100 ng/ml), DAPT (5 µM), or HSA, DMSO as control. Data are presented as means ± SEM from at least three independent experiments. *p<0.05, **p<0.01, *** p<0.001 compared to time point control.

3.4.2.2 HES5 dependency

The suggestion that DAPT as well as Wnt-3a effects on neuronal differentiation depend on the Notch intracellular domain 1 lead to the question which NICD1 target gene may be responsible for the observed effect. Because Kageyama et al. (2008) showed that NICD was not able to inhibit neurogenesis without HES1 and HES5. As shown above, NICD1 was able to increase HES5 (Figure 12, B). Therefore, HES5 was overexpressed in ReNcell VM cells to investigate if HES5 is able to reverse the effects of Wnt-3a and DAPT in the differentiating cells.

HES5 overexpressing ReNcell VM cells were treated with HSA, Wnt-3a, DMSO, and DAPT and were compared to GFP transfected cells. Strikingly, overexpression of HES5 efficiently inhibited the differentiation of the cells. After 3 days of differentiation the cells displayed clearly proliferation morphology and not the typical neuron like morphology with long axons and small and defined cell bodies (Figure 26).

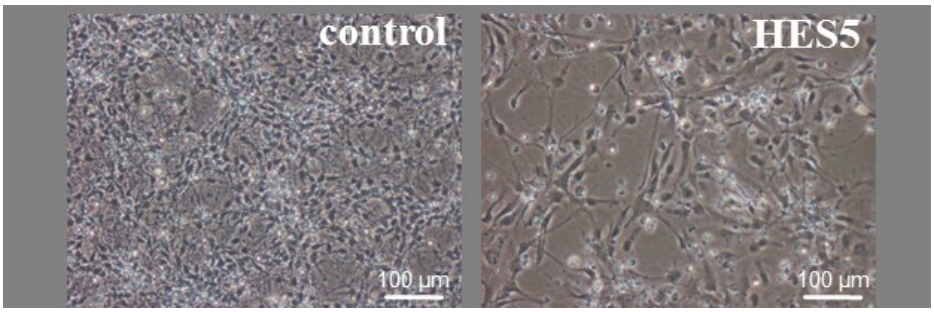

Figure 26: Overexpression of HES5 in ReNcell VM cells. Phase contrast of 3 days differentiated cells transfected with HES5 or GFP as control, respectively. Scale bar 100 µm.

The overexpression of HES5 led to a decrease of Tuj1 as well as HuC/D positive cells compared to GFP transfected cells (Figure 27, A and B). In the case of the HuC/D positive cells, HES5 not only was able to inhibit the effect of Wnt-3a and DAPT, namly the induction of neurogenesis but also reversed this effect (Figure 27, B). Simultaneously, the amount of cells positive for Tuj1 under DAPT treatment was also reduced by HES5 overexpression (Figure 27, A). Interestingly, HES5 transfected cells positive for GFAP were increased compared to GFP transfected cells, but only under Wnt-3a treatment (Figure 27, C). The increase of HES5 transfected cells positive for GFAP was also not significant but visibly by tendency. The same was true for Tuj1 positive cells under Wnt-3a treatment; they were, in this experiment, not significantly increased by Wnt-3a compared to HSA as seen in experiments described above. Simultaneously, there were no differences detectable in cells positive for S100β (Figure 27, D).

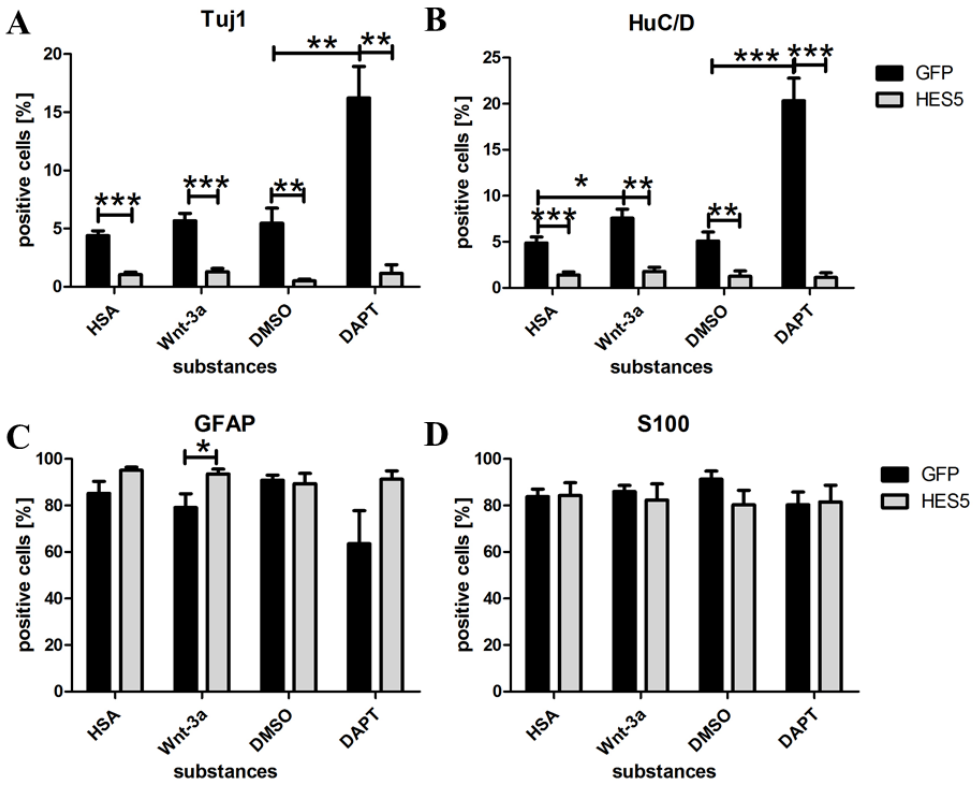

Figure 27: HES5 overexpression in ReNcell VM cells. Flow cytometric data showing percentages of hHES5 transfected cells positive for Tuj1 (**A**), HuC/D (**B**), GFAP (**C**) and S100β (**D**) differentiated for 3 days in the presence of Wnt-3a (100 ng/ml), DAPT (5 µM) or HSA, DMSO as control. Data are presented as means ± SEM from at least three independent experiments. *p<0.05, **p<0.01, *** p<0.001 compared to time point control.

In addition, qRT-PCRs were performed to analyze the effects of HES5 on HES1, GFAP and MASH1. Overexpression of HES5 in ReNcell VM cells led to a strong, down to 0.1 fold, reduction of HES1 mRNA level already 24 h after transfection, which was the time point (0 h) of induction of differentiation, until 72 h of differentiation (Figure 28, A). The mRNA level of the proneural gene MASH1 was reduced after 0 h up to 72 h as well (Figure 28, C). Surprisingly, the level of GFAP mRNA was also reduced by HES5 overexpression at all time points (Figure 28, D). This seemed to be in contrast to the flow cytometric data, where the amount of GFAP positive cells was increased (Figure 27, C). Overexpression of HES5 was, in addition, clearly detectable by the up to 370-fold increase of HES5 mRNA (Figure 28, B) and in western blot analysis (Figure 10).

In summary, HES5 was able to strongly reduce neuronal differentiation which was also accompanied by MASH1 mRNA reduction. Interestingly, HES5 was able to reduce HES1 levels and strongly reduced GFAP mRNA level.

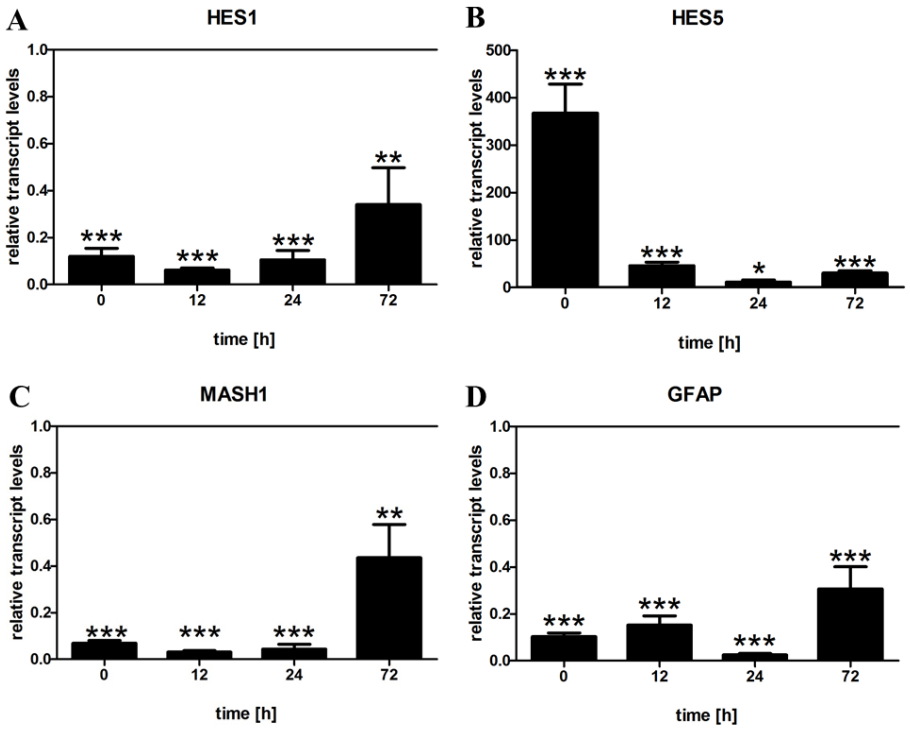

Figure 28: Modulation of genes in ReNcell VM cells by HES5 overexpression. qRT-PCR of HES1 (**A**), HES5 (**B**), MASH1 (**C**) and GFAP (**D**) in cells transfected with hHES5. Data are normalized to GFP transfected cells (time point control, indicated as black line). Data are presented as means ± SEM from at least three independent experiments. *p<0.05, **p<0.01, *** p<0.001 compared to time point control.

3.4.2.3 HES1 dependency

As described above, NICD1 was able to induce HES5 and slightly reduce HES1 (Figure 12, B). In addition, it was shown that the effect of Wnt-3a and DAPT seemed to depend on NICD1 as well as HES5. This arose the question what impact HES1 may have on the differentiation of ReNcell VM cells and whether HES1 may be a mediator of the effects of Wnt-3a and DAPT. To answer this question, HES1 transfected cells were treated with HSA, Wnt-3a, DMSO and DAPT as control. GFP transfected cells served as control.

In general, HES1 overexpression led to a significant reduction of Tuj1 as well as HuC/D positive cells compared to GFP control transfected cells (Figure 30, A and B). This reduction was not as strong as the reduction caused by HES5 transfected cells (see Figure 27). This fits well to the slight inhibition of the differentiation of ReNcell VM cells by HES1 compared to HES5 as judged by phase contrast microscopy (Figure 29).

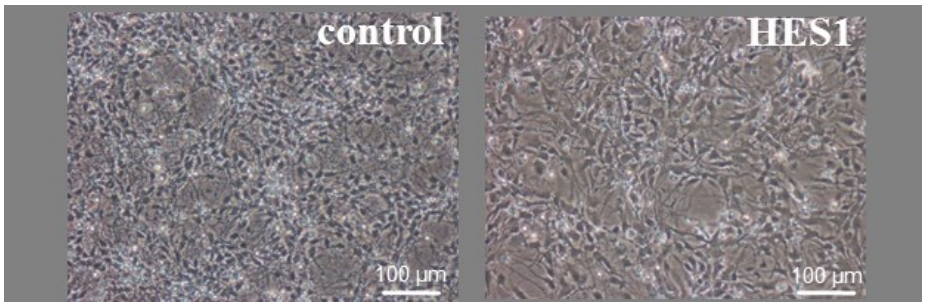

Figure 29: Overexpression of HES1 in ReNcell VM cells. Phase contrast of 3 days differentiated cells transfected with HES1 or GFP as control, respectively. Scale bar 100 µm.

Interestingly, the number of HES1 transfected cells positive for HuC/D were still able to be induced by Wnt-3a as well as DAPT compared to control treated cells (Figure 30, B). Even if this induction was not as high as GFP control transfected cells, it led to the suggestion that the Wnt-3a and DAPT effect may be independent of HES1. Overexpression of HES1 in combination with Wnt-3a treatment led to a significant induction of GFAP positive cells compared to GFP transfected and Wnt-3a treated cells (Figure 30, C). In all other treatments, an induction was only visible by tendency. HES1, furthermore, significantly induced the amount of S100β positive cells in HSA control treated cells (Figure 30, D). This effect was not detectable in other treatments.

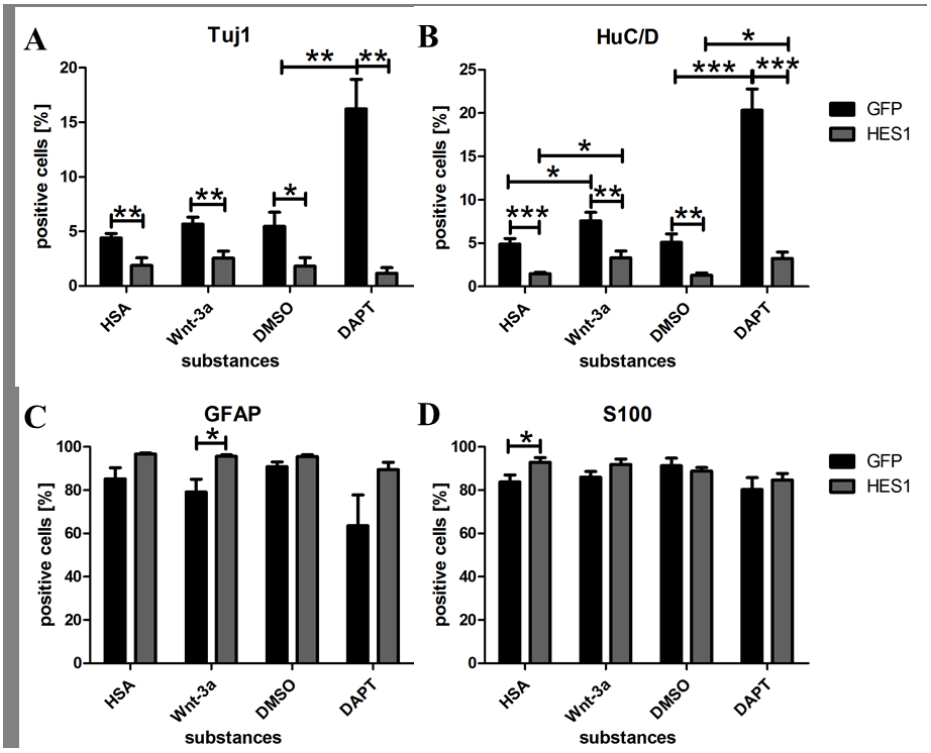

Figure 30: HES1 overexpression in ReNcell VM cells. Flow cytometric data showing percentages of hHES1 transfected cells positive for Tuj1 (**A**), HuC/D (**B**), GFAP (**C**) and S100β (**D**) differentiated for 3 days in the presence of Wnt-3a, DAPT or HSA, DMSO as control. Data are presented as means ± SEM from at least three independent experiments. *p<0.05, **p<0.01, *** p<0.001 compared to time point control.

HES1 overexpression led to a strong increase in HES1 (mRNA level: Figure 31, A; protein: Figure 9) and to a reduction of HES5 (Figure 31, B). Despite the fact that HES1 was still increased after 72 h the reduction of HES5 was lost after 72 h of differentiation. MASH1 mRNA level was also decreased by HES1 overexpression but was lost after 72 h of differentiation (Figure 31, C). Similar to that, GFAP levels were decreased up to 24 h of differentiation but at the level of control treated cells after 72 h (Figure 31, D).

In summary, HES1 reduced HES5, GFAP and MASH1 transcript levels but after 72 h they were no longer regulated by HES1. HES1 furthermore reduced the neuronal differentiation and increased S100β positive cells in HSA control treated cells. However, its effects on ReNcell VM differentiation were weaker than those observed in HES5 overexpression experiments.

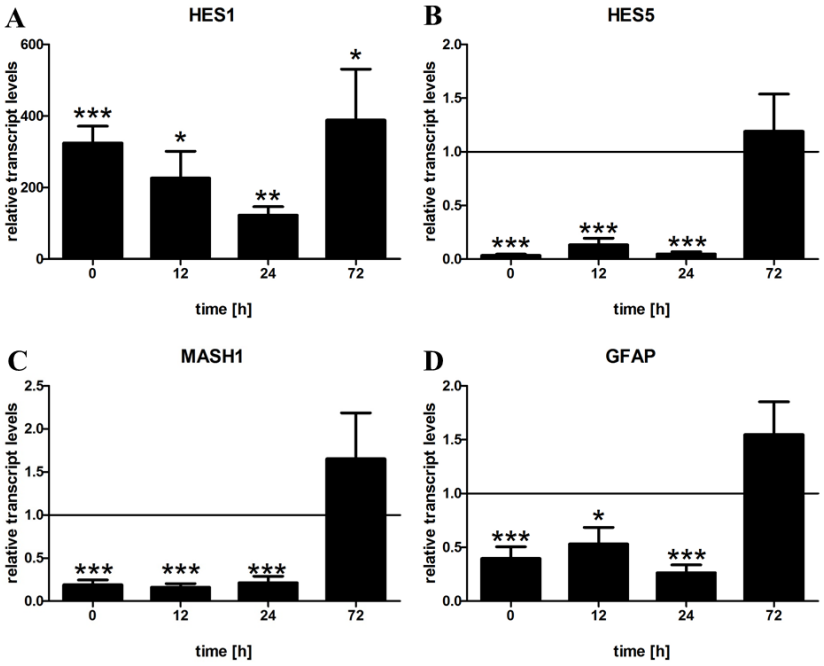

Figure 31: Modulation of genes in ReNcell VM cells by HES1 overexpression. qRT-PCR of HES1 (**A**), HES5 (**B**), MASH1 (**C**) and GFAP (**D**) in cells transfected with hHES1. Data are normalized to GFP transfected cells (time point control, indicated as black line). Data are presented as means ± SEM from at least three independent experiments. *p<0.05, **p<0.01, *** p<0.001 compared to time point control.

3.4.3 Analysis of the BMP pathway dependency

The bone morphogenetic protein pathway is not only known to regulate bone formation, but also plays a major role in diverse diseases, during embryonic development and in adult tissue homeostasis (Bandyopadhyay et al., 2013). Furthermore, BMP is able to modulate the

differentiation of neural stem cells (Song et al., 2011). Nakashima et al. (2005) described an inhibition of the BMP target gene ID1 by Wnt-3a treatment in C2C12 cells. In addition, it was shown that BMP2 enhance Notch induced transcriptional activation of HES5 in mouse neuroepithelial cells (Takizawa et al., 2003). This led to the suggestion that Wnt-3a may be able to inhibit the BMP pathway in ReNcell VM cells, thereby potentially regulating the differentiation independently of β-catenin.

3.4.3.1 Effect of Wnt-3a on the BMP pathway

The best described target genes of the BMP pathway are the bHLH transcription factors inhibitor of differentiation 1 and 3 (ID1 and ID3; Obayashi et al., 2009). To verify a BMP inhibition by Wnt-3a, these target genes were analyzed.

Wnt-3a treatment of ReNcell VM cells led to a significant reduction of ID1 as well ID3 after 3 h, 6 h and 8 h (Figure 32, A and B). The reduction was lost after 24 h of treatment on ID1, but ID3 was slightly induced after 24 h of Wnt-3a treatment.

In summary, Wnt-3a was able to reduce the BMP target genes ID1 and ID3 for up to 8 h significantly but lost its effect after 24 h of treatment. These data indicated that BMP signaling was active in these cells and Wnt-3a was able to inhibit this pathway.

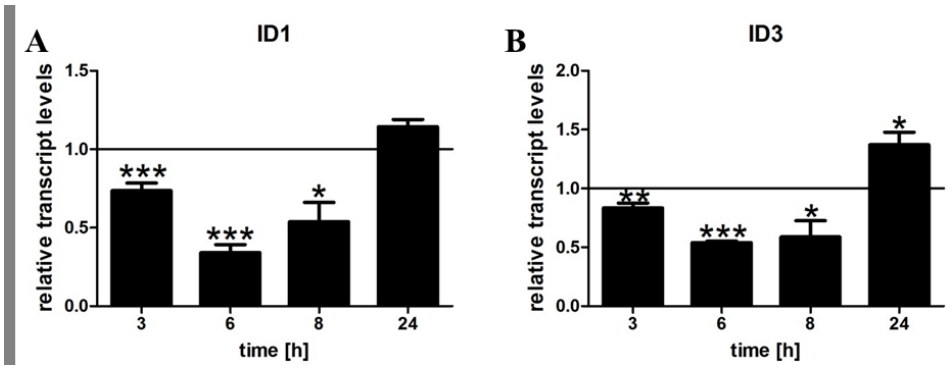

Figure 32: Modulation of BMP target genes in ReNcell VM cells by Wnt-3a. qRT-PCR of ID1 (**A**) and ID3 (**B**), in cells treated with Wnt-3a. Data are normalized to HSA treated cells (time point control, indicated as black line). Data are presented as means ± SEM from at least three independent experiments. *p<0.05, **p<0.01, *** p<0.001 compared to time point control.

3.4.3.2 Inhibition of the BMP pathway

Due to the fact that Wnt-3a was at least able to reduce ID1 and ID3 up to 8 h after induction of differentiation, it was aimed to mimic the Wnt-3a effect by inhibiting the BMP pathway

with known inhibitors. In addition, HES5 and GFAP were analyzed to check if the inhibition of BMP is able to modulate Notch target genes in the same manner as Wnt-3a.

There are three well described substances to inhibit the BMP pathway. Noggin binds the ligand BMP2, 4 and 7 and therefore inhibits the SMAD1, 5, 8 and MAPK p38 (Yu et al., 2008). Dorsomorphin inhibits BMP4 induced signaling and does not affect MAPK p38 (Yu et al., 2008). SB431542 inhibits the TGF-β signaling pathway and therefore SMAD2 and 3 (Inman and Hill, 2002).

Noggin

Noggin (500 ng/ml; Yu et al., 2008) was able to reduce the amount of ID1 mRNA levels already after 3 h down to 0,2-fold und up to 24 h of treatment (Figure 33, A). ID3 was also reduced however less strongly down to 0,4-fold after 3 h of treatment but similarly up to 24 h (Figure 33, B). Interestingly, Noggin reduced HES5 after 3 h of treatment down to 0,8-fold afterwards it increased HES5 over to 2-fold after 8 h and 24 h of treatment (Figure 33, C). GFAP instead was only faintly downregulated by Noggin after 8 h (Figure 33, D) but no regulation was detectable in all other time points. To clarify if Noggin was able to modulate the cell fate of ReNcell VM cells the amount of cells positive for the markers Tuj1, HuC/D, GFAP and S100β was analyzed. Noggin was not able to increase neurogenesis like Wnt-3a; instead it significantly decreased the amount of cells positive for the neural marker HuC/D (Figure 33, E). Simultaneously, the marker Tuj1 was reduced by Noggin treatment only by tendency (Figure 33, F) and S100β and GFAP were not affected (Figure 33, G and H).

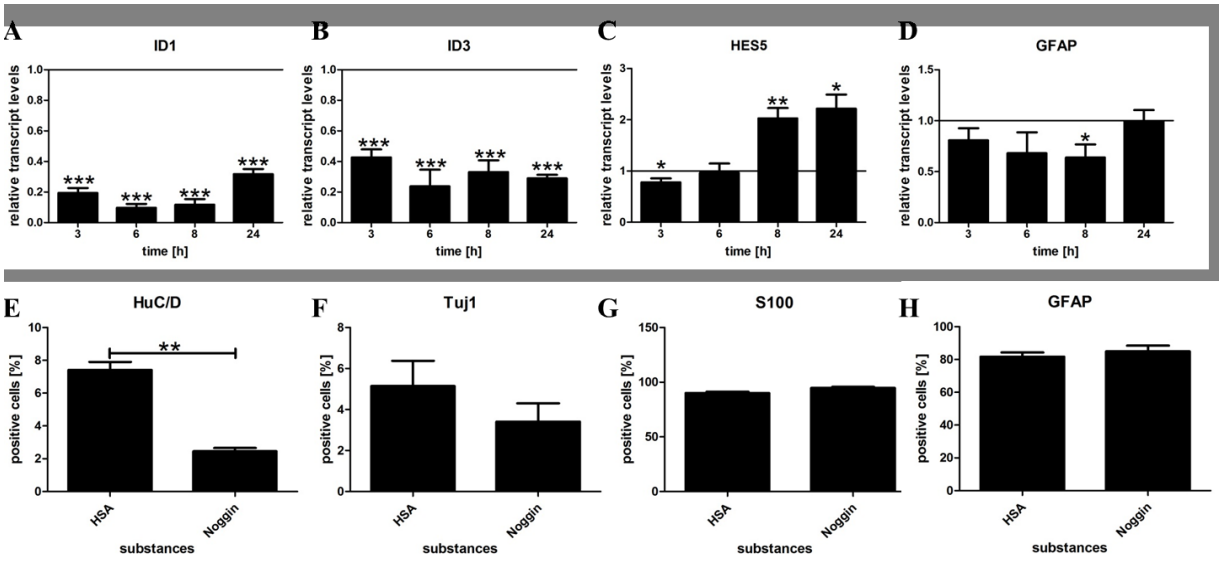

Figure 33: Modulation of ReNcell VM cells by Noggin. A-D: qRT-PCR of ID1 (**A**), ID3 (**B**),HES5 (**C**) and GFAP (**D**) in cells treated with Noggin. Data are normalized to HSA treated cells (time point control, indicated as black line). **E-H**: Flow cytometric data showing percentages of treated cells positive for HuC/D (**E**), Tuj1 (**F**),

S100β (**G**) and GFAP (**H**) differentiated for 3 days in the presence of Noggin or HSA as control. Data are presented as means ± SEM from at least three independent experiments. *p<0.05, **p<0.01, *** p<0.001 compared to time point control.

Dorsomorphin alias Compound C

Dorsomorphin (1 µM; Yu et al., 2008) was able to reduce ID1 in all analyzed time points to 0,4-fold (3 h of treatment) and to 0,7-fold at 8 h of treatment (Figure 34, A). In comparison, ID3 was similar down regulated after 3 h and 6 h of treatment but Dorsomorphin lost its impact on ID3 after 8 h and 24 h (Figure 34, B). Interestingly, neither HES5 nor GFAP was affected by Dorsomorphin treatment (Figure 34, C and D). But there was a significant reduction of HuC/D was well as Tuj1 positive cells under Dorsomorphin treatment (Figure 34, E and F). The numbers of cells positive for the marker S100β and GFAP were not affected (Figure 34, G and H).

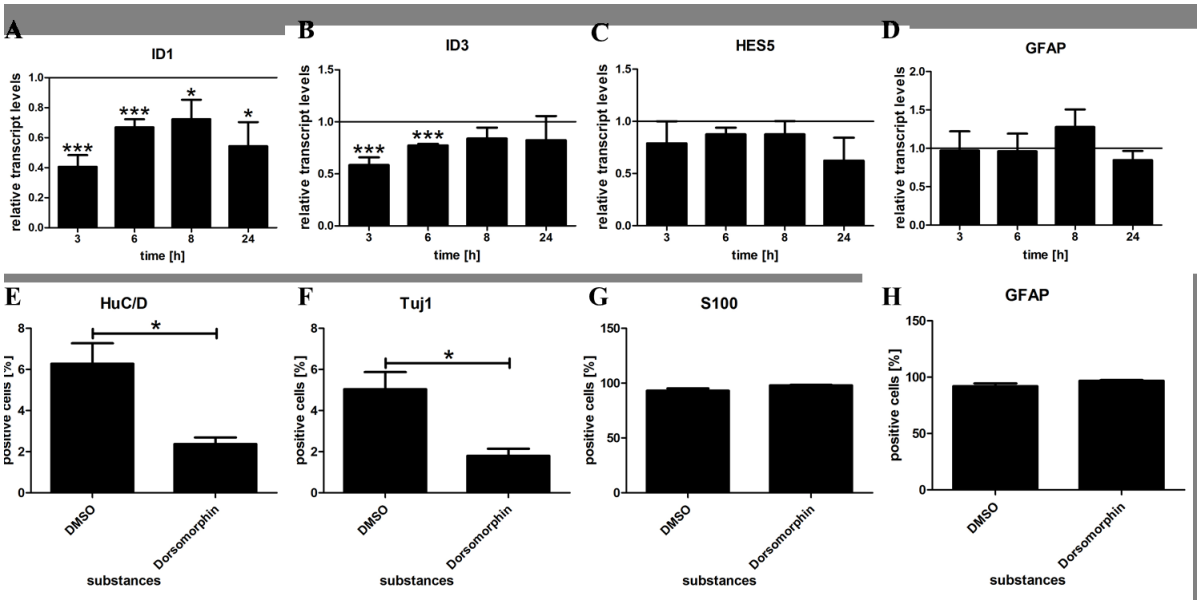

Figure 34: Modulation of ReNcell VM cells by Dorsomorphin. A-D: qRT-PCR of ID1 (**A**), ID3 (**B**), HES5 (**C**) and GFAP (**D**) in cells treated with Dorsomorphin. Data are normalized to DMSO treated cells (time point control, indicated as black line). **E-H**: Flow cytometric data showing percentages of treated cells positive for HuC/D (**E**), Tuj1 (**F**), S100β (**G**) and GFAP (**H**) differentiated for 3 days in the presence of Dorsomorphin or DMSO as control. Data are presented as means ± SEM from at least three independent experiments. *p<0.05, **p<0.01, *** p<0.001 compared to time point control.

SB431542

The impact of SB431542 on ReNcell VM cells was analyzed by FACS, to investigate the main effect: the modulation of differentiation. SB431542 slightly reduced the amount of cells

positive for HuC/D and Tuj1 by tendency (Figure 35, A and B) but did not affect S100β or GFAP (Figure 35, C and D).

In summary, Wnt-3a as well as Noggin and Dorsomorphin were able to inhibit the BMP pathway alike. But the inhibition pattern of Wnt-3a and Dorsomorphin, with the loss of ID3 inhibition after 24 h, was equal. Nevertheless, neither Noggin nor Dorsomorphin nor SB431542 were able to increase neurogenesis like Wnt-3a or reduce GFAP positive cells. But interestingly, Noggin as well as Dorsomorphin was able to reduce cells positive for HuC/D.

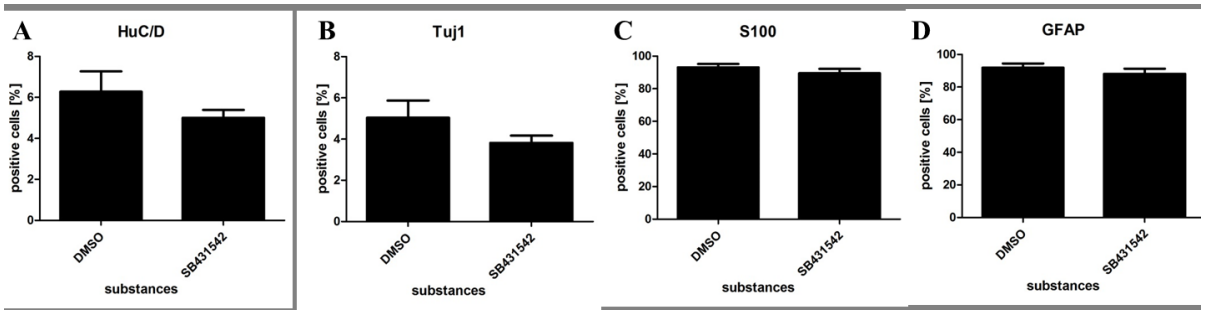

Figure 35: Modulation of ReNcell VM cells by SB431542. Flow cytometric data showing percentages of SB431542 treated cells positive for HuC/D (**A**), Tuj1 (**B**), S100β (**C**) and GFAP (**D**) differentiated for 3 days in the presence of SB431542 or DMSO as control. Data are presented as means ± SEM from at least three independent experiments. *p<0.05, **p<0.01, *** p<0.001 compared to time point control.

3.4.4 Analysis of the JAK/STAT3 pathway dependency

As described above, one of the effects of Wnt-3a and DAPT was the modulation of the neuronal differentiation and GFAP positive cells in ReNcell VM cells. The neuronal differentiation and GFAP are both regulated by transcription factors like HES5. Another well described transcription factor, which regulates GFAP together with HES5 (Nakashima et al., 1999, Kamakura et al., 2004) and therefore is able to regulate neurogenesis, is the signal transducer and activator of transcription 3 (STAT3). In 2006 Hao and colleagues demonstrated that Wnt-3a was able to upregulate STAT3 in mouse embryonic stem cells. Furthermore, Fragoso et al. (2012) identified Wnt-3a as an activator of STAT3, where an upregulation of phosphorylated STAT3 at Tyr 705, in the retinal pigment epithelium ARPE-19 cell line was observed. This led to the suggestion that Wnt-3a could act through the activation of pSTAT3.

3.4.4.1 Activation and inhibition of pSTAT3 in ReNcell VM cells

The first step to show an active STAT3 signaling pathway in ReNcell VM cells was to detect both the total STAT3 and the active form of STAT3, pSTAT3; at TYR705. Due to the fact, that STAT3 is a transcription factor which forms dimers and subsequently translocates into the nucleus (Darnell et al., 1994) the second step was to detect nuclear pSTAT3. This activation and translocation can be activated with the small molecule AICAR (Zang et al., 2008) and be inhibited by Jak-Inhibitor-1 (Pedranzini et al., 2006).

In total cell lysates of differentiating ReNcell VM cells was a strong STAT3 as well as a faint pSTAT3 signal detectable (Figure 36, A). Furthermore, a pSTAT3 signal was slightly inducible by AICAR while STAT3 was not affected. Simultaneously, a modulation of STAT3 or pSTAT3 using the Jak-Inhibitor-1 was not detectable in total cell lysates (Figure 36, A). Therefore, nuclear levels of pSTAT3 and STAT3 were analyzed. There were no differences detectable in STAT3 levels (data not shown). But after 30 min of AICAR treatment was an increase of pSTAT3 detectable (Figure 36, B) while Jak-Inhibitor-1 decreased the amount of pSTAT3 by tendency.

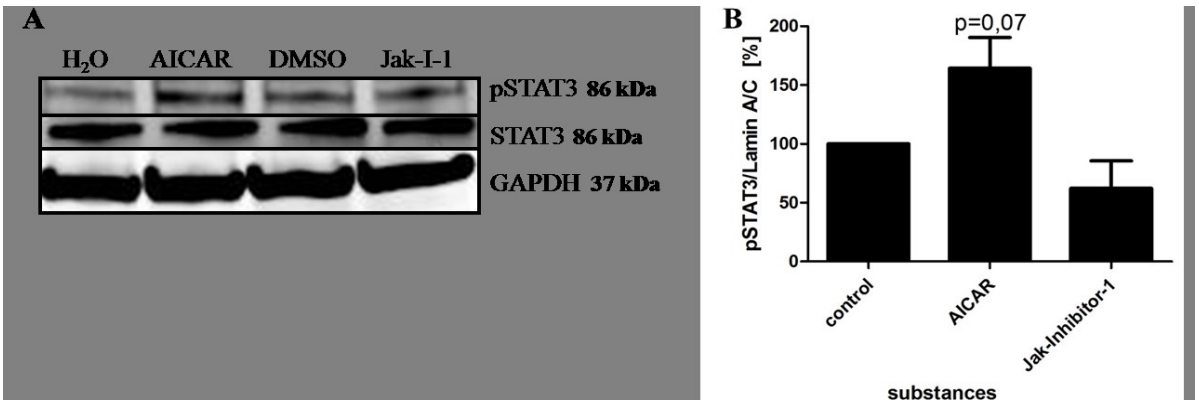

Figure 36: pSTAT3 and STAT3 in ReNcell VM cells. Western blot analysis of pSTAT3 and STAT3 in ReNcell VM cells in differentiation **A:** Western blot analysis of total protein lysates under 30 min H_2O, AICAR, DMSO or Jak-Inhibitor-1 (Jak-I-1) treatment. **B:** Quantification of western blot analysis of nuclear pSTAT3 in cells treated for 30 min with H_2O, AICAR, DMSO or Jak-Inhibitor-1 (Jak-I-1). Data are normalized to Lamin A/C (control set to 100 %). Data are presented as means ± SEM from three independent experiments.

STAT3 together with HES5 is able to induce GFAP and inhibit neurogenesis in rat and mouse NSCs (Gu et al., 2005, Cao et al., 2010). This led to the question, what effect a treatment with AICAR and Jak-Inhibitor-1 may have on differentiating ReNcell VM cells.

Strikingly, AICAR reduced the amount of cells positive for the neuronal marker HuC/D (Figure 38, A) and Tuj1 (Figure 38, B) drastically from 7 % of control cells, down to less than

1 %. Simultaneously, GFAP positive cells increased from 75 % up to 90 % (Figure 38, D), while S100β was not affected (Figure 38, C). Interestingly, treatment with Jak-Inhibitor-1 resulted in no significant changes in the amount of cells positive for the analyzed markers, however neuronal markers were reduced by tendency (Figure 38, A to D). Phase contrast microscopy analysis revealed undifferentiated cells as assessed by cell morphology of ReNcell VM cells compared to control cells which fits well with the observed reduction of neuronal markers (Figure 37). In contrast, cells treated with AICAR revealed no differences in their morphology compared to control cells (data not shown).

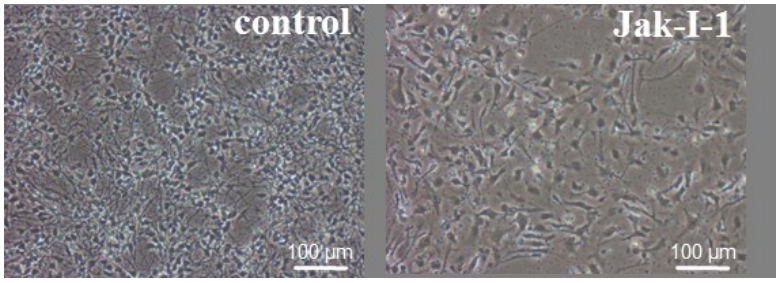

Figure 37: Treatment of ReNcell VM cells with Jak-Inhibitor-1 (Jak-I-1). Phase contrast of 3 days differentiated cells treated with 4 µM Jak-Inhibitor-1 or DMSO as control, respectively. Scale bar 100 µm.

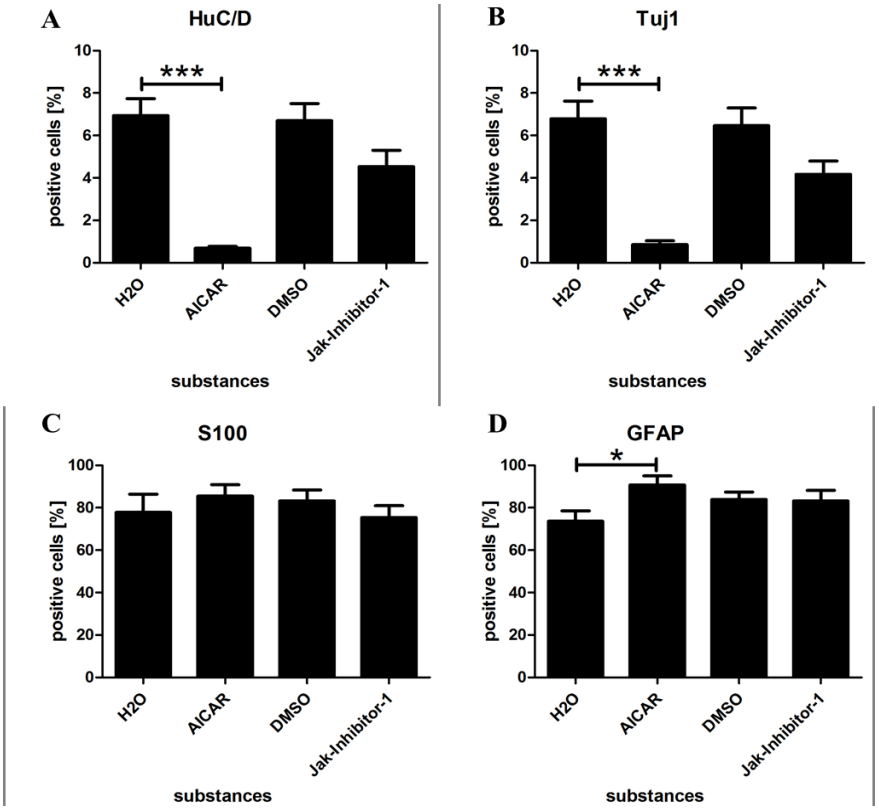

Figure 38: Modulation of ReNcell VM cells by AICAR and Jak-Inhibitor-1. Flow cytometric data showing percentages of AICAR or Jak-Inhibitor-1 treated cells positive for HuC/D (**A**), Tuj1 (**B**), S100β (**C**) and GFAP (**D**) differentiated for 3 days in the presence of AICAR, Jak-Inhibitor or H_2O or DMSO as control. Data are

presented as means ± SEM from at least three independent experiments. *p<0.05, **p<0.01, ***p<0.001 compared to time point control.

3.4.4.2 Does the Wnt or Notch pathway modulate pSTAT3?

The phosphorylation and translocation of transcription factors is fast and delicate. The analyzed time point was chosen by the fact that after 6 h Wnt-3a as well as DAPT were able to modulate GFAP levels. Analysis of the pSTAT3 level in nuclear cell extracts of ReNcell VM cells treated with Wnt-3a detected no significant changes compared to control cells (Figure 39). Treatment with DAPT instead led to a significant decrease of pSTAT3 compared to DMSO from 100 % down to 32 %. A similar downregulation was observable by treatment with DAPT+Wnt-3a (Figure 39).

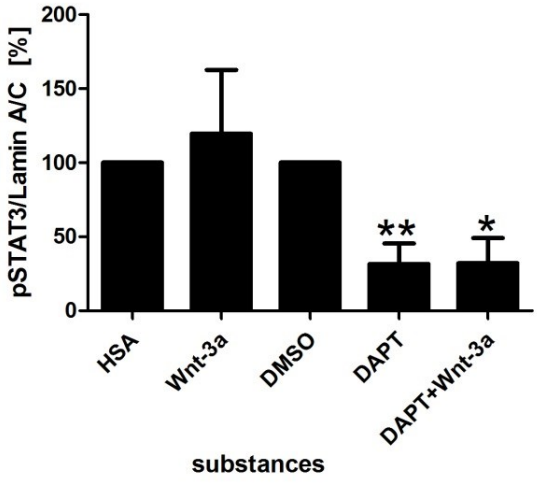

Figure 39: Modulation of pSTAT3 by Wnt-3a and DAPT. Western blots of nuclear pSTAT3 in cells treated for 6 h with HSA, Wnt-3a, DMSO, DAPT or DAPT+Wnt-3a were quantified. Data are normalized to Lamin A/C (HSA and DMSO control set to 100 %). Data are presented as means ± SEM from three independent experiments. *p<0.05, **p<0.01, ***p<0.001 compared to time point control.

Since DAPT was able to reduce pSTAT3, but Wnt-3a had no effect and AICAR was able to induce pSTAT3, it was analyzed whether AICAR was able to rescue the effect of DAPT on neurogenesis.

ReNcell VM cells were treated with DAPT and DAPT+AICAR for 3 days of differentiation. Afterwards, the amount of positive cells for the marker HuC/D, Tuj1, GFAP, and S100β was analyzed. Interestingly, AICAR was able to rescue the neuronal induction of DAPT. It reduced the amount of cells positive for HuC/D from 33 % down to 3 % (Figure 40, A) and

the Tuj1 positive cells from 20 % down to 1 % (Figure 40, B). Simultaneously, AICAR in combination with DAPT increased the amount of cells positive for S100β compared to DAPT alone (Figure 40, C). In addition, AICAR rescued the effect of DAPT on GFAP positive cells and increased the amount of positive cells up to 98 % from 70 % of DAPT or 85 % of DMSO treated cells, respectively (Figure 40, D).

In summary, DAPT was able to reduce nuclear pSTAT3 levels while Wnt-3a had no effect on pSTAT3 levels. Furthermore, AICAR was able to effectively inhibit the effect of DAPT on neuronal differentiation and on the numbers of cells positive for GFAP.

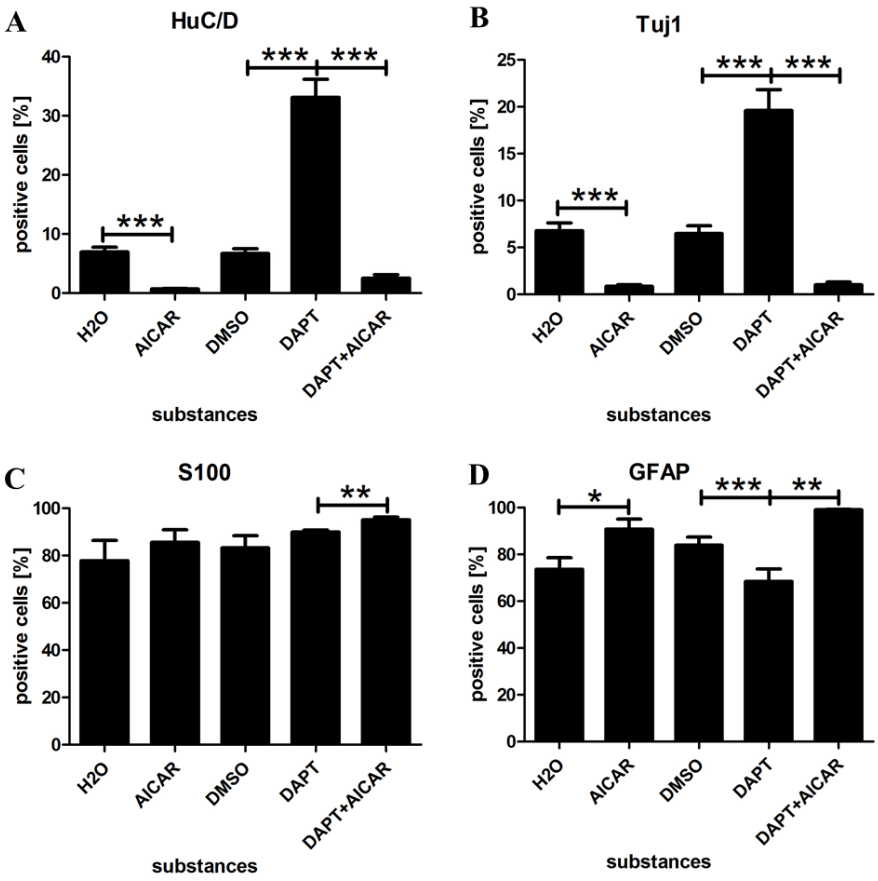

Figure 40: Modulation of ReNcell VM cells by AICAR and DAPT. Flow cytometric data showing percentages of treated cells positive for HuC/D (**A**), Tuj1 (**B**), S100β (**C**) and GFAP (**D**) differentiated for 3 days in the presence of AICAR+DAPT or H_2O or DMSO as control. Data are presented as means ± SEM from at least three independent experiments. *p<0.05, **p<0.01, ***p<0.001 compared to time point control.

3.5 Induced pluripotent stem cell derived neural progenitor cells (iPS-NPCs)

Signaling pathways are known to have different outcomes depending on the cellular context and time dependency. To verify the results observed using ReNcell VM cells and to clarify

that it is not a cell type depending phenomenon, another cell model was used. This model is based on neural progenitor cells (NPCs) which were derived from induced pluripotent stem cells (iPSC). These cells do express the same neural markers like ReNcell VM cells, Nestin and SOX2 (Trilck et al., 2013), and are able to differentiate into neuronal cells. Therefore, this cell line was ideal to verify the results obtained using the human neural progenitor cell line ReNcell VM.

3.5.1 The Notch pathway in iPS-NPCs

To demonstrate active Notch pathway in iPS-NPCs, DAPT was used to inhibit the Notch pathway. Similar to the ReNcell VM cell treatment, iPS-NPCs were treated once after induction of differentiation with 5 µM DAPT and HES1/HES5 mRNA levels were analyzed by qRT-PCR after 3 h, 6 h and 24 h. These time points were chosen because the first 24 h of differentiation seemed to be most important for the cell fate at least in ReNcell VM cells.
DAPT was able to reduce the HES1 (Figure 41, A) as well as the HES5 (Figure 41, B) mRNA levels. Strikingly, DAPT was able to reduce HES5 obviously more potent than HES1 levels, which was also observable in ReNcell VM cells (Figure 11). In the analyzed time points in NPCs no MASH1 or GFAP mRNA levels were detectable.

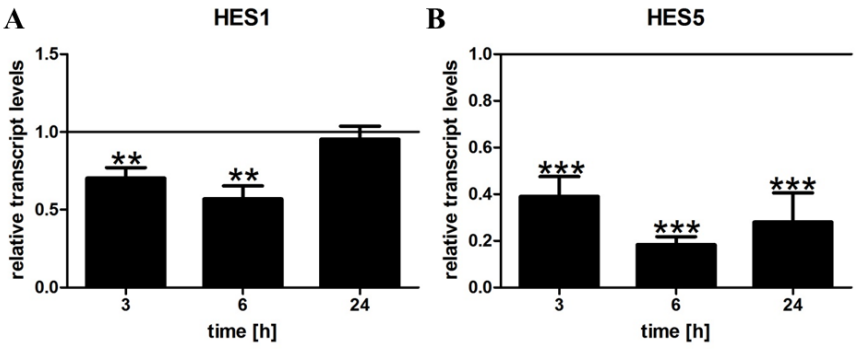

Figure 41: Inhibition of the Notch pathway in iPS-NPCs. qRT-PCR of HES1 (**A**) and HES5 (**B**), in cells treated with DAPT. Data are normalized to DMSO treated cells (time point control, indicated as black line). Data are presented as means ± SEM from at least three independent experiments. *p<0.05, **p<0.01, ***p<0.001 compared to time point control.

3.5.2 The effect of Wnt-3a in differentiating iPS-NPCs

As described before AXIN2 is one of the main target genes of the Wnt signaling pathway, therefore it was used to confirm the activation of the Wnt pathway in NPCs upon Wnt-3a

treatment. Furthermore, the effect of Wnt-3a on the Notch target genes HES1 and HES5 was analyzed.

Wnt-3a was able to significantly increase AXIN2 in iPS-NPCs (Figure 42, A) as well as in ReNcell VM cells (Hübner et al., 2010). Likewise it induced HES1 mRNA level after 3 h and 6 h (Figure 42, B) while HES5 levels were decreased after 6 h of treatment (Figure 42, C). Notably, HES1 induction was, compared to ReNcell VM cells, remarkably stronger and HES5 downregulation less prominent. Regrettably the standard deviations in some time points were very high. In addition, Wnt-3a treatment led to an increase of the active form of β-catenin (non-phosphorylated at SER33/37/THR41) in total cell lysates analyzed via western blot (Figure 42, D). Thus, Wnt-3a was able to induce the β-catenin dependent signaling pathway, which led to an increase of active β-catenin and afterwards an induction of AXIN2.

In summary, Wnt-3a was able to activate the β-catenin dependent Wnt pathway and induced HES1 and reduced HES5 mRNA levels after 6 h of treatment.

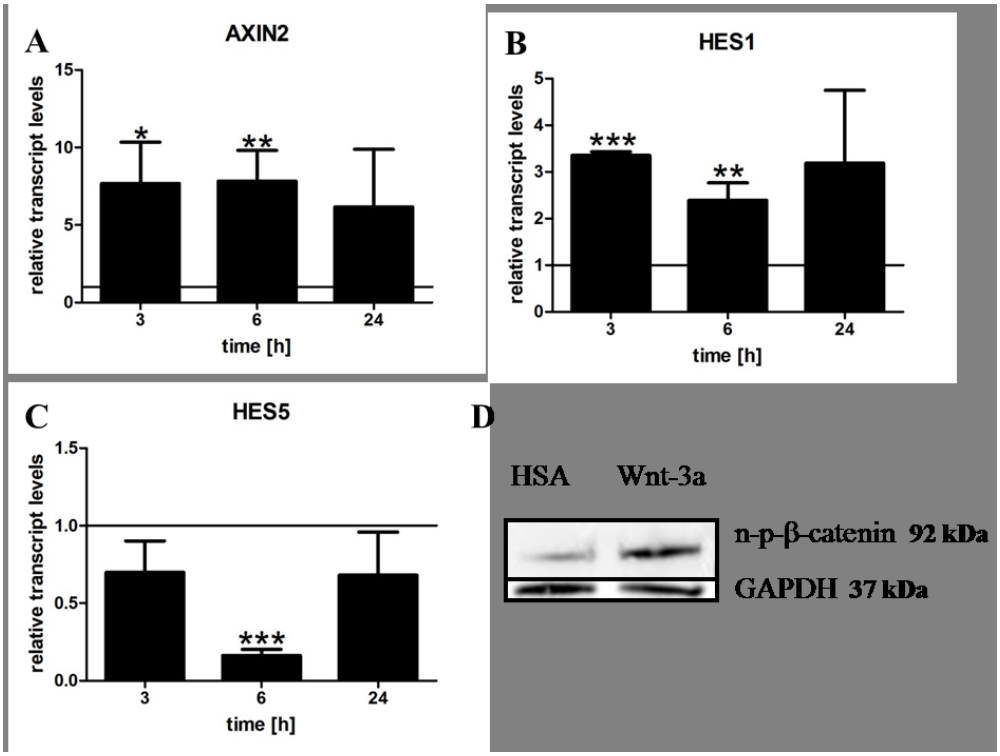

Figure 42: Activation of the Wnt pathway and modulation of Notch target genes by Wnt-3a in iPS-NPCs. qRT-PCR of AXIN2 (**A**), HES1 (**B**) and HES5 (**C**) in cells treated with Wnt-3a (100 ng/ml). Data are normalized to HSA treated cells (time point control, indicated as black line). Data are presented as means ± SEM from at least three independent experiments. *p<0.05, **p<0.01, ***p<0.001 compared to time point control. **D**: Western blot analysis of active non-phospho-β-catenin (n-p-β-catenin) under 6 h of Wnt-3a treatment.

3.5.3 The Wnt-3a and DAPT effect in the differentiation of iPS-NPCs

To verify the ReNcell VM cell results, iPS-NPCs were treated in combination with Wnt-3a plus DAPT and were compared to DAPT alone to illustrate the additive effect of Wnt-3a even to DAPT. Therefore the cells were treated once at the induction of differentiation with substances and the medium was changed every 48 h. In addition, the effects of Wnt-3a and DAPT treatment on the cell fate of iPS-NSCs were analyzed by detecting cells positive for the neuronal marker HuC/D, the mature glial marker S100β and the stem cell/glial marker GFAP. In the case of iPS-NPCs, GFAP has to be seen as a glial marker, in contrast to ReNcell VM cells, due to the fact that neither GFAP positive cells were detectable nor GFAP mRNA levels via qRT-PCR in proliferating cells (data not shown).

As described before, HES1 was reduced upon DAPT treatment, but could be induced by Wnt-3a+DAPT compared to DAPT alone after 3 h and 6 h of treatment (Figure 43, A). There was no Wnt-3a+DAPT induced regulation detectable after 24 h of treatment compared to DAPT alone, which was the same pattern as with Wnt-3a treatment alone (Figure 42, B). The double treatment with Wnt-3a+DAPT compared to DAPT alone had its most prominent effect on HES5 mRNA level after 6 h of treatment (Figure 43, B). Which was the same time point were Wnt-3a alone was able to reduce HES5 most of all. Interestingly, Wnt-3a only in combination with DAPT was able to reduce HES5 after 3 h and 24 h significantly compared to DAPT single treatment, while Wnt-3a alone was not able to reduce it compared to HSA (Figure 42, C). DAPT as well as Wnt-3a+DAPT were able to significantly reduce the amount of cells positive for the glial marker GFAP compared to DMSO (Figure 43, E). But the effect of DAPT and Wnt-3a+DAPT was most prominent in S100β positive cells (Figure 43, D). S100β was significantly reduced by Wnt-3a+DAPT down to 20 % compared to DAPT treated cells (30 %) or DMSO treated cells (47 %). A significant reduction of S100β upon Wnt-3a treatment was not detectable but a tendency was observable. Surprisingly, there were no differences of HuC/D positive cells detectable (Figure 43, E).

In summary, Wnt-3a alone was not able to significantly modulate the fate of differentiating iPS-NPCs. But Wnt-3a+DAPT induced HES1 while HES5 was reduced compared to DAPT. In addition the double treatment was able to reduce the glial marker GFAP and S100β significantly compared to DMSO; whereas the already high amount of HuC/D positive cells was not changed.

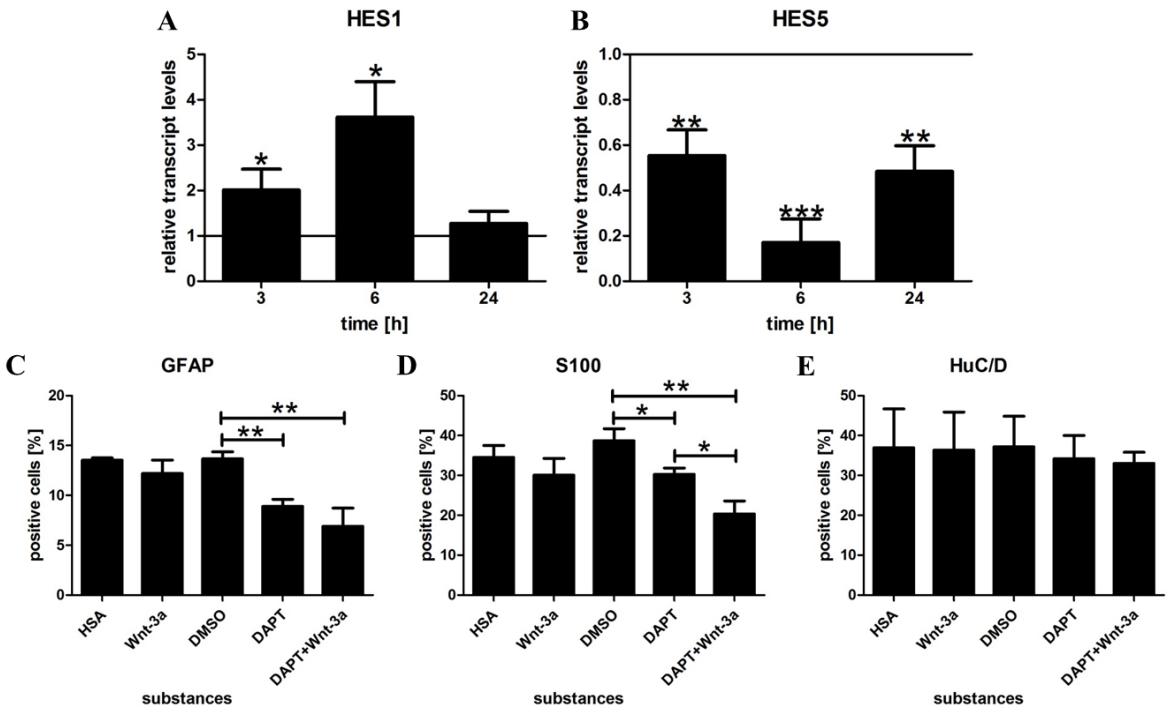

Figure 43: Modulation of genes in iPS-NPCs. A-B: qRT-PCR of HES1 (**A**) and HES5 (**B**) in cells treated with DAPT+Wnt-3a. Data are normalized to DAPT treated cells (time point control, indicated as black line). **C-E:** Flow cytometric data showing percentages of treated cells positive for GFAP (**C**), S100β (**D**) and HuC/D (**E**) differentiated for 18 days in the presence of Wnt-3a, DAPT, DAPT+Wnt-3a or DMSO or HSA as control. Data are presented as means ± SEM from at least three independent experiments. *p<0.05, **p<0.01, ***p<0.001 compared to time point control.

4 Discussion

The most challenging diseases of humankind are the neurodegenerative diseases, since degeneration of neurons is irreversible and often lethal. Currently, we are not able to cure diseases like stroke or spinal cord injuries. A promising approach is the stem cell therapy. But at the moment there is, due to the fragmentary knowledge of differentiation of human neural stem and progenitor cells, no successful therapy availably (Martino and Pluchino, 2006).

Differentiation of NPCs is controlled by a multitude of different pathways and their crosstalk, which regulates the neurogenesis as well as gliogenesis. Understanding these mechanisms will definitely provide the basis for directing differentiation of human NPCs for clinical applications. However, most of the knowledge is based on murine models and derived cell systems. Therefore, the cells of choice for identifying the pathways underlying neuronal differentiation are human neural progenitor cells like ReNcell VM cells, which have two defining properties: self-renewal and multipotentiality. These cells have the ability to differentiate into multiple neuronal cell types. ReNcell VM cells are a v-myc retrovirally immortalized human cell line and were derived from the ventral midbrain of a 10-week old male fetus (Donato et al., 2007). This cell line is able to differentiate after 3 days into S100β positive astrocytes and into HuC/D and Tuj1 positive neurons. Furthermore, proliferating cells express the neuronal marker Nestin and SOX2 as well as GFAP.

The glial fibrillary acidic protein (GFAP) belongs to the intermediate filaments which are regulated developmentally and tissue-specific. It was mainly described as a marker protein for mature astrocytes (Gomes et al., 1999). However, recent findings reveal GFAP, in addition, as a marker for neural stem cells. For example Garcia et al., 2004 clearly showed that GFAP-expressing progenitors are the principle source of constitutive neurogenesis in adult mouse forebrain. Furthermore, GFAP gene deletion seems not to have a distinct effect on neurogenesis or gliogenesis in mice (Gomi et al., 1995, Pekny et al., 1995). In the here used ReNcell VM cells GFAP is already expressed in proliferation and therefore cannot exclusively be seen as a mature astroglial marker. On this account GFAP was used as a marker for neural stem and progenitor cells.

4.1 Generation of pCAGGS-hHES vectors

The generation of pCAGGS-hHES vectors was successful, but due to the fact that at the beginning of this work the hHES proteins were not detectable in western blot analysis, it was

tried to add a HA-tag to the hHESs to facilitate detection. At first, expression vectors with an N-terminal tag were produced, because Kamakura et al. (2004) were able to overexpress N-terminal tagged GST-HES fusion proteins in mouse E13 neuroepithelia cells. Afterwards, good working antibodies were obtained and the protein levels were again analyzed by western blot, but HA-hHES failed to be higher expressed than non-tagged vectors in ReNcell VM cells. While pCAGGS-HA-hHES5 was able to verify the protein size of hHES5 (Figure 49), hHES1 failed to be expressed using pCAGGS-HA-hHES1 (Figure 48). It is possible that the HA-tag inhibits the correct HES1 folding subsequently inducing its rapid degradation and therefore was not visible in western blot analysis.

4.2 The Notch pathway in ReNcell VM cells

To activate the Notch pathway the Notch transmembrane receptor has to be cleaved at two different sites. One is located at the outside of the membrane and releases the Notch extracellular domain (S2-cleavage) and the second is located at the inside of the membrane (S3-cleavage), which releases the Notch intracellular domain (NICD). This NICD can translocate to the nucleus and induce the transcription of the target genes like HES1 and HES5. There are 4 described Notch receptors in mammals and each release a different intracellular domain (1-4), in addition, NICDs are acting context depended (Bay, 2006). In human esophageal keratinocytes it was indicated, that NICD1 siRNA is able to downregulate HES5 mRNA levels (Ohashi et al., 2010). While Breunig et al. (2007) were able to classify NICD1 as an important Notch intracellular domain in GFAP positive mouse hippocampal cells, there is no such classification for human neural progenitor cells.

Detection of the Notch intracellular domain 1 in differentiating ReNcell VM cells via western blot (Figure 11, B) suggested a regulatory role for NICD1 in human neural progenitor cells. This suggestion was supported by the activation as well as inhibition of NICD1 and its effect on neurogenesis. Precisely, NICD1 overexpression significantly reduced the amount of cells positive for neuronal markers (HuC/D and Tuj1; Figure 12, C and D). In contrast, the known Notch inhibitor DAPT increased the amount of cells positive for neuronal markers and decreased the amount of GFAP positive cells (Figure 12). Reduction of Notch target genes HES1/HES5 upon pharmacological inhibition of Notch signaling using DAPT (Figure 11) revealed that Notch signaling is active in ReNcell VM cells and controls neuronal differentiation. This was described before in other cell systems like hESC-derived NESs by Woo et al. (2009) and Borghese et al. (2010).

DAPT is a small molecule which is able to inhibit a variety of γ-secretases. Therefore, it inhibits not only the release of the Notch intracellular domain but also affects other proteins, which leads to multifarious ramifications. On that account, a rescue experiment verified the specific Notch depended effect. In this experiment the induction of neurogenesis by DAPT was rescued by overexpression of NICD1 (Figure 12). Simultaneously, the reduction of GFAP positive cells by DAPT was also rescued by NICD1 overexpression. Over all, DAPT reduced the mRNA level of the Notch target genes HES1 and HES5 significantly. Interestingly, HES5 was stronger affected than HES1 (Figure 11). This phenomenon has been shown before by Nelson et al. (2007) in chicken E4.5 retinal explants, where DAPT reduced HES5 levels (15-fold) more than HES1 levels (2-fold). Furthermore, Hartl et al. (2008) revealed that in mouse E13.5 (peak of neurogenesis) Notch1 protein and ICD were downregulated in the same magnitude like HES5, while HES1 was upregulated. In contrast, the activation of the Notch pathway by overexpression of NICD1 led not only to an augment of NICD1 but also induced the expression of HES5 while HES1 was decreased (Figure 12). This demonstrates a clear regulation of HES5 transcript levels by NICD1, but arises the question if NICD1 alone regulates HES1. A similar observation was made by Haupt et al. (2012), where the introduction of NICD1 into mouse and human neural stem cells resulted in a higher increase of HES5 than HES1. In addition, it was shown before that HES1 is not solely regulated by Notch (Kageyama et al., 2008). Moreover it is able to be modulated by other pathways (for example Shh; Wall et al., 2009) and by basic helix loop helix transcription factors, for example HES5 or itself (Takebayashi et al., 1994, Kageyama et al., 2009). In contrast, Wu et al., 2002 showed a downregulation of HES5 by HES1 overexpression in rat E14.5 spinal cord cells, which underlines a bilateral interaction.

This work shows that NICD1 and DAPT, and therefore Notch, not only regulate the target genes HES1 and HES5 but also the GFAP and the proneural gene MASH1 (ASCL1; Figure 11 and Figure 12). In addition, a clear downregulation of GFAP, on mRNA level as well as in FACS analysis, by DAPT and the rescue of the protein level by NICD1 overexpression were observed. Strikingly, the regulation of HES1 as well as HES5 by DAPT is very fast, within 2 h, while GFAP is significantly inhibited not until 12 h (Figure 11). This suggests a direct regulation of HES but not a direct regulation of GFAP. The temporal delay suspects a direct regulation of HES, which in turn leads to a regulation of GFAP by HES. This assumption was confirmed in E14.5 rat glial restricted precursors by Wu et al. (2002) and in primary mouse neuroepithelial cells by Kamakura et al. (2004) as well as in mouse mesencephalic neural

crest cells by Ijuin et al. (2008). In contrast, Ge et al. (2002) professed a direct regulation of GFAP by CSL (RBP-J; CBF1/Su(H)/Lag-1) in rat cortical NPCs, but simultaneously predicted a cell context dependent mechanism of GFAP regulation. So it is possible, that Notch can activate GFAP by a direct binding of CSL to the GFAP promoter in rat cortical NPCs but not directly in human fetal ventral midbrain derived ReNcell VM cells.

There is a variety of proneural genes in neural progenitors known to be negatively regulated by HES, like MASH1 (ASCL1), Neurogenin 1, and Neurogenin 2. These genes are known to drive NPCs to a neuronal differentiation (Castella et al., 1999, Kageyama et al., 2009). In ReNcell VM cells only MASH1 mRNA level was able to be detected via qRT-PCR, Neurogenin 1 and 2 levels could not be quantified due to very low mRNA levels (data not shown). The time delay between MASH1 regulation and the start of DAPT treatment (6 h; Figure 11) suggests an indirect regulation of MASH1 by HES. Precisely, HES1 and HES5 were described to inhibit MASH1 function by competitively binding to its heterodimeric bHLH partners E12 and E47 (Nakashima et al., 2001). In contrast, Kageyama et al. (2008) reckoned a direct binding of HES factors to MASH1, which leads to heterodimers who were not able to bind DNA. In both ways a reduction of HES leads to an augment of free and therefore active MASH1 which in turn can drive NPCs in a neuronal differentiation.

4.3 The effect of Wnt-3a treatment and Notch inhibition in the differentiation of ReNcell VM cells

Wnt-3a was previously known as a classical “canonical” (β-catenin dependent-) Wnt pathway ligand. In this “canonical” pathway Wnt-3a binds to the receptor Frizzeld and to the co-receptor LRP6 to inhibit the destruction complex and stabilizes β-catenin (Gordon and Nusse 2006; Angers and Moon 2009). But Avila et al. (2010) detected that Wnt-3a can also activate the “non-canonical” Ca^{2+} dependent pathway in mature hippocampal rat neurons.

Our working group was able to show, that Wnt-3a activates the β-catenin dependent Wnt pathway (Hübner et al., 2010, Mazemondet et al., 2011) as well as (the β-catenin independent) Ca^{2+} pathway (personal communication: V. Talabatulla) in ReNcell VM cells. In addition, Wnt-3a was able to increase the neuronal differentiation of ReNcell VM cells, shown in Wnt-3a overexpressing cells and cells treated with recombinant protein. In detail, Wnt-3a augmented HuC/D and Tuj1 positive cells, while stabilized β-catenin failed to mimic this effect (Hübner et al., 2010). This led to the suggestion of a β-catenin independent effect of Wnt-3a on ReNcell VM cells. In this work, the induction of the neuronal differentiation by

treatment with recombinant Wnt-3a was confirmed (Figure 16). In addition, a reduction of GFAP was detectable, while S100β was not affected (Figure 16). Similar results were detected via Wnt-3a transfection, where the transcript levels of the stem cell marker Nestin were reduced by Wnt-3a overexpression but not by overexpression of S33Y, the stabilized form of β-catenin (Hübner et al., 2010). This suggests that Wnt-3a increases the neuronal differentiation by reducing the stem-cell-ness of ReNcell VM cells and therefore pushing the cells to differentiation.

Simultaneously, Wnt-3a modulated the Notch target genes HES1 and HES5. As outlined above, HES genes are known to regulate neurogenesis as well as gliogenesis in a plurality of different cell models (Ohtsuka et al., 2001; Wu et al., 2002; Kageyama et al., 2008). Precisely, HES5 was downregulated after 3 h up to 24 h with a short period without a significant downregulation at 8 h and 12 h of treatment (Figure 14). In contrast, HES1 was upregulated in early time points (2 h, 6 h and 8 h) and not significantly regulated in later time points (Figure 14). Compared to Hirsch et al. (2007), where the HES5 mRNA levels were regulated in the same way, while HES1 levels were decreased after 24 h-treatment with Wnt-3a in neonatal mouse cortical neural progenitors. The differences may be occurring due to the source of the cell lines and the different cell contexts. Furthermore, HES1 is known to be modulated by different pathways such as the Wnt signaling pathway in a cell context dependent manner (Peignon et al., 2011), this interaction may cause the differential regulation. While Jörgi et al. (2002) described, that it is possible that differentiation is initiated by a short-lived upregulation of HES1 (in PC12 cells), DAPT treatment, which induced a fast and strong downregulation of HES1, clearly resulted in a marked increase in neuronal differentiation. This displays that the short induction of HES1 is not mandatory for the differentiation in ReNcell VM cells. But the strong, fast and consistent modulation of HES5 led to the suggestion, that it is directly regulated by Wnt-3a and is important for the neural differentiation. Furthermore, it seems to be sufficient to downregulate HES5 for 24 h to influence the differentiation as seen by Wnt-3a treatment.

The mRNA level of GFAP was significantly downregulated by Wnt-3a after 6 h (Figure 14, C). This short time delay of 6 h may be due to an indirect regulation of GFAP. As outlined before, GFAP is in the majority of cases directly upregulated by HES5 and only in a second plain by Wnt-3a. But compared to the HES5 mRNA levels, GFAP levels did not get back to control levels after 24 h, instead, they kept downregulated. In sum, these data show that Wnt-3a induces a temporary HES5 downregulation which in consequence potentially leads to a

reduction of GFAP. This effect may be caused by a disruption of the HES oscillation. It is known, that the oscillation of HES genes is important such as for a functional segmentation clock, but also occurs in the proliferation and differentiation of stem cells (Kageyama et al., 2007, Kageyama et al., 2012). In addition, Nakaya et al. (2005) described Wnt-3a as a modulator of this segmentation clock, by regulating the Delta/Notch pathway. But in comparison, DAPT was not able to reduce GFAP in a stronger way than Wnt-3a, despite it had a stronger effect on HES5 mRNA levels at all-time points. This suggests that HES5 may be a mediator of the Wnt-3a effect but does not solely regulate GFAP, which is also observable by HES5 overexpression where GFAP mRNA levels were reduced (Figure 27). It is also possible, that the disruption of the putative HES5 oscillation led to a more prominent effect when it occurs at an early time point (up to 24 h) and when the oscillation is restored after 24 h. To further analyze the effect of the HES oscillation on differentiation it would be needed to do single cell analysis. Due to the fact, that ReNcell VM cells are not synchronized, an oscillation would likely not be detected by total mRNA or protein level analysis.

Interestingly, MASH1 significantly increases after 24 h of Wnt-3a treatment, when HES1 is no longer upregulated but HES5 displayed its strongest downregulation (Figure 14). On the first glance this would suggests a HES5 dependent regulation of MASH1 and not a HES1 dependent regulation, as it was described by Kageyama et al. (2008). But Fischer et al. (2007) reported a model in which HES1 is able to be an activator of MASH1 by binding to the transcriptional co-factor CBP or, in contrast, be a repressor by binding to the transcriptional co-factor TLE. The fact that MASH1, HES1 and HES5 were stronger affected by DAPT than by Wnt-3a, leads to the suggestion that MASH1 is a direct target of HES and, while HES is a target of Wnt-3a, only an indirect target of Wnt-3a. In this case, it is not possible to discriminate which HES regulates MASH1 or if both are necessary. Further analysis with a specific knockdown of HES1 and/or HES5 may reveal an answer to that question. Unfortunately, a knockout of one of the two HES genes in mice did not lead to a phenotype, only double knockout mice exhibit premature neurogenesis (Hatakeyama et al., 2004), which may be due to a potential compensatory effect.

While Wnt-3a is able to modulate Notch target genes and DAPT is more potent to do that, it arises the question if it is able to act in addition to DAPT. A direct regulation of Notch by Wnt-3a is not probabilistic to be the solely modulator of the “Wnt-3a-effect” on neuronal differentiation, because Wnt-3a was able to modulate the Notch target genes in reverse directions and GFAP in a more secular way than DAPT. Therefore, the cells were treated in

combination with Wnt-3a and DAPT and were compared to DAPT single treatment. This method visualizes the additive effects of Wnt-3a on target genes compared to DAPT (Figure 15). Strikingly, Wnt-3a was still able to upregulate HES1 mRNA level after 2 h of treatment despite the downregulation of HES1 using DAPT. In total, HES1 mRNA was 3-fold upregulated compared to DAPT single treatment, respectively, around 1.5-fold compared to HSA/DMSO. But after 6 h and 48 h, Wnt-3a reduced the HES1 mRNA level even further than DAPT alone. So there is an additive effect of Wnt-3a on HES1 mRNA detectable, but its effect seems to be time dependent. In contrast, the downregulation of HES5 mRNA was further decreased by Wnt-3a, compared to DAPT alone, in nearly all time points analyzed. This shows a more distinct impact of Wnt-3a on HES5 than on HES1 mRNA levels. Together with the observation that DAPT had also a more potent effect on HES5 than on HES1, HES5 seems to be straighter regulated than HES1 in differentiating ReNcell VM cells.

The GFAP mRNA level was already after 3 h of double treatment with DAPT+Wnt-3a significantly downregulated compared to DAPT alone (Figure 15). This implies a strong additive effect of Wnt-3a on the regulation of not only direct Notch target genes, but also on the proposed indirect target of Notch, namly GFAP. In addition, the effect on mRNA level was verified with FACS analysis, where the DAPT+Wnt-3a treated cells positive for GFAP were significantly decreased compared to DMSO as well as compared to DAPT (Figure 16). Simultaneously, Wnt-3a had no additive effect on the mRNA level of the proneural gene MASH1 (Figure 15) and nor on the amount of cells positive for the neuronal markers HuC/D and Tuj1 compared to DAPT single treatment (Figure 16). But in both cases was a tangentially increase detectable, which was significantly when compared to DMSO. The Wnt-3a effect and the additive effect of Wnt-3a compared to DAPT treated neural progenitor cells is described for the first time in this work. This outstanding decrease of GFAP positive cells in combination with the highest increase of cells positive for the neuronal markers is a remarkably step forward to drive NPCs to neurons instead of glial cells. In conclusion, Wnt-3a seemed to have a straight effect on HES5, which in turn had a straight effect on GFAP and MASH1, which finally regulated the fate of differentiating ReNcell VM cells to an increase in neuronal differentiation and a decrease of GFAP (Figure 16). In contrast, DAPT had a more potent effect on HES1 and HES5 and maybe, therefore, a stronger effect on MASH1 and on the differentiation to neurons but affected GFAP less potent than Wnt-3a. This lead to the suggestion that Wnt-3a upregulates the neuronal differentiation by reduction of the stemness, which can act in addition to the DAPT-induced increase of neurogenesis.

4.4 Time dependency in the differentiation of ReNcell VM cells

The cells were treated once with Wnt-3a (100 ng/ml) at the beginning of differentiation (time point 0 h), this may be the reason why Wnt-3a lost its impact on HES genes after 24 h. Taelman et al. (2010) clearly showed a sequestration of the Wnt induced receptor signaling complex into multivesicular bodies but were not able to finally discover the fate of the Wnt ligand. They found a co-localization of the multivesicular bodies and Rab7, a lysosomal marker, which may led to the suggestion that the Wnt ligand can be degraded in the lysosomes and therefore depleted. Taken together, Wnt-3a may lose its impact on target genes because it was depleted during differentiation.

It is widely known that the output of the Wnt signaling pathway and also of the Notch pathway is extremely cell context dependent. In addition, the time plays a major role, too. This led to the analysis of the time dependency of the "DAPT/Wnt-3a effect" on differentiating ReNcell VM cells, which was not described before in the literature and, therefore, is a complete new experimental design. Cells were treated once with substances, these were washed out after an indicated time period and after a total of three days of differentiation cells were analyzed. All cells were differentiated for three days but with a changing time frame of differentiation, in combination with substances. In all analyzed markers the first significant effects were detectable after 24 h of treatment, while the strongest effects were reached after 48 h of treatment (Figure 18). This reveals a time frame were the substances are able to effect the differentiation of ReNcell VM cells. In sum, the cells have to be treated for at least 24 h to direct them into a neuronal fate. A longer treatment of 48 h, results in a stronger effect, but a treatment for 72 h did not resulte in a further augment. This suggests that the effect is saturated after 48 h and a further increase is unlikely.

The differences between the two neuronal markers HuC/D and Tuj1 are of interest. While the first Tuj1 positive cells were detectable after treatment for 24 h, the first HuC/D positive cells were observable after treatment for 3 h, where all cells were differentiated for 3 days (Figure 18). This indicates HuC/D as a very fast and sensitive neuronal marker. Hu proteins are RNA-binding proteins to stabilize specific target mRNAs, HuC and HuD are, therefore, the earliest markers of the neuronal cell lineage (Perrone-Bizzozero and Bird 2013). In contrast Tuj1 is a β-tubulin which is able to heterodimerize with α-tubulins to form microtubules, which are essential components of the cytoskeleton. And it is a marker for terminally differentiated neurons of the central and peripheral nervous system (Perrone-Bizzozero and Bird, 2013). Therefore, the time-dependent differences of the neuronal markers are due to the different

source of the protein-marker. This means, a RNA-binding protein is usually faster affected by a cellular signal than a cytoskeleton protein and therefore a faster and more sensitive marker for changes in cell fate. This was, in addition, visible by cells differentiated for only 24 h. There was the significant effect of treatment detectable, precisely DAPT and DAPT+Wnt-3a were able to increase the amount of HuC/D positive cells compared to control (Figure 19).
Interestingly, the only significant reduction of S100β was detectable after 48 h of treatment with DAPT+Wnt-3a compared to DMSO (Figure 18). The effect was lost after 72 h of treatment due to the high standard deviation. But it shows that double treatment can have an effect on astrocytes and led not only to an increase of cells positive for neuronal markers.
To increase the neuronal differentiation, the cells needed to be treated right after the start of differentiation with the substances. After 18 h of differentiation the cells were able to change the differentiation program to neuronal differentiation, demonstrated by the increase of HuC/D positive cells, but were not able to finally differentiate into more mature -Tuj1 positive cells (Figure 20). As described above, HuC/D is an early marker for neuronal differentiation and therefore can be seen as a marker which is able to detect the beginning changes in neuronal differentiation. Tuj1, on the other hand, is a marker for more mature neuronal differentiation and therefore detects the final amount of mature neurons, respectively, the final outcome of the differentiation. The treatment did not have any effect on the amount of mature neurons, if treated after 24 h or 66 h (Figure 20). Simultaneously, the amount of cells positive for S100β and GFAP were not affected when treated after the start of differentiation. In summary, the cells have to be treated at the beginning of differentiation to significantly increase the amount of mature neurons and decrease the amount of GFAP positive cells. This shows that the cells need time to react on the treatment and also to run the whole differentiation program to finally differentiate into mature neurons.

4.5 The mechanism behind the Wnt-3a effect

The two major pathways controlling neuronal and glial differentiation are the Wnt and Notch Signaling pathways (Kunke et al., 2009; Kageyama et al., 2005). Over the past years, it became obvious that crosstalk of these pathways is fundamental in controlling events during vertebrate and non-vertebrate development. This work assessed the role of Notch signaling and its crosstalk with the Wnt/β-catenin pathway in the human neural progenitor cell line ReNcell VM.

4.5.1 Wnt pathway dependency

Our group previously showed that Wnt-3a as well as stabilized β-catenin and inhibition of GSK3 activate target genes of the Wnt/β-catenin pathway in ReNcell VM cells (Hübner et al., 2010; Mazemondet et al., 2011; Schmöle et al., 2010). Hübner et al. (2010) revealed moreover that Wnt-3a, but not stabilized β-catenin, is able to increase neurogenesis. In addition, stabilized β-catenin was not able to modulate Notch target genes HES1/HES5 or GFAP (Rayk Hübner, personal communication). This leads to the suggestion, that Wnt-3a may modulate the Notch pathway in ReNcell VM cells over Wnt-pathway-proteins upstream of β-catenin.

The main Wnt-pathway-protein upstream of β-catenin, which is known to be able to modulate a variety of different proteins such as SMAD1 and Notch, is GSK3β (Ribeiro et al., 2009). Taelman et al. (2010) detected that over 20 % of the proteome containing three or more consecutive potential GSK3 sites. Furthermore, Espinosa et al. (2003) suggested that Notch phosphorylation by GSK3β regulates crosstalk between the Notch and Wnt pathways. While Wnt-3a inhibits the GSK3β, its inhibition with small molecules should mimic the effects of Wnt-3a. But in ReNcell VM cells the inhibition of GSK3β by SB216763 and IM12 was not able to mimic the effect. While SB216763 was able to increase the mRNA level of AXIN2, it did not augment the mRNA levels of HES1, did not reduce HES5 or GFAP levels (Figure 21) in the same way like Wnt-3a and did not increase the amount of cells positive for HuC/D and Tuj1 or reduced the amount of GFAP positive cells (Figure 22). Interestingly, SB216763 reduced HES1 as well as HES5 mRNA levels in later time points and reduced the amount of cells positive for the mature astrocyte marker S100β. In summary, SB216763 did not mimic the effect of Wnt-3a and therefore seemed not to be the link between the Wnt and Notch pathway in ReNcell VM cells. While Taelman et al. (2010) described stabilized β-catenin as an inducer of the sequestration of the signaling complex (containing Wnt-3a, LRP6 as well as GSK3β) and while this sequestration inhibits GSK3β, confirms the inhibition of GSK3 that the Wnt-3a effect is independent of β-catenin.

There are plenty of different Wnt pathways known in the literature. Beside the best described pathway the β-catenin dependent pathway there are, in addition, a rising number of β-catenin independent pathways described. The main β-catenin independent pathways are the PCP- and Ca^{2+}-pathway but there are additional downstream events triggered by Wnts in combination with Frizzled or specific co-receptors like ROR and RYK (Niehrs 2012). In all described β-

catenin dependent pathways the co-receptor LRP5/6 is involved. The binding of Wnt to the co-receptor LRP5/6 can be inhibited in NPCs by Dkk-1 (Munji et al., 2011).

In ReNcell VM cells the effect of Wnt-3a on the mRNA level of Notch target genes is not inhibited by Dkk-1 while AXIN2 is significantly decreased (Figure 23). In addition, the induction of HuC/D and Tuj1 positive cells by Wnt-3a is as well not inhibited by Dkk-1 (see appendix 7.5). Furthermore, Dkk-1 treatment led to an additional decrease of HES5 mRNA level. This additional effect suggests a competitive mechanism of Wnt-3a in which Wnt-3a, can activate the β-catenin dependent pathway by binding to LRP and simultaneously activates the unknown "β-catenin, GSK3 and LRP independent" pathway. These two pathways are in competition with each other for the Wnt-3a ligand. One can speculate that Dkk-1 inhibits the "β-catenin, GSK3 and LRP dependent" pathway, thus raising the level of Wnt-3a available to activate the "β-catenin, GSK3 and LRP independent" pathway which further decreases HES5. A similar effect was described by Nalesso et al. (2011). They found that Wnt-3a can simultaneously activate the β-catenin dependent pathway and the Ca^{2+} pathway with distinct and independent outcomes in human articular chondrocytes.

In contrast, the inhibition of the Wnt-3a and Frizzled receptor interaction by sFRP1 did not significantly modulate HES5 mRNA level compared to control, but increased it by tendency (Figure 24). To more clearly verify the impact of Frizzled in this pathway a better AXIN2 inhibition is needed to get a better view of the dependencies. Nevertheless, these data suggest a Wnt-3a effect which is not trigged by LRP or GSK3 neither by β-catenin. But it leads to the suggestion of an activation of a β-catenin independent pathway by Wnt-3a which was already demonstrated by V. Talabattula (personal communication) who was able to induce Calcium signaling by Wnt-3a treatment in ReNcell VM cells. In addition, the increase of components of the PCP pathway in differentiating cells suggested a possibly active or activatable pathway (Mazemondet et al., 2010). In addition, it is highly improbable RYK dependent due to the fact that it is activated by the cleavage of a γ-secreatase which releases its intracellular domain and starts transcription after translocation into the nucleus (Lyu et al., 2008). If the Wnt-3a effect depends on this pathway DAPT would inhibit this cleavage and, therefore, no additive effect of Wnt-3a and DAPT compared to DAPT would be detectable. In contrast, DAPT would inhibit the effect of Wnt-3a on the RYK dependent pathway.

In sum, the effect of Wnt-3a is independent of β-catenin, of the upstream protein GSK3β, of the co-receptor LRP5/6 and seems to be independent of the receptor Frizzled. Up to now there

is no pathway known in which Wnt is able to activate a pathway independent of Frizzled, therefore, independency of Frizzled should be verified.

4.5.2 Notch pathway dependency

As described before, the effect of DAPT on ReNcell VM cells depends on the Notch intracellular domain 1 (NICD1). In addition, the effect of Wnt-3a depends as well as DAPT effects on NICD1. As long as NICD1 was overexpressed, neither DAPT nor Wnt-3a was able to increase neurogenesis (Figure 25). This led to the suggestion that the DAPT as well as the Wnt-3a effect on neuronal differentiation depends on the Notch intracellular domain 1, which was able to augment HES5 while HES1 was decreased and without HES1 and HES5, NICD was unable to inhibit neurogenesis (Kageyama et al., 2008). To verify this effect of the NICD1, HES1 and HES5 were overexpressed. The overexpression of HES5 led to an inhibition of the neuronal differentiation of ReNcell VM cells (Figure 27). The inhibitory effect of HES5 on differentiation was described before in NSCs by Kageyama et al. (2008) and in rat embryonic neural stem cells by Liu et al. (2010). In contrast, DAPT, which inhibits HES5, was described to reduce proliferation and increase differentiation (Nelsen et al., 2007, Borghese et al., 2010). This was shown in the reduction of the stem cell marker GFAP in ReNcell VM cells. Unfortunately, the reduction of Wnt-3a+DAPT treated GFP-transfected cells positive for GFAP compared to HES5 overexpressing cells under control-treatment was not significant (Figure 27). This may be due to the experimental procedure since cells were transfected and transfected cells generally showed a higher amount of cells positive for GFAP.

Interestingly, the overexpression of HES1 inhibited the differentiation of the progenitor cells (Figure 30) but not to the same extent like HES5, while the amounts of HES transcripts in the overexpressing cells were similar. This led to the suggestion that HES5 had a stronger effect on differentiation than HES1. Furthermore, overexpression of HES5 (Figure 27) resulted in a stronger decrease of HuC/D and Tuj1 positive cells compared to HES1 overexpressing cells (Figure 30). In addition, the substances DAPT and Wnt-3a were still able to increase the amount of HuC/D positive cells when HES1 is overexpressed (Figure 30). In contrast, HES5 overexpressing cells were not affected by the substances (Figure 27). These data strongly suggest that HES5 is a modulator of the effect of Wnt-3a as well as DAPT. Simultaneously, the mRNA levels of HES5 and HES1 correlate with each other. Precisely, HES1 overexpression leads to a reduction of HES5 (Figure 31) and vice versa (Figure 28). The bilateral interaction of HES proteins was described before in mouse C3H10T1/2 cells by

Takebayashi et al. (1994) and in mouse spinal cord by Wu et al. (2002). But Hatakeyama et al. (2004), in addition, described that the HES proteins were able to compensate each other. But, it is the first time that this effect is verified in human neuronal progenitor cells. This may explain that the HES1 overexpressing cells did have a decreased amount of Tuj1 and HuC/D positive cells, despite HES5 was downregulated. Moreover, HES5 (Figure 28) as well as HES1 (Figure 31) overexpressing cells showed the expected downregulation of MASH1 mRNA levels. This fits to the upregulation of MASH1 under DAPT treatment (Figure 11), where in contrast the HES1 and HES5 mRNA levels were downregulated. Unfortunately, due to the potential compensatory effect and the bilateral interaction it was not possible to finally clarify which HES regulates MASH1. The MASH1 regulation is controversially discussed in literature. Cao et al. (2010) revealed a HES5 dependent regulation of MASH1 in striatal tissues from E14-E15 mouse embryos, while Zhang et al. (2009) described that HES1 repressed the transcription of MASH1 in mouse NPCs from the anterior subventricular zone. In contrast, Fischer et al. (2007) suspected that HES1 can function as an activator as well as an inhibitor of MASH1 depending on the present co-transcription factors. Precisely, they suppose that HES1 in combination with TLE (transducing-like enhancer of split) repress MASH1 and HES1 in combination with CBP (CREB binding protein) activates MASH1. In sum, without a deletion of HES1 or HES5 it will not be possibly to clarify wich HES is responsible for MASH1 regulation and even than it is difficulte to answer that question due to their compensatory effect. Therefore the MASH1 poromotor has to be analyzed to verify which HES binds to it.

Strikingly, the GFAP mRNA levels were clearly decreased by HES1 (Figure 31) and HES5 (Figure 28) overexpressing cells. However, the amount of GFAP positive cells was not affected (Figure 27 and Figure 30). It was suggested that decreased HES5 levels would lead to a decrease of GFAP as shown by Kabos et al. (2002) and Wu et al. (2002). In addition, Ijuin et al. (2008) reported that HES1 and HES5 overexpression induces GFAP expression in mouse mesencephalic neural crest cells, which were also GFAP positive in proliferation as ReNcell VM cells. This contradicts the results in ReNcell VM cells. The decrease of GFAP mRNA level was detectable at all time points between 0 h and 72 h and is not in line with the not changed amount of cells positive for GFAP. The differences may be due to the distinct methods used, the flow cytomeric analysis counts only positive cells but does not show a downregulation of the amount of GFAP protein in GFAP positive cells (data not shown). A feedback regulation is partially possible, due to the fact that GFAP mRNA level was

downregulated in all time points but the amount of positive cells was not changed after 3 days of differentiation. If a feedback regulation of GFAP would be true in ReNcell VM cells, this would lead to the suggestion that GFAP proteins have a very long half-life. Interestingly, Rolland et al. (1990) analyzed the expression and turnover of GFAP in astroglial primary cultures. They found via radioactive labeling two pools of GFAP, the first one was a fast decaying pool with a half-life of 16-18 h and the second was a stable one with a half-life of 5-6 days. It is possible that the overexpression of HES1 and HES5 led to a decrease of the mRNA level of GFAP, but the amount of cells positive for GFAP was not affected due to the protein half-life of 5-6 days. To check this hypothesis the amount of cells positive for GFAP should be analyzed after 6-7 days. It is not much known about the different GFAP pools, but they may occur due to distinct splice variations of GFAP. Thomsen et al. (2013) revealed that at least two of the 8 known splice variants have distinct subcellular localization patterns. In this work a qRT-PCR primer was used which is able to detect all splice variations without the variation GFAPγ. Therefore it can be speculated that GFAPγ may be the upregulated protein which is measured by flow cytometry while its mRNA level was not able to be detected.

4.5.3 BMP pathway dependency

The target genes ID1 and ID3 are the best described target genes of the BMP pathway (Obayashi et al., 2009). They were described to be regulated not only by BMP but additionally by Wnt-3a in C2C12 cells (Nakashima et al, 2005). Precisely, Fuentealba et al. (2007) revealed that GSK marked SMAD1 for degradation by phosphorylation. In contrast, Guo et al. (2009) described that Wnt-3a activates, over AXIN2 induction, the BMP inhibitor SMAD7. In ReNcell VM cells, Wnt-3a was not only able to decrease ID1 but, in addition, ID3 (Figure 32). However, inhibition of the BMP pathway was not able to mimic the effect of Wnt-3a. There are three well described substances to inhibit the BMP pathway. Noggin binds the ligand BMP2, 4 and 7 and therefore inhibits the SMAD1, 5, 8 and MAPK p38 (Yu et al., 2008). Dorsomorphin inhibits BMP4 induced signaling and does not affect MAPK p38 (Yu et al., 2008). SB431542 inhibits the TGF-β signaling pathway and therefore SMAD2 and 3 (Inman and Hill, 2002). Noggin led to an increase of HES5 mRNA level and simultaneously decreased the amount of HuC/D positive cells (Figure 33). Dorsomorphin did not affect HES5 or GFAP mRNA levels but reduced the amount of cells positive for HuC/D and Tuj1 (Figure 34). SB431542 treatment, in addition, was not able to affect the differentiation of ReNcell VM cells (Figure 35). This clearly showed that HES5 is not solely mandatory for the decision

if cells differentiate into neurons or not, otherwise the HES5 mRNA level would be augmented by Dorsomorphin alike by Noggin treatment. In sum, the reduction of ID1 and/or ID3 did not led to the increase of cells positive for neuronal marker by Wnt-3a treatment, due to the fact that ID reduction by BMP inhibitor led to a decrease of neurons. The differences between the inhibitors Noggin and Dorsomorphin may be due to the different inhibitory mechanisms. While Noggin binds the ligand BMP2, 4 and 7 and therefore inhibits the SMAD1, 5, 8 and MAPK p38, Dorsomorphin inhibits BMP4 induced signaling and does not affect MAPK p38 (Yu et al., 2008). But when the inhibition of ID led to a decrease of neurons it arises the question whether the Wnt-3a induced ID reduction counteracts the induction of neuronal differentiation. Thus ID1 and ID3 may have a compensatory role in regulating neuronal differentiation.

4.5.4 JAK/STAT3 pathway dependency

The signal transducer and activator of transcription 3 (STAT3) was described to negatively regulate the neuronal differentiation by regulating, in combination with other transcription factors, proneural genes and to stimulate astrogliogenesis by activating GFAP (Rajan et al., 1998 Nakashima et al., 1999). STAT3 is a transcription factor which, upon phosphorylation at Tyr 705 forms dimers and translocates to the nucleus (Darnell et al., 1994). Therefore an analysis via qRT-PCR would not be useful compared to other transcription factors which are not known to be regulated by posttranslational modifications like the bHLH genes HES1, HES5 and MASH1. In addition, no post-translational modifications are known for GFAP. The activation and translocation can be triggerd with the small molecule AICAR (Zang et al., 2008) and inhibited by Jak-Inhibitor-1 (Pedranzini et al., 2006).

At first, the detection of phosphorylated STAT3 in ReNcell VM cells demonstrated an active JAK/STAT3 pathway (Figure 36). In addition, AICAR was able to activate STAT3 and led to an augment of pSTAT3 in the nucleus, while Jak-Inhibitor-1 was only able to decrease the amount of pSTAT3 by tendency (Figure 36). Interestingly, cells treated with Jak-Inhibitor-1 showed a less differentiated phenotype than control cells (Figure 37). Constitutively active STAT3 was observed in a large number of human tumors stimulating cell proliferation and preventing apoptosis. The inhibition with Inhibitor 2 ((E)-2-cyano-N-[(S)-1-phenylethyl]-3-(pyridin-2-yl) acrylamide), in contrast, led to an induction of apoptosis in glioma cells (Swiatek-Machado et al., 2012). In ReNcell VM cells an obvious increase of apoptosis was not detectable via microscopy analysis, but an apoptosis assay would maybe reveal clearer

results. In addition, AICAR was able to strongly reduce the amount of cells positive for the neuronal marker HuC/D and Tuj1 while Jak-Inhibitor-1 only reduced them by tendency (Figure 38). In contrast, the amount of GFAP positive cells were increased by AICAR but not affected by Jak-Inhibitor-1 treatment (Figure 38).

In sum, pSTAT3 was found in ReNcell VM cells and AICAR was able to induce the phosphorylation of STAT3 at Tyr 705 and the subsequent dimerization and translocation to the nucleus. The activation of the STAT pathway led to a decrease of neuronal differentiation and an increase of GFAP positive cells. This shows that the JAK/STAT3 pathway is active, is able to be modulated in ReNcell VM cells and its activation inhibits differentiation.

The γ-secretase inhibitor DAPT inhibits the Notch pathway and, therefore, reduces the amount of HES1 and HES5 in ReNcell VM cells (Figure 11). Kamakura et al. (2004) revealed that STAT3 is an effector of HES1 and HES5 mediated astrocytic differentiation in mice. They described HES as scaffolding proteins that induces STAT3 phosphorylation by JAK2 and, therefore, induces GFAP expression. This work revealed that the treatment with DAPT leads to a reduction of pSTAT3 (Figure 39) which maybe caused by the inhibition of HES1 and HES5. In contrast, the inhibition of PKC using the inhibitor GF109203X in ReNcell VM cells (Hübner, 2010), which subsequently activates the phosphorylation of pSTAT3 (Mattagajasingh et al., 2012), leads to an increase of Tuj1 and HuC/D positive cells. This underlines the impact of pSTAT3 on the differentiation of human neural progenitor cells. Furthermore, AICAR was able to inhibit the effect of DAPT on differentiating ReNcell VM cells (Figure 40). A small augment of pSTAT3 caused by AICAR seems therefore, to be able to inhibit the strong effect of DAPT. In sum data suggest, that the inhibitory effect of DAPT on the notch pathway is able to increase the neurogenesis by reduction of the active, while post-translational phosphorylated, STAT3. In contrast, the regulation of Wnt-3a seems to be independent of the post-translational phosphorylation of STAT3 because it did not significantly affect pSTAT3 (Figure 39).

Doubtful is the fact that GFAP is mainly regulated by STAT3, due to the fact that in ReNcell VM cells Wnt-3a (Figure 13) downregulates GFAP mRNA level stronger than DAPT (Figure 11). If STAT3 would primarily regulate the transcription of GFAP a decrease of pSTAT3 would lead to a decrease of GFAP mRNA. But the decrease of pSTAT3 was only detected by DAPT treated cells (Figure 39) and the decrease of GFAP mRNA was stronger and faster by Wnt-3a treated cells compared to DAPT treated cells. This contradicts the mechanism of a mainly by STAT3 regulated GFAP. It can be speculated that this contradicting regulation may

be due to the two different GFAP pools with different half-lifes. Hypothetically, DAPT may downregulate the stable GFAP pool over pSTAT3, which is detectable by FACS but not by qRT-PCR due to the splice variant GFAPγ. Wnt-3a, in contrast, maybe downregulates only the instable GFAP pool, GFAP mRNA levels without the GFAPγ, over a yet unknown mechanism.

4.6 Induced pluripotent stem cell derived neural progenitor cells (iPS-NPCs)

To verify that the described effects in ReNcell VM cells are not a cell-type specific phenomenon a second cell line was used. This cell line consists of neural progenitor cells which were derived from induced pluripotent stem cells. These cells express the same neural markers like ReNcell VM cells, Nestin and SOX2, and are able to differentiate into neuronal cells.

This work revealed that iPS-NPCs exhibit an active Notch pathway, detectable by HES1 and HES5 expression, which is able to be inhibited by DAPT (Figure 41). Interestingly, DAPT reduced the mRNA level of HES5 stronger than the HES1 mRNA level. These results are in common with the ReNcell VM cell results (Figure 11). But in contrast to ReNcell VM cells, the inhibition of HES1 and HES5 by DAPT did not change the amount of HuC/D positive cells and therefore had no detectable effect on neurogenesis in iPS-NPCs (Figure 43). This may be due to the high standard deviations or because of the already high (37 %) number of HuC/D positive cells compared to that 8 % of the ReNcell VM cells and suggest a saturating effect. The inhibition of the Notch pathway, furthermore, decreased the amount of cells positive for the glial marker S100β and GFAP (Figure 43). The amount of cells positive for the glial marker GFAP is, compared to ReNcell VM cells, strongly reduced, where 80 % of ReNcell VM cells and 14 % of iPS-NPCs are positive. This reduction may occur due to the fact that GFAP is a stemness marker in ReNcell VM cells and is already detectable in proliferating cells. In iPS-NPCs GFAP is solely a glial marker and may increase during differentiation length (Qian et al., 2000). The regulation of S100β by DAPT and DAPT+Wnt-3a in iPS-NPCs (Figure 43) is a clear difference compared to ReNcell VM cells (Figure 11 and Figure 15) and may be cell type specific. Another difference between ReNcell VM cells and iPS-NPCs is the speed of differentiation. While ReNcell VM cells need three days to differentiate into cells with neuronal morphology expressing neuronal markers, iPS-NPCs need at least 17 days. Since iPS-NPCs differentiated only for 48 hours in the presence of Wnt-

3a –afterwards the medium was changed-, this treatment duration may not be sufficient to promote the effect on neuronal differentiation. Thus iPS-NPCs have to be treated in the whole time of differentiation which means to treat them after every change of medium again.
Moreover, iPS-NPCs were able to respond to Wnt-3a. Precisely, Wnt-3a treatment led to an increase of active non-phosphorylated β-catenin protein, an augment of AXIN2 mRNA and to an induction of HES1 mRNA and a reduction of HES5 mRNA (Figure 42). These data demonstrate that Wnt-3a was able to activate Wnt/beta-catenin signaling accompanied by modulation of Notch pathway which was similar to ReNcellVM cells. In contrast, Wnt-3a was not able to affect the amount of cells positive for glial and/or neuronal markers (Figure 43). This may be due to high standard deviations, especially the cells positive for the glial markers were at least decreased by tendency. Furthermore, the additive effect of DAPT+Wnt-3a was similarly observable in iPS-NPCs (Figure 43) as well as in ReNcell VM cells (Figure 15). In both cell lines, Wnt-3a intensified the effects on HES1 and HES5 mRNA levels compared to DAPT treatment alone. This shows that even if Wnt-3a alone is not able to modulate HES genes and markers as effective as in ReNcell VM cells, the combinatory treatment is, like in ReNcell VM cells, able to strongly increase the effect of DAPT. The combination of DAPT and Wnt-3a, therefore, seems to activate an important mechanism of the neuronal differentiation in neural progenitor cells.
In sum, the modulation of HES1 and HES5 by Wnt-3a and DAPT+Wnt-3a in ReNcell VM cells were verified in iPS-NPCs but the effect on neuronal markers was not confirmed. Tomita et al. (2001) revealed that in the absence of proneural genes such as MASH1 the neuronal differentiation is inhibited and neural stem cells remain in earlier stages. Thus, the absence of MASH1 may be the reason that the amount of cells positive for the neuronal marker HuC/D was not changed.

4.7 ReNcell VM cells

ReNcell VM cells are a v-myc retrovirally immortalized human cell line and were derived from the ventral midbrain of a 10-week old male fetus. V-myc is the viral homologe of c-myc and is the most potent transforming gene known. The potency of neural progenitors to differentiate is not influenced by v-myc. But a v-myc transformation inhibits the potential to diffentiate under treatment with substances like retinoic acid (Lee et al 1999). There is no Wnt or Notch mediated regulation of v-myc known. However, Liu et al., 2011 showed that c-myc is stimulated by Wnt-3a in intestinal epithelial cells (IEC-6) through LRP6 and β-catenin.

This result does not influence the veracity of this work due to the fact that the Wnt-3a effect shown in this work is not mediated through LRP6 and β-catenin. It is not known if the overexpression of v-myc is able to modulate the Wnt pathway. Recently Zinin et al., 2014 discovered a negative regulation of Notch1, HES1 and HES5 by c-myc in radial glial precursors. In this work Notch1 is detactable in v-myc retrovirally transfected cell line (ReNcell VM cells) and seems not be strongly downregulated by v-myc. This maybe indicates a celltype specific regulation. In addition, HES1 and HES5 were detectable in ReNcell VM cells on RNA levels and protein levels.

In sum, ReNcell VM cells are a fast differentiating cell line of neural progenitor cells. The speed of proliferation and differentiation is maybe due to the v-myc transfection, but it is unclear if v-myc is able to modulte the Wnt and Notch pathway. Therefore in this study was also a second cell line used, the induced pluripotent stem cell derived neural progenitor cells which showed similar results like the ReNcell VM cells. This shows that the v-myc overexpression is not essential for the descriped Wnt-3a effect.

4.8 Outlook

The ReNcell VM cells are fast differentiating cells which are able to express neuronal markers and show the typical neuronal morphology after three days of differentiation. In contrast, iPS-NPCs need at least 17 days to differentiate. Due to the short treatment periode of 48 hours – afterwards the medium was changed - iPS-NPCs neuronal differentiation was not affected by treatment with Wnt-3a and DAPT. Thus iPS-NPCs have to be treated in the whole time of differentiation which means to treat them after every change of medium again. This could be done with conditioned medium from Wnt-3a overexpressing cells to reduce costs.

To confirm HES5 as the main mediator of the Wnt-3a and DAPT effect on neuronal differentiation, a specific knockdown of HES1 and/or HES5 is needed. Even if a knockout of one of the two HES genes in mice did not lead to a phenotype (Hatakeyama et al., 2004) may lead a knockout in neuronal precursor cells to a significant difference in neuronal differentiation and/or in MASH1 mRNA levels.

The inhibition of the Wnt-3a and Frizzled receptor interaction by sFRP1 did not significantly modulate HES5 mRNA level compared to control, but increased it by tendency (Figure 24). To more clearly verify the impact of Frizzled in this pathway a better AXIN2 inhibition is needed to get a better view of the dependencies. In addition an independency of Frizzled should be verified by a Frizzled knock out, because up to now there is no pathway known in

which Wnt is able to activate a pathway independent of Frizzled. This would be a completely new pathway induced by Wnt-3a.

5 Summary

The aim of this study was to shed light on the poorly understood network of signaling pathways which are responsible for the cell fate determination and differentiation of human neural progenitor cells initiated by Wnt-3a treatment and Notch pathway inhibition.

Wnt-3a was not only able to induce the β-catenin dependent Wnt pathway, but also regulated the Notch target genes HES1 and HES5 in a β-catenin independent manner, while stabilized β-catenin was not able to modulate them. Furthermore, Wnt-3a differentially regulated HES1 and HES5 independent of the Notch pathway while additive to the inhibition of Notch by DAPT. This regulation was independent of the β-catenin dependent pathway, because it was independent of GSK3β inhibition, independent of the formation of a Wnt-3a-LRP6-Frizzled receptor complex and independent of the inhibition of the BMP signaling pathway which is known to be initiated by Wnt ligands through β-catenin. This all suggested a β-catenin independent mechanism and therefore an activation of the β-catenin independent pathway by Wnt-3a. In sum, Wnt-3a activated a signaling cascade which activated HES1 transcription and inhibited HES5 and subsequently inhibited GFAP and increased MASH1 transcription while the phosphorylation level of STAT3 was not affected by Wnt-3a. The involved receptor combination is still unknown but was independent of LRP6 and possibly of Frizzeld. Simultaneously, using iPS-NPCs in this study revealed for the first time that the modulation of the Notch target genes by Wnt-3a is a common mechanism in human neural progenitor cells.

Wnt-3a was able to downregulate GFAP and upregulate MASH1 mRNA level which were not solely dependent on the modulation of HES5. Moreover, GFAP seemed to be stronger regulated by Notch inhibition through DAPT which in turn was strongly dependent on phosphorylated STAT3. AICAR, the inducer of pSTAT3, in contrast, could rescue the effect of DAPT on the amount of cells positive for GFAP. HES5, in the meantime, seemed to be involved in the glial differentiation but did not solely regulate the neuronal differentiation. Furthermore, HES5 seems to be regulated mainly by Notch and in ReNcell VM cells at least by NICD1, while HES1 was not solely modulated by Notch.

In the differentiation of ReNcell VM cells Wnt-3a was able to repress BMP pathway target genes, but this reduction was not responsible for the increase in neuronal differentiation since the inhibition of BMP signaling led to a decrease of cells positive for neuronal markers. This

suggests that Wnt-3a simultaneously initiated pro- and antineurogenic signal cascades which underlines that the final outcome of differentiation strongly depends on the cell context.

The differentiation of ReNcell VM cells needs 3 days to establish the maximal numbers of cells positive for the neuronal markers HuC/D and Tuj1. To modulate this process the first hours are crucial, 24 h after induction of differentiation the treatment is not anymore sufficient to increase neurogenesis. This demonstrates a defined time window for the modulation of the differentiation of ReNcell VM cells.

In sum, the combined treatment with Wnt-3a and DAPT and the thereout resulting increase of cells positive for neuronal markers and decrease of stemness marker is an outstanding step forward to drive NPCs from an undifferentiated state to neurons instead of glial cells which is a prerequisite for cell based therapies utilizing neuronal cells.

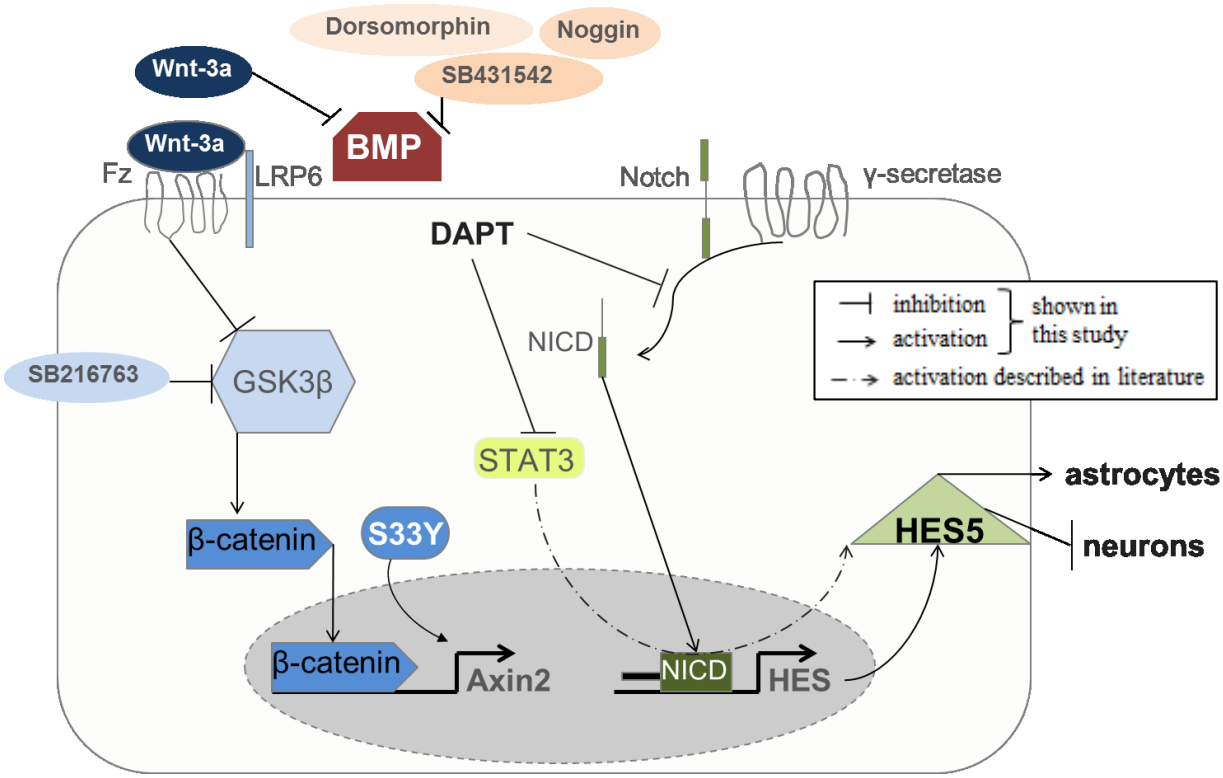

Figure 44: Simplified scheme of the crosstalk between Wnt-3a and the Wnt, BMP and Notch pathway in hNPCs. Blue: Wnt pathway components: when Wnt-3a binds to Frizzled and LRP5/6, GSK3β is phosphorylated and inactivated. This allows β-catenin to accumulate and translocate to the nucleus, where it activates the transcription of target genes like AXIN2. SB216763 can be used to inhibit GSK3β like Wnt-3a and S33Y is a stabilized form of β-catenin which is able to activate target genes upon overexpression. **Red:** BMP pathway components: Wnt-3a is able to inhibit the BMP pathway which does not lead to increased neuronal differentiation in hNPCs. BMP can also be inhibited by Dorsomorphin, SB431542 and Noggin. **Green:** Notch pathway components: The notch receptor is cleaved by γ-secretase to release NICD which translocates to the nucleus and starts transcription of the target genes HES.

6 Literature

Aberle H, Schwartz H, Kemler R. Cadherin-catenin complex: protein interactions and their implications for cadherin function. J Cell Biochem. 1996;61(4):514-23. Review.

Ables JL, Decarolis NA, Johnson MA, Rivera PD, Gao Z, Cooper DC, Radtke F, Hsieh J, Eisch AJ. Notch1 is required for maintenance of the reservoir of adult hippocampal stem cells. J Neurosci. 2010 Aug 4;30(31):10484-92. doi: 10.1523/JNEUROSCI.4721-09.2010.

Ables JL, Breunig JJ, Eisch AJ, Rakic P. Not(ch) just development: Notch signalling in the adult brain. Nat Rev Neurosci. 2011 May;12(5):269-83. doi: 10.1038/nrn3024. Review.

Ahn VE, Chu ML, Choi HJ, Tran D, Abo A, Weis WI. Structural basis of Wnt signaling inhibition by Dickkopf binding to LRP5/6. Dev Cell. 2011 Nov 15;21(5):862-73. doi: 10.1016/j.devcel.2011.09.003.

Androutsellis-Theotokis A, Leker RR, Soldner F, Hoeppner DJ, Ravin R, Poser SW, Rueger MA, Bae SK, Kittappa R, McKay RD. Notch signalling regulates stem cell numbers in vitro and in vivo. Nature. 2006;442(7104):823–826. doi: 10.1038/nature04940.

Angers S, Moon RT: Proximal events in Wnt signal transduction. Nat Rev Mol Cell Biol. 2009;10(7):468-477.

Avila ME, Sepúlveda FJ, Burgos CF, Moraga-Cid G, Parodi J, Moon RT, Aguayo LG, Opazo C, De Ferrari GV. Canonical Wnt3a modulates intracellular calcium and enhances excitatory neurotransmission in hippocampal neurons. J Biol Chem. 2010 Jun 11;285(24):18939-47. doi: 10.1074/jbc.M110.103028.

Bailey A M, Posakony J W. Suppressor of Hairless directly activates transcription of the Enhancer of split complex genes in response to Notch receptor activity. Genes Dev. 1995; 9:2609–2622.

Bandyopadhyay A, Yadav PS, Prashar P. BMP signaling in development and diseases: a pharmacological perspective. Biochem Pharmacol. 2013 Apr 1;85(7):857-64. doi: 10.1016/j.bcp.2013.01.004.

Bai G, Pfaff SL. Protease regulation: the Yin and Yang of neural development and disease. Neuron. 2011 Oct 6;72(1):9-21. doi: 10.1016/j.neuron.2011.09.012. Review.

Bray SJ. Notch signalling: a simple pathway becomes complex. Nat Rev Mol Cell Biol 2006;7(9):678-689.

Bayer SA, Altman J, Russo RJ, Dai XF, Simmons JA. Cell migration in the rat embryonic neocortex.J Comp Neurol. 1991 May 15;307(3):499-516.

Berndt, J. D. Mindbomb 1, an E3 ubiquitin ligase, forms a complex with RYK to activate Wnt/β-catenin signaling. J. Cell Biol. 194, 737–750 (2011).

Böhm C, Wassmann H, Paulus W. No evidence of tumour cells in blood of patients with glioma. Mol Pathol. 2003;56(3):187-9.

Borghese L, Dolezalova D, Opitz T, Haupt S, Leinhaas A, Steinfarz B, Koch P, Edenhofer F, Hampl A, Brüstle O. Inhibition of notch signaling in human embryonic stem cell-derived neural stem cells delays G1/S phase transition and accelerates neuronal differentiation in vitro and in vivo. Stem Cells. 2010 May;28(5):955-64. doi: 10.1002/stem.408.

Bovolenta P, Esteve P, Ruiz JM, Cisneros E, Lopez-Rios J. Beyond Wnt inhibition: new functions of secreted Frizzled-related proteins in development and disease. J Cell Sci. 2008 Mar 15;121(Pt 6):737-46. doi: 10.1242/jcs.026096. Review.

Breunig JJ, Silbereis J, Vaccarino FM, Sestan N, Rakic P. Notch regulates cell fate and dendrite morphology of newborn neurons in the postnatal dentate gyrus. Proc Natl Acad Sci U S A. 2007 Dec 18;104(51):20558-63.

Cadigan KM. TCFs and Wnt/beta-catenin signaling: More than one way to throw the switch. Curr Top Dev Biol. 2012; 98:1–34.

Cai J, Weiss ML, Rao MS. In search of "stemness". Exp Hematol. 2004;32(7):585-98. Review.

Cao F., Hata R., Zhu P., Nakashiro K., Sakanaka M. Conditional deletion of Stat3 promotes neurogenesis and inhibits astrogliogenesis in neural stem cells. Biochemical and Biophysical Research Communications 394 (2010) 843–847

Castella P, Wagner JA, Caudy M. Regulation of hippocampal neuronal differentiation by the basic helix-loop-helix transcription factors HES-1 and MASH-1. J Neurosci Res. 1999 May 1;56(3):229-40.

Chen D., Zhao M., Mundy G. R. Bone morphogenetic proteins. Growth Factors 22 233–241. doi: 10.1080/08977190412331279890.

Chen J, Lu L, Shi S, Stanley P. Expression of Notch signaling pathway genes in mouse embryos lacking beta4galactosyltransferase-1. Gene Expr Patterns. 2006 Apr;6(4):376-82.

Cheng Z, Biechele T, Wei Z, Morrone S, Moon RT, Wang L, Xu W. Crystal structures of the extracellular domain of LRP6 and its complex with DKK1. Nat Struct Mol Biol. 2011 Oct 9;18(11):1204-10. doi: 10.1038/nsmb.2139.

Ciani L., Salinas P. C. WNTs in the vertebrate nervous system: from patterning to neuronal connectivity. Nat. Rev. Neurosci. 6

Cooper MT, Bray SJ. Frizzled regulation of Notch signalling polarizes cell fate in the Drosophila eye. Nature. 1999 Feb 11;397(6719):526-30

Darnell JE Jr, Kerr IM, Stark GR. Jak-STAT pathways and transcriptional activation in response to IFNs and other extracellular signaling proteins. Science. 1994 Jun 3;264(5164):1415-21. Review.

De A. Wnt/Ca2+ signaling pathway: a brief overview. Acta Biochim Biophys Sin (Shanghai). 2011 Oct;43(10):745-56. doi: 10.1093/abbs/gmr079. Epub 2011 Sep 7.

Denham M, Dottori M. Signals involved in neural differentiation of human embryonic stem cells. Neurosignals. 2009;17(4):234-41. doi: 10.1159/000231890. Epub 2009 Sep 30.

Derynck R., Zhang Y. E. Smad-dependent and Smad-independent pathways in TGF-beta family signalling. Nature 425 577–584. doi: 10.1038/nature02006.

Donato R, Miljan EA, Hines SJ, Aouabdi S, Pollock K, Patel S, Edwards FA, Sinden JD. Differential development of neuronal physiological responsiveness in two human neural stem cell lines. BMC Neurosci. 2007;8:36.

Dworkin S, Jane SM, Darido C. The planar cell polarity pathway in vertebrate epidermal development, homeostasis and repair. Organogenesis. 2011 Jul-Sep;7(3):202-8. doi: 10.4161/org.7.3.18431.

Dziennis S., Alkayed N. J. Role of signal transducer and activator of transcription 3 in neuronal survival and regeneration. Rev. Neurosci. 19, 341–361. doi: 10.1515/REVNEURO.2008.19.4-5.341.

Episkopou V. SOX2 functions in adult neural stem cells. Trends Neurosci. 2005 May;28(5):219-21.

Espinosa L, Inglés-Esteve J, Aguilera C, Bigas A. Phosphorylation by glycogen synthase kinase-3 beta down-regulates Notch activity, a link for Notch and Wnt pathways. J Biol Chem. 2003 Aug 22;278(34):32227-35.

Feng X. H., Derynck R. Specificity and versatility in TGF-β signaling through Smads. Annu. Rev. Cell Dev. Biol. 21 659–693. doi: 10.1146/annurev.cellbio.21.022404.142018.

Fischer T, Guimera J, Wurst W, Prakash N. Distinct but redundant expression of the Frizzled Wnt receptor genes at signaling centers of the developing mouse brain. Neuroscience. 2007 Jul 13;147(3):693-711.

Fortini ME, Bilder D. Endocytic regulation of notch signaling. Curr Opin Genet Dev. 2009;19(4):323–328. doi: 10.1016/j.gde.2009.04.005.

Fragoso MA, Patel AK, Nakamura RE, Yi H, Surapaneni K, Hackam AS The Wnt/β-catenin pathway cross-talks with STAT3 signaling to regulate survival of retinal pigment epithelium cells. PLoS One. 2012;7(10):e46892. doi: 10.1371/journal.pone.0046892.

Fuentealba L. C., Eivers E., Ikeda A., Hurtado C., Kuroda H., Pera E. M., et al. Integrating patterning signals: Wnt/GSK3 regulates the duration of the BMP/Smad1 signal. Cell 131 980–993. doi: 10.1016/j.cell.2007.09.027.

Furuhashi M, Yagi K, Yamamoto H, Furukawa Y, Shimada S, Nakamura Y, Kikuchi A, Miyazono K, Kato M. Axin facilitates Smad3 activation in the transforming growth factor beta signaling pathway. Mol Cell Biol. 2001 Aug;21(15):5132-41.

Garcia AD, Doan NB, Imura T, Bush TG, Sofroniew MV. GFAP-expressing progenitors are the principal source of constitutive neurogenesis in adult mouse forebrain. Nat Neurosci. 2004;7(11):1233-41.

Ge W, Martinowich K, Wu X, He F, Miyamoto A, Fan G, Weinmaster G, Sun YE. Notch signaling promotes astrogliogenesis via direct CSL-mediated glial gene activation.
J Neurosci Res 2002;69:848–860.

Gomes FC, Paulin D, Moura Neto V. Glial fibrillary acidic protein (GFAP): modulation by growth factors and its implication in astrocyte differentiation. Braz J Med Biol Res. 1999 May;32(5):619-31. Review.

Gomi H, Yokoyama T, Fujimoto K, Ikeda T, Katoh A, Itoh T, Itohara S. Mice devoid of the glial fibrillary acidic protein develop normally and are susceptible to scrapie prions. Neuron. 1995 Jan;14(1):29-41.

Gordon M. D., Nusse R. Wnt signaling: multiple pathways, multiple receptors, and multiple transcription factors. J. Biol. Chem. 281 22429–22433. doi: 10.1074/jbc.R600015200.

Green JL, La J, Yum KW, Desai P, Rodewald LW, Zhang X, Leblanc M, Nusse R, Lewis MT, Wahl GM. Paracrine Wnt signaling both promotes and inhibits human breast tumor growth. Proc Natl Acad Sci U S A. 2013 Apr 23;110(17):6991-6. doi: 10.1073/pnas.1303671110.

Gu F, Hata R, Ma YJ, Tanaka J, Mitsuda N, Kumon Y, Hanakawa Y, Hashimoto K, Nakajima K, Sakanaka M. Suppression of Stat3 promotes neurogenesis in cultured neural stem cells. J Neurosci Res. 2005 Jul 15;81(2):163-71.

Guo C, Yang G, Khun K, Kong X, Levy D, Lee P, Melamed J. Activation of Stat3 in renal tumors Am J Transl Res. 2009 Feb 28;1(3):283-90.

Guo CJ, Yang XB, Wu YY, Yang LS, Mi S, Liu ZY, Jia KT, Huang YX, Weng SP, Yu XQ, He JG. Involvement of caveolin-1 in the Jak-Stat signaling pathway and infectious spleen and kidney necrosis virus infection in mandarin fish (Siniperca chuatsi). Mol Immunol. 2011 Apr;48(8):992-1000. doi: 10.1016/j.molimm.2011.01.001.

Habib SJ, Chen BC, Tsai FC, Anastassiadis K, Meyer T, Betzig E, Nusse R. A localized Wnt signal orients asymmetric stem cell division in vitro. 2013 Mar 22;339(6126):1445-8. doi: 10.1126/science.1231077.

Hao J, Li TG, Qi X, Zhao DF, Zhao GQ. WNT/beta-catenin pathway up-regulates Stat3 and converges on LIF to prevent differentiation of mouse embryonic stem cells. Dev Biol. 2006 Feb 1;290(1):81-91.

Hardwick JC, Kodach LL, Offerhaus GJ, van den Brink GR. Bone morphogenetic protein signalling in colorectal cancer. Nat Rev Cancer. 2008 Oct;8(10):806-12. doi: 10.1038/nrc2467. Epub 2008 Aug 29. Review.

Hartl D, Irmler M, Römer I, Mader MT, Mao L, Zabel C, de Angelis MH, Beckers J, Klose J. Transcriptome and proteome analysis of early embryonic mouse brain development. Proteomics. 2008 Mar;8(6):1257-65. doi: 10.1002/pmic.200700724.

Hatakeyama J, Bessho Y, Katoh K, Ookawara S, Fujioka M, Guillemot F, Kageyama R. Hes genes regulate size, shape and histogenesis of the nervous system by control of the timing of neural stem cell differentiation. Development. 2004 Nov;131(22):5539-50. Epub 2004 Oct 20.

Hatzis P, van der Flier LG, van Driel MA, Guryev V, Nielsen F, Denissov S, Nijman IJ, Koster J, Santo EE, Welboren W, Versteeg R, Cuppen E, van de Wetering M, Clevers H, Stunnenberg HG. Genome-wide pattern of TCF7L2/TCF4 chromatin occupancy in colorectal cancer cells. Mol Cell Biol. 2008;28:2732–2744.

Haupt S, Borghese L, Brüstle O, Edenhofer F. Non-genetic modulation of Notch activity by artificial delivery of Notch intracellular domain into neural stem cells. Stem Cell Rev. 2012 Sep;8(3):672-84.

Hayward P, Kalmar T, Arias AM. Wnt/Notch signalling and information processing during development. Development. 2008 Feb;135(3):411-24. doi: 10.1242/dev.000505. Review.

He X, Semenov M, Tamai K, Zeng X. LDL receptor-related proteins 5 and 6 in Wnt/beta-catenin signaling: arrows point the way. Development. 2004 Apr;131(8):1663-77. Review.

Hill C. S. Nucleocytoplasmic shuttling of Smad proteins. Cell Res. 19 36–46. doi: 10.1038/cr.2008.325.

Hinck A. P. Structural studies of the TGF-betas and their receptors – insights into evolution of the TGF-beta superfamily. FEBS Lett. 586 1860–1870. doi: 10.1016/j.febslet.2012.05.028.

Hipper A, Isenberg G. Cyclic mechanical strain decreases the DNA synthesis of vascular smooth muscle cells. Pflugers Arch. 2000 May;440(1):19-27.

Hirata H, Ohtsuka T, Bessho Y, Kageyama R. Generation of structurally and functionally distinct factors from the basic helix-loop-helix gene Hes3 by alternative first exons. J Biol Chem. 2000 Jun 23;275(25):19083-9.

Hirsch C, Louise M. Campano, Wöhrle S, Hecht A. Canonical Wnt signaling transiently stimulates proliferation and enhances neurogenesis in neonatal neural progenitor cultures. Experimental Cell Research 2007;313(3):572-587.

Ho, H. Y. Wnt5a–Ror–Dishevelled signaling constitutes a core developmental pathway that controls tissue morphogenesis. Proc. Natl Acad. Sci. USA 109, 4044–4051 (2012).

Hsieh J. Orchestrating transcriptional control of adult neurogenesis. Genes Dev. 26 1010–1021. doi: 10.1101/gad.187336.112.

Hübner R., Role of Wnt Signaling in Proliferation and Differentiation of Human Neural Progenitor Cells (ReNcell VM) Doc.-Thesis Albrecht-Kossel Institute, University of Rostock, Germany

Hübner R, Schmöle AC, Liedmann A, Frech MJ, Rolfs A, Luo J. Differentiation of human neural progenitor cells regulated by Wnt-3a. Biochem Biophys Res Commun. 2010 Sep 24;400(3):358-62. doi: 10.1016/j.bbrc.2010.08.066.

Ijuin K, Nakanishi K, Ito K. Different downstream pathways for Notch signaling are required for gliogenic and chondrogenic specification of mouse mesencephalic neural crest cells. Mech Dev. 2008 May-Jun;125(5-6):462-74. doi: 10.1016/j.mod.2008.01.008.

Imayoshi I, Shimojo H, Sakamoto M, Ohtsuka T, Kageyama R. Genetic visualization of notch signaling in mammalian neurogenesis. Cell Mol Life Sci. 2013 Jun;70(12):2045-57. doi: 10.1007/s00018-012-1151-x. Review.

Inestrosa N. C., Arenas E. Emerging roles of Wnts in the adult nervous system. Nat. Rev. Neurosci. 11 77–86. doi: 10.1038/nrn2755.

Inman GJ, Hill CS. Stoichiometry of active smad-transcription factor complexes on DNA. J Biol Chem. 2002 Dec 27;277(52):51008-16. Epub 2002 Oct 8. Erratum in: J Biol Chem. 2003 May 9;278(19):17580.

Jiang J, Chan YS, Loh YH, Cai J, Tong GQ, Lim CA, Robson P, Zhong S, Ng HH A core Klf circuitry regulates self-renewal of embryonic stem cells. Nat Cell Biol. 2008 Mar;10(3):353-60. doi: 10.1038/ncb1698.

Jin YH, Kim H, Ki H, Yang I, Yang N, Lee KY, Kim N, Park HS, Kim K. Beta-catenin modulates the level and transcriptional activity of Notch1/NICD through its direct interaction. Biochim Biophys Acta. 2009 Feb;1793(2):290-9. doi: 10.1016/j.bbamcr. 2008.10.002.

Jögi A, Persson P, Grynfeld A, Påhlman S, Axelson H. Modulation of basic helix-loop-helix transcription complex formation by Id proteins during neuronal differentiation. J Biol Chem. 2002 Mar 15;277(11):9118-26. Epub 2001 Dec 27.

Kabos P, Kabosova A, Neuman T. Blocking HES1 expression initiates GABAergic differentiation and induces the expression of p21(CIP1/WAF1) in human neural stem cells. J Biol Chem. 2002 Mar 15;277(11):8763-6.

Kabos P, Kabosova A, Neuman T. Neuronal injury affects expression of helix-loop-helix transcription factors. Neuroreport. 2002 Dec 20;13(18):2385-8.

Kabos P, Matundan H, Zandian M, Bertolotto C, Robinson ML, Davy BE, Yu JS, Krueger RC Jr. Neural precursors express multiple chondroitin sulfate proteoglycans, including the lectican family. Biochem Biophys Res Commun. 2004 Jun 11;318(4):955-63.

Kageyama R, Ohtsuka T, Kobayashi T. The Hes gene family: repressors and oscillators that orchestrate embryogenesis. Development. 2007 Apr;134(7):1243-51. Review.

Kageyama R, Ohtsuka T, Kobayashi T. Roles of Hes genes in neural development. Dev Growth Differ. 2008 Jun;50 Suppl 1:S97-103. doi: 10.1111/j.1440-169X.2008.00993.x. Review.

Kageyama R, Ohtsuka T, Shimojo H, Imayoshi I. Dynamic regulation of Notch signaling in neural progenitor cells. Curr Opin Cell Biol. 2009 Dec;21(6):733-40. doi: 10.1016/j.ceb.2009.08.009. Review.

Kageyama R, Niwa Y, Isomura A, González A, Harima Y. Oscillatory gene expression and somitogenesis. Wiley Interdiscip Rev Dev Biol. 2012 Sep-Oct;1(5):629-41. doi: 10.1002/wdev.46. Epub 2012 Mar 22.

Kamakura S, Oishi K, Yoshimatsu T, Nakafuku M, Masuyama N, Gotoh Y. Hes binding to STAT3 mediates crosstalk between Notch and JAK-STAT signalling. Nat Cell Biol. 2004 Jun;6(6):547-54.

Kandel ER, Squire LR. Neuroscience: breaking down scientific barriers to the study of brain and mind. Science. 2000 Nov 10;290(5494):1113-20.

Kikuchi A, Yamamoto H, Sato A. Selective activation mechanisms of Wnt signaling pathways. Trends Cell Biol. 2009 Mar;19(3):119-29. doi: 10.1016/j.tcb.2009.01.003. Review.

Kopan R, Ilagan MX. The canonical notch signaling pathway: unfolding the activation mechanism. Cell. 2009;137(2):216–233. doi: 10.1016/j.cell.2009.03.045.

Kørbling M, Estrov Z. Adult stem cells for tissue repair - a new therapeutic concept? N Engl J Med. 2003 Aug 7;349(6):570-82. Review.

Koval A, Katanaev VL. Wnt3a stimulation elicits G-protein-coupled receptor properties of mammalian Frizzled proteins. Biochem J. 2011 Feb 1;433(3):435-40. doi: 10.1042/BJ20101878.

Kühl M, Sheldahl LC, Park M, Miller JR, Moon RT. The Wnt/Ca2+ pathway: a new vertebrate Wnt signaling pathway takes shape. Trends Genet. 2000 Jul;16(7):279-83. Review.

Kunke D, Bryja V, Mygland L, Arenas E, Krauss S. Inhibition of canonical Wnt signaling promotes gliogenesis in P0-NSCs. Biochem Biophys Res Commun. 2009 Sep 4;386(4):628-33. doi: 10.1016/j.bbrc.2009.06.084.

Lee E, Salic A, Krüger R, Heinrich R, Kirschner MW. The roles of APC and Axin derived from experimental and theoretical analysis of the Wnt pathway. PLoS Biol. 2003;1:E10.

Lendahl U, Zimmerman LB, McKay RD. CNS stem cells express a new class of intermediate filament protein. Cell. 1990;60(4):585-95.

Liu Z, Tang Y, Qiu T, Cao X, Clemens TL. A dishevelled-1/Smad1 interaction couples WNT and bone morphogenetic protein signaling pathways in uncommitted bone marrow stromal cells. J Biol Chem. 2006 Jun 23;281(25):17156-63.

Liu H, Huang GW, Zhang XM, Ren DL, X Wilson J. Folic Acid supplementation stimulates notch signaling and cell proliferation in embryonic neural stem cells. J Clin Biochem Nutr. 2010 Sep;47(2):174-80. doi: 10.3164/jcbn.10-47.

Loebel DA, Watson CM, De Young RA, Tam PP. Lineage choice and differentiation in mouse embryos and embryonic stem cells. Dev Biol. 2003;264(1):1-14.

Louvi A, Artavanis-Tsakonas S. Notch and disease: a growing field. Semin Cell Dev Biol. 2012 Jun;23(4):473-80. doi: 10.1016/j.semcdb.2012.02.005. Review.

Lyu, J., Yamamoto, V. & Lu, W. Cleavage of the Wnt receptor Ryk regulates neuronal differentiation during cortical neurogenesis. Dev. Cell 15, 773–780 (2008).

Mao B, Wu W, Davidson G, Marhold J, Li M, Mechler BM, Delius H, Hoppe D, Stannek P, Walter C, Glinka A, Niehrs C. Kremen proteins are Dickkopf receptors that regulate Wnt/beta-catenin signalling. Nature. 2002;417(6889):664-7.

Martino G, Pluchino S. The therapeutic potential of neural stem cells. Nat Rev Neurosci. 2006 May;7(5):395-406. Review.

Martin-Rendon E, Watt SM. Stem cell plasticity. Br J Haematol. 2003;122(6):877-91. Review.

Masserdotti G, Badaloni A, Green YS, Croci L, Barili V, Bergamini G, Vetter ML, Consalez GG. ZFP423 coordinates Notch and bone morphogenetic protein signaling, selectively up-regulating Hes5 gene expression. J Biol Chem. 2010 Oct 1;285(40):30814-24. doi: 10.1074/jbc.M110.142869.

Mattagajasingh SN, Yang XP, Irani K, Mattagajasingh I, Becker LC. Activation of Stat3 in endothelial cells following hypoxia-reoxygenation is mediated by Rac1 and protein Kinase C. Biochim Biophys Acta. 2012 May;1823(5):997-1006.

Mazemondet O, Hubner R, Frahm J, Koczan D, Bader BM, Weiss DG, Uhrmacher AM, Frech MJ, Rolfs A, Luo J. Quantitative and kinetic profile of Wnt/β-catenin signaling components during human neural progenitor cell differentiation. Cell Mol Biol Lett. 2011 Dec;16(4):515-38. doi: 10.2478/s11658-011-0021-0.

Mehler M. F., Mabie P. C., Zhang D., Kessler J. A. Bone morphogenetic proteins in the nervous system. Trends Neurosci. 20 309–317. doi: 10.1016/S0166-2236(96)01046-6.

Metcalfe C, Bienz M. Inhibition of GSK3 by Wnt signalling--two contrasting models. J Cell Sci. 2011 Nov 1;124(Pt 21):3537-44. doi: 10.1242/jcs.091991.

Miyazono K., Kamiya Y., Morikawa M. Bone morphogenetic protein receptors and signal transduction. J. Biochem. 147 35–51. doi: 10.1093/jb/mvp148.

Morgan PJ, Ortinau S, Frahm J, Krüger N, Rolfs A, Frech MJ. Protection of neurons derived from human neural progenitor cells by veratridine. Neuroreport 2009; 20(13):1225-9.

Mueller T. D., Nickel J. Promiscuity and specificity in BMP receptor activation. FEBS Lett. 586 1846–1859. doi: 10.1016/j.febslet.2012.02.043.

Müller, K., Untersuchung zu Interaktionen der Wnt/Notch-Signalwege in humanen neuralen Progenitorzellen. Albrecht-Kossel-Institute of Neuroregeneration (AKos) Universität Rostock; Bachelor Thesis

Munji RN, Choe Y, Li G, Siegenthaler JA, Pleasure SJ. Wnt signaling regulates neuronal differentiation of cortical intermediate progenitors. J Neurosci. 2011 Feb 2;31(5):1676-87. doi: 10.1523/JNEUROSCI.5404-10.2011.

Nakashima K, Yanagisawa M, Arakawa H, Kimura N, Hisatsune T, Kawabata M, Miyazono K, Taga T. Synergistic signaling in fetal brain by STAT3-Smad1 complex bridged by p300. Science. 1999 Apr 16;284(5413):479-82.

Nakashima K, Takizawa T, Ochiai W, Yanagisawa M, Hisatsune T, Nakafuku M, Miyazono K, Kishimoto T, Kageyama R, Taga T. BMP2-mediated alteration in the developmental pathway of fetal mouse brain cells from neurogenesis to astrocytogenesis. Proc Natl Acad Sci U S A. 2001 May 8;98(10):5868-73.

Nakashima A, Katagiri T, Tamura M. Cross-talk between Wnt and bone morphogenetic protein 2 (BMP-2) signaling in differentiation pathway of C2C12 myoblasts. J Biol Chem. 2005 Nov 11;280(45):37660-8.

Nakaya MA, Biris K, Tsukiyama T, Jaime S, Rawls JA, Yamaguchi TP. Wnt3a links left-right determination with segmentation and anteroposterior axis elongation. Development. 2005 Dec;132(24):5425-36. Epub 2005 Nov 16.

Nalesso G, Sherwood J, Bertrand J, Pap T, Ramachandran M, De Bari C, Pitzalis C, Dell'accio F. WNT-3A modulates articular chondrocyte phenotype by activating both canonical and noncanonical pathways. J Cell Biol. 2011 May 2;193(3):551-64. doi: 10.1083/jcb.201011051.

Nelson BR, Gumuscu B, Hartman BH, Reh TA. Notch activity is downregulated just prior to retinal ganglion cell differentiation. Dev Neurosci. 2006;28(1-2):128-41.

Nelson BR, Hartman BH, Georgi SA, Lan MS, Reh TA. Transient inactivation of Notch signaling synchronizes differentiation of neural progenitor cells. Dev Biol. 2007 Apr 15;304(2):479-98. Epub 2007 Jan 8.

Niehrs C. The complex world of WNT receptor signalling. Nat Rev Mol Cell Biol. 2012 Dec;13(12):767-79. doi: 10.1038/nrm3470. Review.

Niwa H, Yamamura K, Miyazaki J. Efficient selection for high-expression transfectants with a novel eukaryotic vector. Gene. 1991;108(2):193-9.

Niwa Y, Masamizu Y, Liu T, Nakayama R, Deng CX, Kageyama R. The initiation and propagation of Hes7 oscillation are cooperatively regulated by Fgf and notch signaling in the somite segmentation clock. Dev Cell. 2007;13(2):298–304. doi: 10.1016/j.devcel.2007.07.013.

Nomachi, A. (2008) Receptor tyrosine kinase Ror2 mediates Wnt5a‐induced polarized cell migration by activating c‐Jun N‐terminal kinase via actin-binding protein filamin A. J. Biol. Chem. 283, 27973–27981. Schlessinger K., Hall A., Tolwinski N., 2009. Wnt signaling pathways meet Rho GTPases doi: 10.1101/gad.1760809 Genes & Dev. 2009. 23: 265-277

Norton J. D.. ID helix-loop-helix proteins in cell growth, differentiation and tumorigenesis. J. Cell Sci. 113(Pt 22) 3897–3905.

Obayashi S, Tabunoki H, Kim SU, Satoh J. Gene expression profiling of human neural progenitor cells following the serum-induced astrocyte differentiation. Cell Mol Neurobiol. 2009 May;29(3):423-38. doi: 10.1007/s10571-008-9338-2.

Ohashi S, Natsuizaka M, Yashiro-Ohtani Y, Kalman RA, Nakagawa M, Wu L, Klein-Szanto AJ, Herlyn M, Diehl JA, Katz JP, Pear WS, Seykora JT, Nakagawa H. NOTCH1 and NOTCH3 coordinate esophageal squamous differentiation through a CSL-dependent

transcriptional network. Gastroenterology. 2010 Dec;139(6):2113-23. doi: 10.1053/j.gastro.2010.08.040.

Ohl F, Jung M, Radonić A, Sachs M, Loening SA, Jung K. Identification and validation of suitable endogenous reference genes for gene expression studies of human bladder cancer. J Urol. 2006;175(5):1915-20.

Ohtsuka T, Sakamoto M, Guillemot F, Kageyama R. Roles of the basic helix-loop-helix genes Hes1 and Hes5 in expansion of neural stem cells of the developing brain. J Biol Chem. 2001 Aug 10;276(32):30467-74.

Ong CT, Cheng HT, Chang LW, Ohtsuka T, Kageyama R, Stormo GD, Kopan R.J Target selectivity of vertebrate notch proteins. Collaboration between discrete domains and CSL-binding site architecture determines activation probability. Biol Chem. 2006 Feb 24;281(8):5106-19. Epub 2005 Dec 19.

Pan W, Choi S-C, Wang H, Qin Y, Volpicelli-Daley L, Swan L, Lucast L, Khoo C, Zhang X, Li L, Abrams CS, Sokol SY, Wu D. Wnt3a-mediated formation of phosphatidylinositol 4,5-bisphosphate regulates LRP6 phosphorylation. Science. 2008;321:1350–1353.

Parish CL, Castelo-Branco G, Rawal N, Tonnesen J, Sorensen AT, Salto C, Kokaia M, Lindvall O, Arenas E. Wnt5a-treated midbrain neural stem cells improve dopamine cell replacement therapy in parkinsonian mice. J Clin Invest. 2008;118(1):149-60.

Park IH, Zhao R, West JA, Yabuuchi A, Huo H, Ince TA, Lerou PH, Lensch MW, Daley GQ. Reprogramming of human somatic cells to pluripotency with defined factors. Nature. 2008 Jan 10;451(7175):141-6.

Pedranzini L, Dechow T, Berishaj M, Comenzo R, Zhou P, Azare J, Bornmann W, Bromberg J. Pyridone 6, a pan-Janus-activated kinase inhibitor, induces growth inhibition of multiple myeloma cells. Cancer Res. 2006 Oct 1;66(19):9714-21.

Peignon G, Durand A, Cacheux W, Ayrault O, Terris B, Laurent-Puig P, Shroyer NF, Van Seuningen I, Honjo T, Perret C, Romagnolo B. Complex interplay between β-catenin signalling and Notch effectors in intestinal tumorigenesis. Gut. 2011 Feb;60(2):166-76. doi: 10.1136/gut.2009.204719.

Pekny M, Levéen P, Pekna M, Eliasson C, Berthold CH, Westermark B, Betsholtz C. Mice lacking glial fibrillary acidic protein display astrocytes devoid of intermediate filaments but develop and reproduce normally. EMBO J. 1995 Apr 18;14(8):1590-8.

Perrone-Bizzozero N, Bird CW. Role of HuD in nervous system function and pathology. Front Biosci (Schol Ed). Jan 2013 1;5:554-63.

Pfaffl MW. A new mathematical model for relative quantification in real-time RT-PCR. Nucleic Acids Res. 2001;29(9):e45.

Qian X, Shen Q, Goderie SK, et al. Timing of CNS cell generation: a programmed sequence of neuron and glial cell production from isolated murine cortical stem cells. Neuron. 2000;28(1):69–80.

Qiu X, Klebanov L, Yakovlev A. Correlation between gene expression levels and limitations of the empirical bayes methodology for finding differentially expressed genes. Stat Appl Genet Mol Biol. 2005;4:Article34. Epub 2005 Nov 22.

Rajan P, McKay RD. Multiple routes to astrocytic differentiation in the CNS. J Neurosci. 1998 May 15;18(10):3620-9.

Ram P. T., Iyengar R.. G protein coupled receptor signaling through the Src and STAT3 pathway: role in proliferation and transformation. Oncogene 20, 1601–1606. doi: 10.1038/sj.onc.1204186.

Reiss K, Maretzky T, Ludwig A, Tousseyn T, de Strooper B, Hartmann D, Saftig P. ADAM10 cleavage of N-cadherin and regulation of cell-cell adhesion and beta-catenin nuclear signalling. EMBO J. 2005;24:742–752.

Ribeiro M, Hansson ML, Lindberg MJ, Popko-Scibor AE, Wallberg AE. GSK3beta is a negative regulator of the transcriptional coactivator MAML1. Nucleic Acids Res. 2009 Nov;37(20):6691-700. doi: 10.1093/nar/gkp724.

Rolland B, Le Prince G, Fages C, Nunez J, Tardy M. GFAP turnover during astroglial proliferation and differentiation. Brain Res Dev Brain Res. 1990 Oct 1;56(1):144-9.

Saneyoshi T, Kume S, Amasaki Y, Mikoshiba K. The Wnt/calcium pathway activates NF-AT and promotes ventral cell fate in Xenopus embryos. Nature. 2002;417(6886):295-9.

Schlessinger K, Hall A, Tolwinski N. Wnt signaling pathways meet Rho GTPases. Genes Dev. 2009 Feb 1;23(3):265-77. doi: 10.1101/gad.1760809. Review.

Schmöle AC, Brennführer A, Karapetyan G, Jaster R, Pews-Davtyan A, Hübner R, Ortinau S, Beller M, Rolfs A, Frech MJ. Novel indolylmaleimide acts as GSK-3beta inhibitor in human neural progenitor cells. Bioorg Med Chem. 2010 Sep 15;18(18):6785-95. doi: 10.1016/j.bmc.2010.07.045. Epub 2010 Jul 25.

Scholl C., Weibetamuller K., Holenya P., Shaked-Rabi M., Tucker K. L., Wolfl S. Distinct and overlapping gene regulatory networks in BMP- and HDAC-controlled cell fate determination in the embryonic forebrain. BMC Genomics 13:298. doi: 10.1186/1471-2164-13-298.

Semënov MV, Tamai K, Brott BK, Kühl M, Sokol S, He X. Head inducer Dickkopf-1 is a ligand for Wnt coreceptor LRP6. Curr Biol. 2001;11(12):951-61.

Sharma RP, Chopra VL. Effect of the Wingless (wg1) mutation on wing and haltere development in Drosophila melanogaster. Dev Biol. 1976;48:461–465.

Shimizu T, Kagawa T, Inoue T, Nonaka A, Takada S, Aburatani H, Taga T. Stabilized beta-catenin functions through TCF/LEF proteins and the Notch/RBP-Jkappa complex to promote

proliferation and suppress differentiation of neural precursor cells. Mol Cell Biol. 2008 Dec;28(24):7427-41. doi: 10.1128/MCB.01962-07.

Song HW, Kumar BK, Kim SH, Jeon YH, Lee YA, Lee WT, Park KA, Lee JE. Agmatine enhances neurogenesis by increasing ERK1/2 expression, and suppresses astrogenesis by decreasing BMP 2,4 and SMAD 1,5,8 expression in subventricular zone neural stem cells. Life Sci. 2011 Sep 26;89(13-14):439-49. doi: 10.1016/j.lfs.2011.07.003.

Steward MM, Sridhar A, Meyer JS. Neural regeneration. Curr Top Microbiol Immunol. 2013;367:163-91. doi: 10.1007/82_2012_302.

Swiatek-Machado K, Mieczkowski J, Ellert-Miklaszewska A, Swierk P, Fokt I, Szymanski S, Skora S, Szeja W, Grynkiewicz G, Lesyng B, Priebe W, Kaminska B Novel small molecular inhibitors disrupt the JAK/STAT3 and FAK signaling pathways and exhibit a potent antitumor activity in glioma cells .Cancer Biol Ther. 2012 Jun;13(8):657-70. doi: 10.4161/cbt.20083.

Taelman VF, Dobrowolski R, Plouhinec JL, Fuentealba LC, Vorwald PP, Gumper I, Sabatini DD, De Robertis EM. Wnt signaling requires sequestration of glycogen synthase kinase 3 inside multivesicular endosomes. Cell. 2010 Dec 23;143(7):1136-48. doi: 10.1016/j.cell.2010.11.034.

Takada R, Satomi Y, Kurata T, Ueno N, Norioka S, Kondoh H, Takao T, Takada S. Monounsaturated fatty acid modification of Wnt protein: its role in Wnt secretion. Dev Cell. 2006;11(6):791-801.

Takahashi K, Yamanaka S. Induction of pluripotent stem cells from mouse embryonic and adult fibroblast cultures by defined factors. Cell. 2006 Aug 25;126(4):663-76.

Takebayashi K, Sasai Y, Sakai Y, Watanabe T, Nakanishi S, Kageyama R. Structure, chromosomal locus, and promoter analysis of the gene encoding the mouse helix-loop-helix factor HES-1. Negative autoregulation through the multiple N box elements. J Biol Chem. 1994 Feb 18;269(7):5150-6.

Takizawa T, Ochiai W, Nakashima K, Taga T. Enhanced gene activation by Notch and BMP signaling cross-talk. Nucleic Acids Res. 2003 Oct 1;31(19):5723-31.

Tanneberger K, Pfister AS, Brauburger K, Schneikert J, Hadjihannas MV, Kriz V, Schulte G, Bryja V, Behrens J. Amer1/WTX couples Wnt-induced formation of PtdIns(4,5)P2 to LRP6 phosphorylation. EMBO J. 2011;30:1433–1443.

Thomsen R, Daugaard TF, Holm IE, Nielsen AL Alternative mRNA Splicing from the Glial Fibrillary Acidic Protein (GFAP) Gene Generates Isoforms with Distinct Subcellular mRNA Localization Patterns in Astrocytes. PLoS ONE 8(8): e72110. doi:10.1371/journal.pone.0072110

Trilck M., Hübner R., Seibler P., Klein C., Rolfs A., and Frech M. J. Niemann-Pick type C1 patient-specific induced pluripotent stem cells display disease specific hallmarks Orphanet Journal of Rare Diseases 2013, 8:144 doi:10.1186/1750-1172-8-144

Nielsen AL, Holm IE, Johansen M, Bonven B, Jorgensen P, et al. A new splice variant of glial fibrillary acidic protein, GFAP epsilon, interacts with the presenilin proteins. J Biol Chem 277: 29983–29991. doi: 10.1074/jbc.m112121200.

Tomita, K., Moriyoshi, K., Nakanishi, S., Guillemot, F. & Kageyama, R. Mammalian achaete-scute and atonal homologs regulate neuronal versus glial fate determination in the central nervous system. EMBO J. 19, 5460–5472.

Uemura K, Kihara T, Kuzuya A, Okawa K, Nishimoto T, Bito H, Ninomiya H, Sugimoto H, Kinoshita A, Shimohama S. Activity-dependent regulation of beta-catenin via epsilon-cleavage of N-cadherin. Biochem Biophys Res Commun. 2006;345:951–958.

Urist M. R.. Bone: formation by autoinduction. Science 150 893–899. doi: 10.1126/science.150.3698.893.

van Amerongen R., Nusse R.. Towards an integrated view of Wnt signaling in development. Development 136 3205–3214. doi: 10.1242/dev.033910.

Vinals F., Reiriz J., Ambrosio S., Bartrons R., Rosa J. L., Ventura F.. BMP-2 decreases Mash1 stability by increasing Id1 expression. EMBO J. 23 3527–3537. doi: 10.1038/sj.emboj.7600360.

Wall DS, Mears AJ, McNeill B, Mazerolle C, Thurig S, Wang Y, Kageyama R, Wallace VA. Progenitor cell proliferation in the retina is dependent on notch-independent Sonic hedgehog/Hes1 activity. J Cell Biol. 2009;184(1):101–112. doi: 10.1083/jcb.200805155.

WHO statistics 2013-08-21; 10:54 (UTC+01:00): http://www.who.int/healthinfo/global_burden_disease/GBD_report_2004update_part4.pdf

Wawrzak D, Métioui M, Willems E, Hendrickx M, de Genst E, Leyns L. Wnt3a binds to several sFRPs in the nanomolar range. Biochem Biophys Res Commun. 2007 Jun 15;357(4):1119-23.

Weissman IL. Stem cells: units of development, units of regeneration, and units in evolution. Cell. 2000;100(1):157-68. Review.

Wicks S. J., Grocott T., Haros K., Maillard M., ten Dijke P., Chantry A.. Reversible ubiquitination regulates the Smad/TGF-beta signalling pathway. Biochem. Soc. Trans. 34 761–763. doi: 10.1042/BST0340761.

Willert K, Brown JD, Danenberg E, Duncan AW, Weissman IL, Reya T, Yates JR 3rd, Nusse R. Wnt proteins are lipid-modified and can act as stem cell growth factors. Nature 2003;423(6938):448-52.

Winkel, A. Wnt-ligand-dependent interaction of TAK1 (TGF-β-activated kinase-1) with the receptor tyrosine kinase Ror2 modulates canonical Wnt signalling. Cell. Signal. 20, 2134–2144 (2008).

Woo SM, Kim J, Han HW, Chae JI, Son MY, Cho S, Chung HM, Han YM, Kang YK. Notch signaling is required for maintaining stem-cell features of neuroprogenitor cells derived from human embryonic stem cells. BMC Neurosci. 2009;10:97.

Wu Y, Liu Y, Levine EM, Rao MS. Hes1 but not Hes5 regulates an astrocyte versus oligodendrocyte fate choice in glial restricted precursors. Dev Dyn. 2003 Apr;226(4):675-89.

Wu D, Pan W. GSK3: a multifaceted kinase in Wnt signaling. Trends Biochem Sci. 2010 Mar;35(3):161-8. doi: 10.1016/j.tibs.2009.10.002.

Yu PB, Hong CC, Sachidanandan C, Babitt JL, Deng DY, Hoyng SA, Lin HY, Bloch KD, Peterson RT. Dorsomorphin inhibits BMP signals required for embryogenesis and iron metabolism. Nat Chem Biol. 2008 Jan;4(1):33-41.

Zang Y, Yu LF, Pang T, Fang LP, Feng X, Wen TQ, Nan FJ, Feng LY, Li J. AICAR induces astroglial differentiation of neural stem cells via activating the JAK/STAT3 pathway independently of AMP-activated protein kinase. J Biol Chem. 2008 Mar 7;283(10):6201-8.

Zhang LY, Ye J, Zhang F, Li FF, Li H, Gu Y, Liu F, Chen GS, Li Q. Axin induces cell death and reduces cell proliferation in astrocytoma by activating the p53 pathway. Int J Oncol. 2009;35(1):25-32.

Zhu Z and Huangfu D. Human pluripotent stem cells: an emerging model in developmental biology Development 2013 140:705-717; doi:10.1242/dev.086165

7 Appendix

7.1 ReNcell VM cells

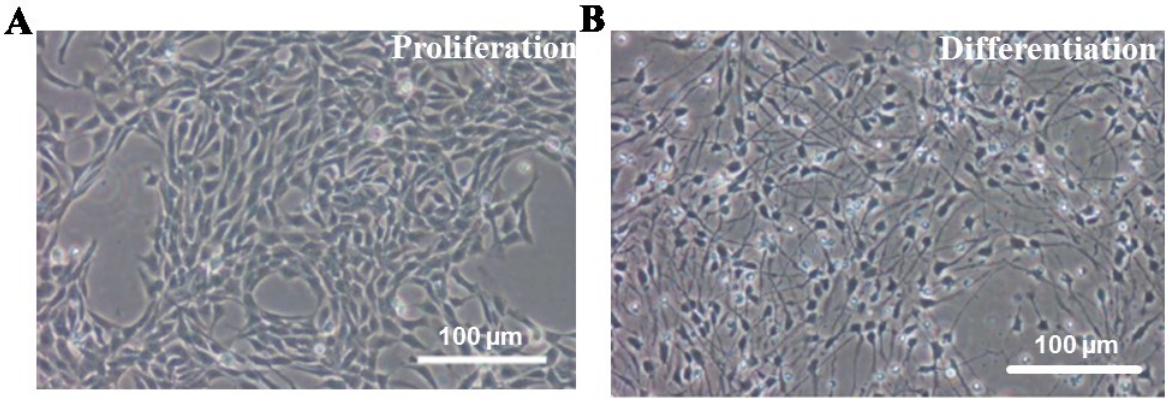

Figure 45: Phasecontrast picture of ReNcell VM cells in proliferation and differentiation. A: Phasecontrast of proliferating ReNcell VM cells. **B**: Phasecontrast of 3 days differentiated ReNcell VM cells.

7.2 iPS-NPCs

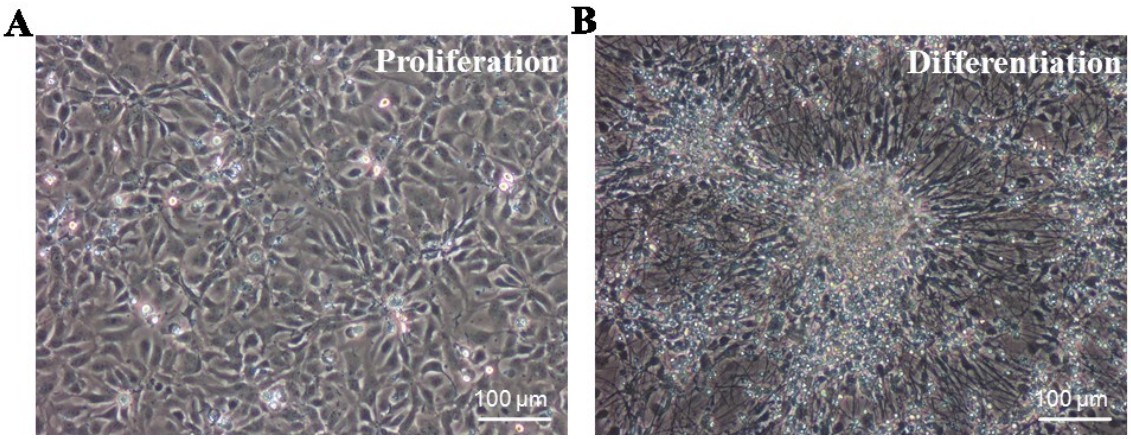

Figure 46: Phasecontrast picture of iPS-NPCs in proliferation and differentiation. A: Phasecontrast of proliferating iPS-NPCs. **B**: Phasecontrast of 18 days differentiated iPS-NPCs.

7.3 Efficiency of transfection and lipofection of ReNcell VM cells

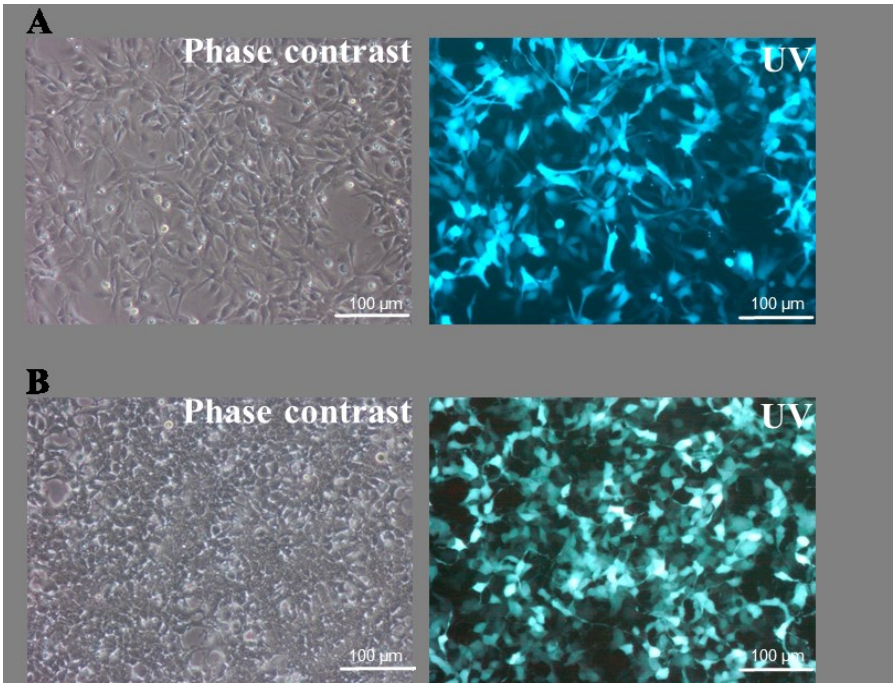

Figure 47: Efficency of transfection and lipofection. **A**: Transfection of 1 Mio ReNcell VM cells with pCAGGS-GFP, 24 h after transfection of 4 µg plasmid DNA. **B**: Lipofection of 0,2 Mio HEK293H with pCAGGS-GFP, 24 h after lipofection of 4 µg plasmid DNA.

7.4 Generation of pCAGGS-HA-HES vectors

7.4.1 Generation of pCAGGS-HA-hHES1

To amplify *hHES1* the plasmid pCMV6-XL4-HES1 (origene) was used as a template, together with the forward primer which includes the *Xho*I restriction site in combination with a HA-Tag and the reverse primer which includes a *Bst*XI restriction site. After amplification of HA-*hHES1* (Figure 48, A) the insert was purified and ligated into pGEM-T easy (Promega) for subsequent blue/white screening and selection. Positive clones were analyzed by digestion with *BstXI* and *Xho*I, expected fragments were ca. 3000 bp and 1011 bp (Figure 48, B). All positive clones were sequenced and used for insert production. The purified insert was ligated into pCAGGS and resulting clones were analyzed by colony PCR. Consequential positive clones were sequenced and transfected in ReNcell VM cells. The expression of N-terminally HA-tagged hHES1 was tested via western blot analysis. Therefore, transfected ReNcell VM cells were proliferated for 24 h after transfection and then differentiated for 24 h. Western blot analysis revealed no specific band neither by HA antibody nor by HES1 antibody (Figure 48, D).

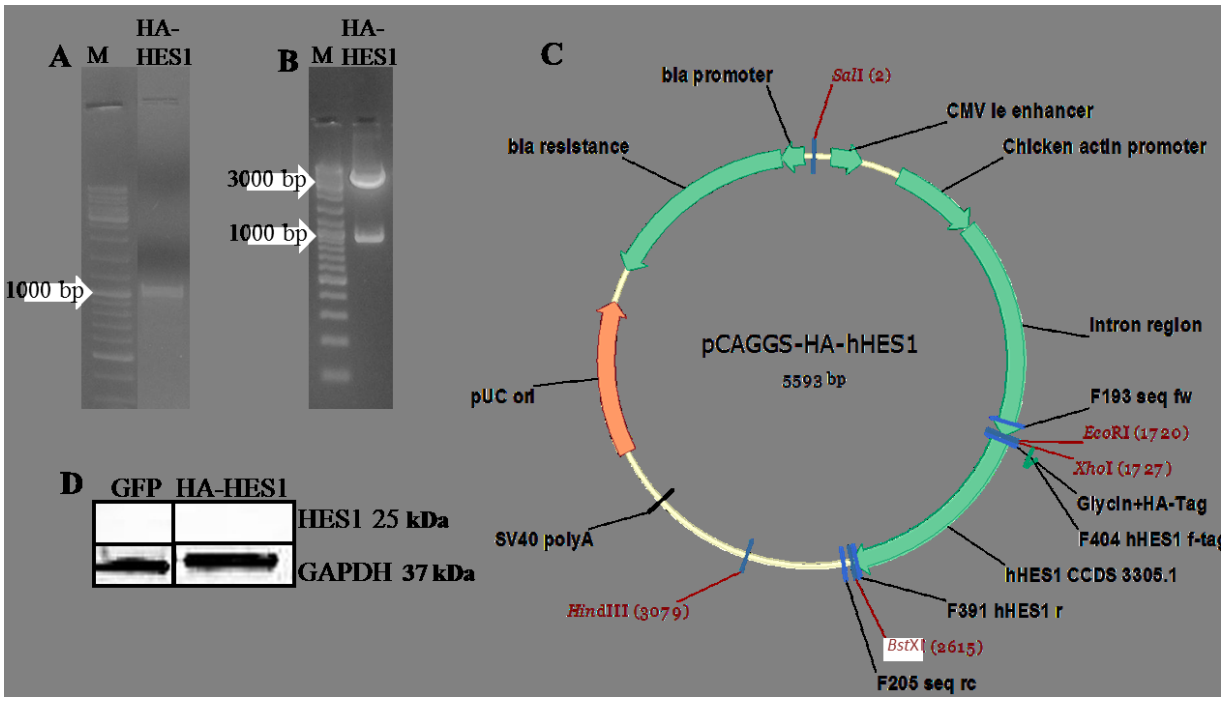

Figure 48: Generation of pCAGGS-HA-hHES1. A: Product of HA-*hHES1* amplification (M=DNA ladder). **B**: Digestion of pGEM-T easy-HA-hHES1 with *Xho*I and *Bst*XI; expected fragments were 3000 bp and 1011 bp. **C**: Plasmid map of pCAGGS-HA-hHES1. **D**: Western blot of pCAGGS-HA-hHES1 transfected ReNcell VM cells after 24 h of differentiation detected by HA antibody, pCAGGS-GFP transfected cells were used as control.

7.4.2 Generation of pCAGGS-HA-hHES5

To amplify *hHES5* the plasmid pCMV6-XL4-HES5 (origene) was used as a template, together with the forward primer which includes the *Xho*I restriction site in combination with a HA-Tag and the reverse primer which includes a *Bst*XI restriction site. After amplification of HA-*hHES5* (Figure 49, A) the insert was purified and ligated into pGEM-T easy (Promega) for subsequent blue/white screening and selection. Positive clones were analyzed by digestion with *BstXI* and *Xho*I, expected fragments were ca. 3000 bp and 590 bp (Figure 49, B). All positive clones were sequenced and used for insert production. The purified insert was ligated into pCAGGS and resulting clones were analyzed by colony PCR. Consequential positive clones were sequenced and transfected in ReNcell VM cells. The expression of N-terminally HA-tagged hHES1 was tested via western blot analysis. Therefore, transfected ReNcell VM cells were proliferated for 24 h after transfection and then differentiated for 24 h. Western blot analysis revealed a very weak band at 20 kDa (Figure 49, D), which was consistent with the pCAGGS-hHES5 vector.

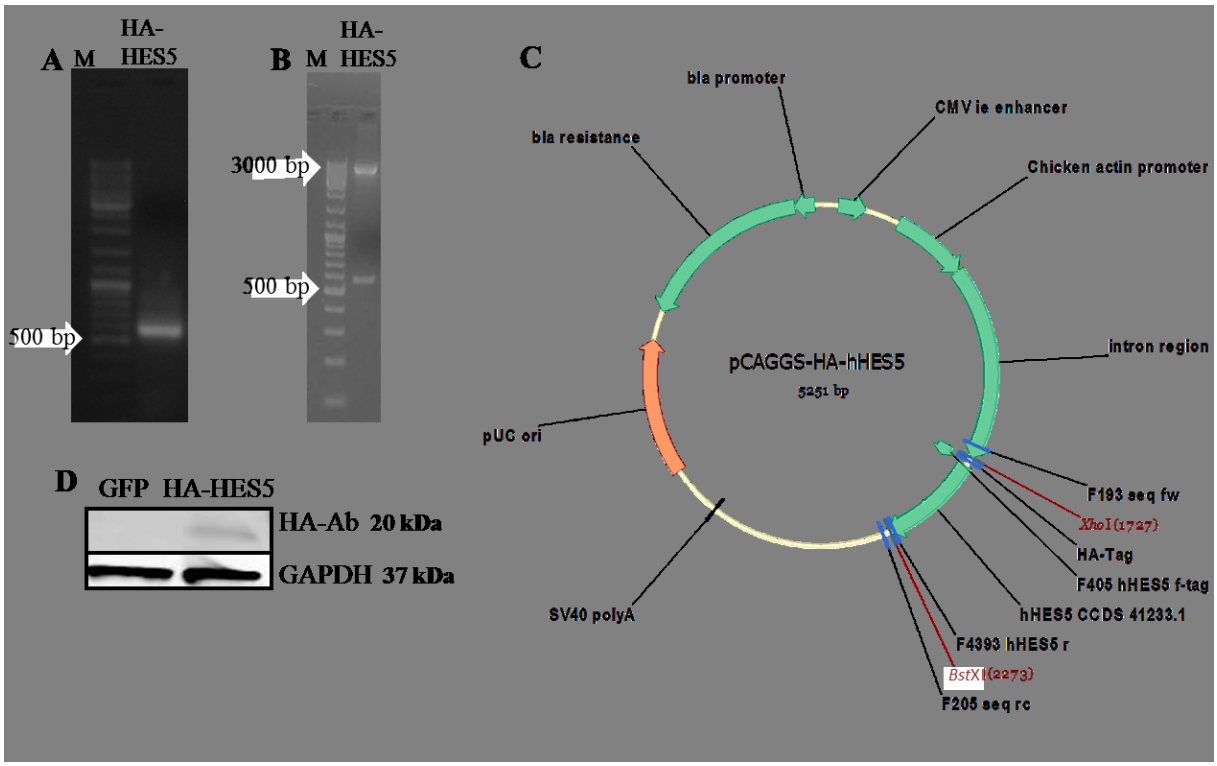

Figure 49: Generation of pCAGGS-HA-hHES5. **A**: Product of HA-*hHES5* amplification (M=DNA ladder). **B**: Digestion of pGEM Teasy-HA-hHES5 with *Xho*I and *Bst*XI; expected fragments were 3000 bp and 590 bp. **C**: Plasmid map of pCAGGS-HA-hHES5. **D**: Western blot of pCAGGS-HA-hHES5 transfected ReNcell VM cells after 24 h of differentiation, pCAGGS-GFP transfected cells were used as control.

7.5 Treatment of ReNcell VM cells with Dkk-1

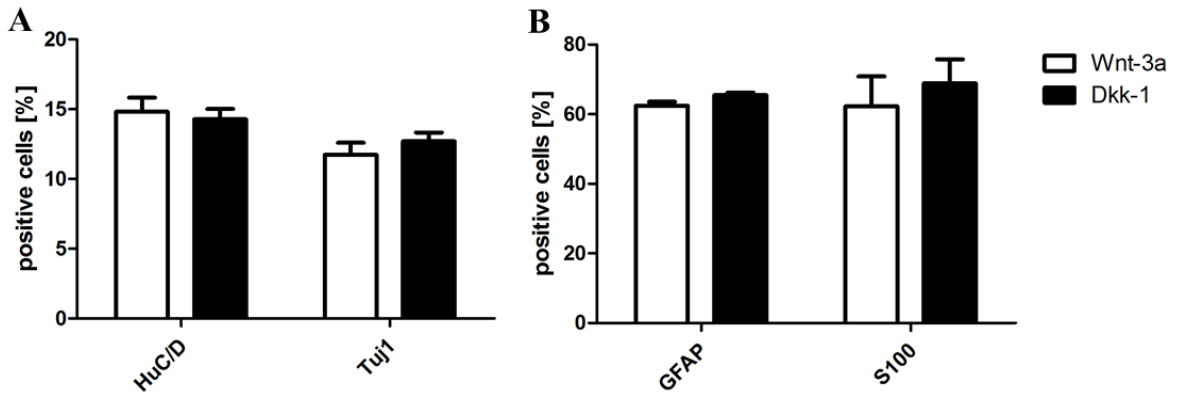

Figure 50: Analysis of Wnt-3a and Dkk-1 treated ReNcell VM cells Flow cytometric data showing percentages of Wnt-3a and Dkk-1 treated cells positive for HuC/D and Tuj1 (A) and GFAP and S100β (B) differentiated for 3 days in the presence of Wnt-3a+Dkk-1 (Dkk-1) or Wnt-3a alone as control. Data are presented as means ± SEM from two independent experiments.

Danksagung

Ich möchte mich bei Prof. Dr. A. Rolfs dafür bedanken, dass ich meine Doktorarbeit im Albrecht-Kossel-Institut für Neuroregeneration erarbeiten durfte. Dies ermöglichte mir an einem interessanten Thema zu arbeiten.

Mein besonderer Dank gilt Prof. Dr. R Schröder für die Funktion als Gutachter.

Dr. R Hübner danke ich für die sehr gute Betreuung in den letzten 3 Jahren, schnellen Antworten und kreativen Ideen.

Ich möchte Amie, Anne, Christian, Frances, Jan, Michi, Moritz, Sabine, Susanne, Susi, Stefan (alias Super-Hiwi), Venkata und Vivian für die Hilfe, die unterhaltsamen Stunden im Labor und für die erfrischenden Gespräche in den Pausen danken.

Ein herzlicher Dank geht an die TAs Ellen, Lea, Norman und Sebastian. Sie waren stets kompetente Ansprechpartner und ihre Anwesenheit eine sehr große Freude.

Mein größter Dank aber gilt meiner Familie. Meinem Ehemann Jens, meinen Großeltern Gerda und Eduard, meinen Eltern Gabriele und Herbert, meinem Bruder Mark mit seiner Frau Jenny, meinem Neffen Bennet, meiner Nichte Leni, meinen Onkeln Thomas und Michael, meiner „Tante“ Anne und „Onkel“ Wilfred, meinen Schwiegereltern Etta und Reinhard, Oma Hilke, Magarethe und Werner, meinen Freunden Domenica, Sarah und Valentina. Ohne sie alle wäre ich heute nicht wer ich bin und ohne ihre Unterstützung und Motivation nicht in der Lage gewesen diese Arbeit zu verfassen.